A STUDY OF THE FLEXIBLE SPACE PLATFORM BASED DEPLOYABLE MANIPULATOR

ITSHAK MAROM

B.Sc., Technion - Israel Institute of Technology, 1974
M.Sc., Technion - Israel Institute of Technology, 1977

A THESIS SUBMITTED IN PARTIAL FULFILMENT OF
THE REQUIREMENTS FOR THE DEGREE OF

DOCTOR OF PHILOSOPHY

in

The Faculty of Graduate Studies
Department of Mechanical Engineering

We accept this thesis as conforming
to the required standard

THE UNIVERSITY OF BRITISH COLUMBIA

July 1993

In presenting this thesis in partial fulfilment of the requirements for an advanced degree at the University of British Columbia, I agree that the Library shall make it freely available for reference and study. I further agree that permission for extensive copying of this thesis for scholarly purposes may be granted by the head of my department or by his or her representatives. It is understood that copying or publication of this thesis for financial gain shall not be allowed without my written permission.

(Signature) _____

Department of Mechanical Engineering
The University of British Columbia
Vancouver, B.C. CANADA

Date: July 1993

ABSTRACT

A relatively general formulation, based on Lagrange's approach, for studying the nonlinear dynamics and control of a flexible, space based, Mobile Deployable Manipulator (MDM) has been developed. The formulation has the following distinctive features:

(i) it is applicable to a two-link deployable manipulator translating along a flexible space platform in any desired orbit;

(ii) the revolute and the prismatic joints are flexible with finite gear ratio and rotor inertia;

(iii) the nonlinear, nonautonomous and coupled equations of motion are presented in a compact form which provide insight into the intricate dynamical interactions and help achieve a highly efficient dynamic simulation.

Validity of the formulation and the computer code were established through checks on conservation of the system energy, and comparison with test-cases.

Results of the dynamical analysis clearly show that under critical combinations of parameters, the system can become unstable.

An inverse kinematic technique, accounting for the linear and angular displacements of the the flexible platform, has been developed to meet the desired position and orientation requirement of the end effector with respect to the chosen reference frame.

A nonlinear control strategy, based on the Feedback Linearization Technique (FLT) has been developed to ensure accurate tracking of a desired trajectory in presence of the system libration as well as the base translation and vibrations. The con-

troller also ensures desired attitude motion in presence of the manipulator's translational and slewing maneuvers. The closed loop simulation results show that a desired degree of system stability and high tracking accuracy can be achieved.

TABLE OF CONTENTS

LIST OF SYMBOLS

$\bar{a}_i$	position vector locating the $(i+1)^{th}$ frame w.r.t. the i^{th} frame
$\bar{a}_0$	shift in the system center of mass
$\bar{a}_5$	deployment generalized coordinate
a_{5d}	required deployment
$[c_j]$	transformation matrix from the j^{th} frame to the $(j-1)^{th}$ frame
C_i	damping coefficient associated with the i^{th} body generalized coordinate
dm_i	mass element in the i^{th} body
d_1	cross-section dimension of the platform
d_4	cross-section dimension of the arm
D_i	damping generalized force in the i^{th} body
E	total energy of the system
EJ	flexural rigidity of the platform
F_0	system frame
F_I	inertial coordinate frame
F_p	platform truss fixed reference frame
F_r	orbital coordinate frame
F_i	i^{th} body fixed coordinate frame
GM	earth gravitational constant
[H]	homogeneous transformation
h	angular momentum per unit mass w.r.t. the inertial frame
h_1	location of the manipulator base along the platform

h_2	distance between joint 1 and the center line of the platform
[I]	system instantaneous moment of inertia w.r.t. the system frame
$[I_i]$	moment of inertia matrix of the i^{th} body w.r.t. the system frame
$\hat{i}, \hat{j}, \hat{k}$	unit vectors along the X,Y,Z coordinates, respectively
k_3, k_5	equivalent torsional stiffness of joints 1 and 2, respectively
K_{m3}, K_{m5}	torque motor gains for joint 1 and joint 2, respectively
$[K_p], [K_v]$	position and velocity feedback gain matrices, respectively
$\bar{l}_{rc}$	direction cosine vector for $\bar{r}_c$ w.r.t. the system frame
l_1	semi-major length of the platform
l_4	length of arm 1
m	total mass of the system
m_i	mass of the i^{th} body
[M]	system mass matrix
$\overline{N}$	nonlinear force vector; Eq. (2.37)
n	number of bodies in the system
nom	number of flexible modes
n_3, n_5	gear ratios of joints 1 and 2, respectively
$\bar{q}_d$	required generalized coordinate vector
$\bar{q}$	generalized coordinate vector
q_i	generalized coordinate associated with the i^{th} mode
$\overline{Q}$	generalized force vector
r_c	radius of the orbit
$\bar{R}_i$	position vector of a mass element w.r.t. the inertial frame

$\bar{r}_i$	position vector of a mass element w.r.t. the body frame
r_5	effective linear actuator radius
t	time
T_i	generalized control torque exerted on the i^{th} body
T	system kinetic energy
T_{j3}, T_{j5}	kinetic energies of joints 1 and 2, respectively
U	system potential energy
U_i	potential energy stored in the i^{th} body
U_g	gravitational potential energy
U_e	elastic potential energy
[U]	the unit matirx
X_i, Y_i, Z_i	i^{th} body fixed coordinate frame
α_1	local slope of the deformed platform
β_i	rotation angle of the i^{th} body fixed coordinate frame
β_3	rotation of joint 1 w.r.t. the base
β_4	slew of arm 1 w.r.t. the base
β_{4d}	required slew
β_5	rotation of joint 2 w.r.t. the arm
δ_0	platform deflection at midpoint
δ_1	platform transverse deflection
$\delta(-)$	denotes change in (-)
ϵ	orbit eccentricity
θ	true anomaly

ξ_i	damping ratio in the i^{th} degree of freedom
$\bar{\rho}_i$	position vector of a mass element w.r.t. the i^{th} body frame
$\bar{\phi}_1$	vector containing the mode shapes of the platform
ψ	system rotation about the orbit normal Z_r; system libration
ψ_i	rotation of the i^{th} body fixed frame w.r.t. the $(i-1)^{th}$ frame
ω_i	eigenvalues of the i^{th} generalized coordinate
$\overline{\Omega}$	system frame angular velocity
τ	orbital period

ABBREVIATIONS

c (–)	cos (–)
c.m.	center of mass
d.o.f.	degree(s) of freedom
deg	degrees
FLT	Feedback Linearization Technique
Hz	Hertz
I.C.	Initial Condition
J	Joule
kg	kilogram
m	meter
MDM	Mobile Deployable Manipulator
MSS	Mobile Servicing System
Nm	Newton-meter
r.h.s.	right hand side
s	seconds
SPDM	Sepecial Purpose Dexturous Manipulator
s (–)	sin (–)
w.r.t.	with respect to

Dot ($\dot{}$) and prime ($'$) represent differentiations with respect to time and spatial coordinate, respectively. Subscripts $_o$ and $_d$ indicate initial conditions and required values, respectively. Subscript $_i$ indicates the i^{th} body or the i^{th} mode. Superscript ^{T} represents transpose of a matrix. Overbar ($\bar{}$) represents a vector.

LIST OF FIGURES

LIST OF TABLES

ACKNOWLEDGEMENTS

I would like to thank Prof. V.J. Modi for his useful guidance throughout this research project.

Thanks are also due to colleagues Dr. Alfred Ng, Mr. Satyabrata Pradhan and Mr. Anant Grewal who facilitated the progress of this work by sharing their technical know-how.

Special appreciation is extended to my family for their understanding and support.

The investigation reported here was supported by the Natural Sciences and Engineering Research Council of Canada, Grant No. A-2181; and the Networks of Centers of Excellence Program, Institute of Robotics and Intelligent Systems, Grant No. IRIS/C-8, 5-55380.

1. INTRODUCTION

1.1 Preliminary Remarks

The proposed Space Station "Freedom", as shown in Figure 1-1, is intended to be operational in the late nineties. Spanning over 110 meters in its permanently manned configuration, and carrying solar panels extending to 66 meters tip-to-tip, the Space Station is a highly flexible structure. The primary design requirements of the space station is to serve as a permanent operational base for scientific explorations as well as processing and manufacture in the favourable microgravity and high vacuum environment. It will also be used as a platform for satellite launch and repair, as well as assembly of space structures.

Canada's contribution will be through the Mobile Servicing System (MSS), a complex robotic manipulator, which will be used to assemble, service and maintain the entire station. The MSS comprises the maintenance depot and the Special Purpose Dexterous Manipulator (SPDM). The SPDM, when attached to the station manipulator, will give the MSS an additional precision capability for tasks requiring a higher degree of accuracy.

The normal operation of the Space Station is designed to be by remote or teleoperation of several robotic manipulators from a central control post, where the Mobile Servicing System (MSS) will operate as the main handling tool. Forming an integral part of the space station, the MSS may have one or two arms supported by a mobile base, which traverses the power boom through translational and rotational maneuvers.

The Space Station based MSS is inherently a highly complex and variable inertia system. Structural and joints flexibilities further accentuate the problem. The inter-

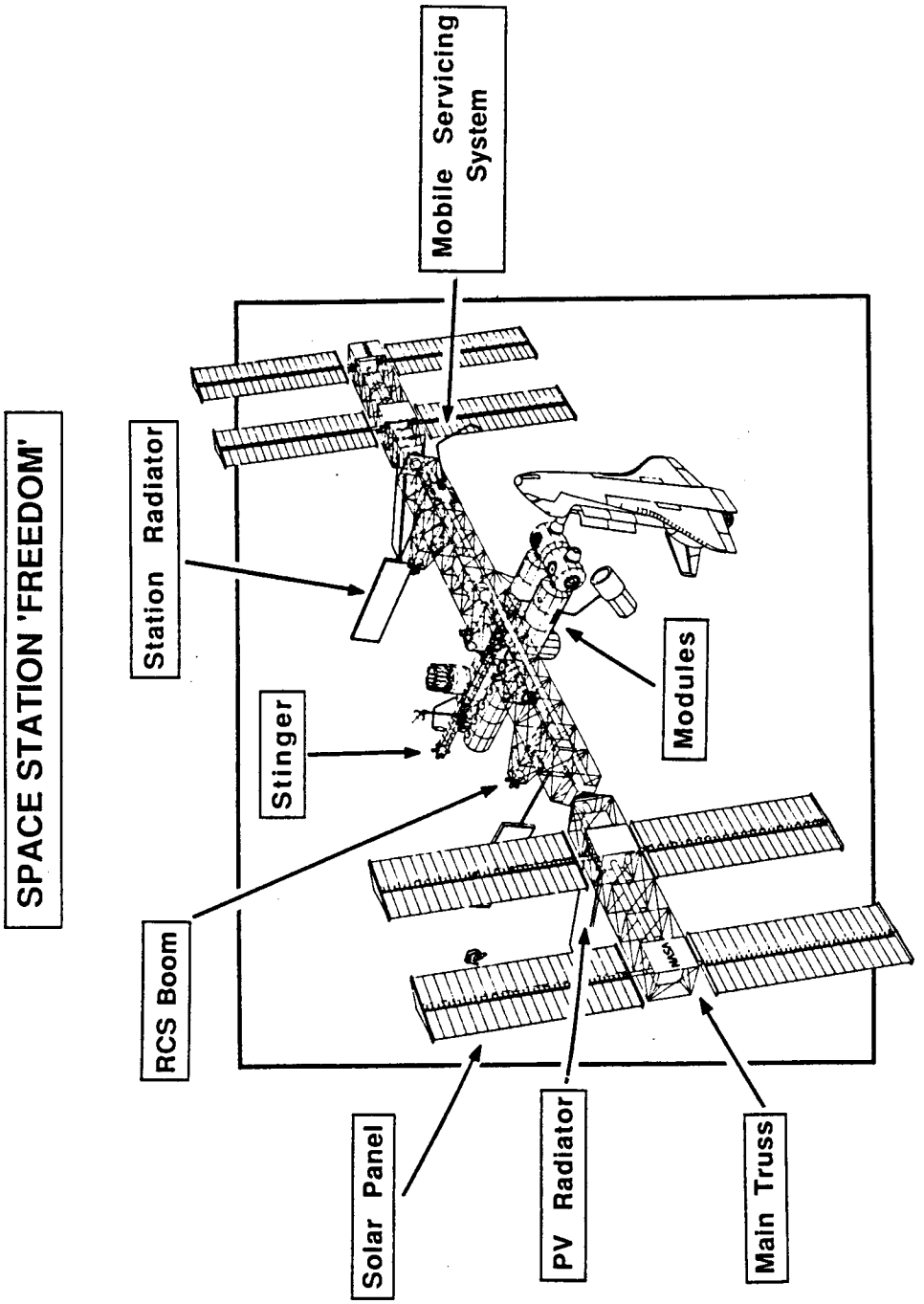

Figure 1-1 The proposed Space Station *Freedom* configuration as of 1988. It has undergone several revisions and is in the process of further change.

active dynamics involving the space station and the MSS is challenging as it involves relative slewing and translational motion of the flexible manipulator on a highly flexible platform. Both the structural elasticity and joint compliance may adversely affect its performance in following a desired trajectory as well as assuring precise orientation of the payload.

The study of an orbiting two-link deployable manipulator with elastic and dissipative joints, operating on a highly flexible space station and carrying an arbitrary shaped payload represents a challenge that has never been encountered before. This class of problems is particular to space-based systems and seldom, if ever, encountered by robots operating on the ground. They normally tend to be rigid and operate from fixed, rigid supporting platforms.

1.2 A Brief Survey of the Relevant Literature

The literature review focuses on the topics that are considered relevant to the study in hand as follows:

- robotics in general, with emphasis on deployable manipulators;
- dynamics of flexible structures in space;
- control of space station based flexible manipulators.

1.2.1 Robotics

A ground based robot is a general purpose, computer controlled, manipulator consisting of several rigid links connected in series by revolute or prismatic joints. Each link is connected, at the most, to two others; and a closed chain is usually avoided. The joints normally have only one degree of freedom. A revolute joint permits rotation about an axis, while a prismatic joint allows sliding along an axis

with no rotation. The manipulator is attached to a fixed, rigid base; while its end is free and equipped with a grip to manipulate objects, or to perform assembly tasks. In general, motion of the joints leads to link motion resulting in to spatial scanning by the grip.

Unlike the ground based manipulators which are thoroughly described in the textbooks by Paul [1] and Fu [2], space manipulators tend to be flexible and often operate from a mobile base as discussed by Chan [3]. Recently, in order to meet the demands of higher speed and efficiency, the new generation of fast robots have been developed with lightweight, low inertia arms which are usually flexible [4]. In general, flexibility arises from two sources: elasticity of the structure and compliance of the motor and the transmission unit at the joint. The structural and joint flexibilities of the manipulator can cause end-effector oscillations, thus limiting its ability to perform a given task with a desired degree of accuracy.

Dynamic analysis of a flexible robot is complicated by coupling between the nonlinear rigid body motion and elastic displacements of the deformed structure [5]. Derivation of the coupled, nonlinear governing equations of motion is enormously time consuming, and efforts have been made to simplify the process. Book [6] developed a recursive Lagrangian approach to generate full nonlinear dynamics of multilink flexible manipulators using homogeneous transformation matrices. Centinkunt et al. [7] have proposed the use of symbolic manipulation programs to overcome algebraic complexities, and thus facilitate the formulation.

1.2.2 Flexible structures in space

With the advent of large space structures, flexibility has become increasingly important, and accurate modelling of the elastic behavior is fundamental to the dynam-

ics and control studies, as discussed by Nurre [8]. The problem is further accentuated by the demanding performance requirements associated with these systems.

A comprehensive literature review on the dynamics of flexible satellites was given by Modi [9]. In treating flexibility, the continuous system is described in terms of discrete and distributed coordinates. The resultant governing equations of motion are transformed into a set of ordinary differential equations, using assumed mode methods with time dependent generalized coordinates [10-12].

Dynamic simulation codes have been developed for multibody systems consisting of rigid and flexible components. However, these programs have certain limitations as pointed out by Singh et al. [13]. Kane et al. [14] have investigated dynamics of a moving elastic cantilever beam, and observed conventional methods to predict erroneous divergence under extreme conditions.

Of particular interest is the class of spacecraft with deployment of flexible appendages from the central body. This class of systems involve transient inertia dynamics, similar to that experienced by the space station during the MSS maneuvers. Reddy et al. [15], and Bainum and Kumar [16] have provided considerable insight into the behavior of complex large space system, by modelling basic structural elements such as flexible beams and plates in orbit.

Systems with deployable appendages have been analyzed, with varying levels of simplifying assumptions, by Lang and Honeycutt [17], Cloutier [18], Hughes [19], Sellpan, Bainum [20] and others. These investigators have treated flexible members as point masses or rigid bodies. A general formulation for studying librational dynamics of a spacecraft, with a rigid central body, deploying an arbitrary number of flexible appendages was presented by Modi and Ibrahim [21]. The formulation also accounted for a shift in the centre of mass.

Slewing appendages impose transient inertias in the study of system dynamics. Hablani [22] derived equations of motion for a chain of hinge-connected bodies in the gravitational field. Conway [23] included dissipative elastic joints in the system which was subjected to arbitrary external forces. Both the studies considered only rigid bodies and are based on the Newton-Euler formulation procedure.

The *Canadarm* on the space shuttle represents a flexible manipulator system capable of relatively fast and large slewing maneuvers. The associated literature [24-30] would be of some value in understanding the dynamics of a large scale manipulator, although it is smaller than the MSS and fixed w.r.t. the space shuttle, which is assumed to be rigid unlike the Space Station.

Meirovitch and Quinn [31] derived the equations of motion for a maneuvering flexible spacecraft using a perturbation approach. Longman et al. [32] addressed the problem of slew induced reaction moment on the librational response, and modified the joint angle commmands, through the kinematic equations, to position the end-effector of a rigid remote manipulator at its desired target.

1.2.3 Control of flexible manipulators

With the high precision positioning critical to the success of certain missions, the problem of maneuvering a flexible spacecraft while suppressing the induced vibrations and the attitude librations is becoming increasingly important. Hale et al. [33] have discussed simultaneous optimization of structural and control parameters for maneuvering flexible spacecraft.

Nonlinear feedback control was explored by Carrington [34], while Yuan [35] has studied the robust beam-pointing and attitude control of a flexible spacecraft. The research related to the control of flexible orbiting structures intensified with two ex-

periments proposed by NASA: Spacecraft COntrol Laboratory Experiment (SCOLE) and COntrol of Flexible Spacecraft (COFS). Recently these have been replaced by Control Structure Interaction (CSI) studies, however, the scope of the project remains essentially the same.

Control of flexible robots, considering the elasticity at the joints, has been investigated by many researchers [36-41]. Garcia [36] presents a formulation for modelling a single-link flexible beam. It undergoes slew motion with an actively controlled pinned end while the other end of the beam is kept free. Position and velocity sensors provided input for proportional feedback control about the slew axis. The motor characteristics, gear ratio and the position feedback determined the equivalent torsional spring constant (servo-stiffness). The investigation concluded that, for moderate or low values of the ratio of the servo stiffness to beam flexibility, it is necessary to consider effects of the servo-drives on the dynamics of the flexible beam.

In studying control of flexible space station based manipulators, Modi et al. [42] considered a mobile, two link manipulator with flexible joints. The inverse control technique was used to achieve high tracking accuracy of the end effector in the presence of maneuvers induced as well as other external and internal disturbances. Two different schemes based on the Quasi-Closed Loop Control (QCLC) and Quasi-Open Loop Control (QOLC) were developed. Though quite effective, authors suggested more attention be given towards the robustness issue.

This brief literature survey provides a synopsis of the research activities in the field of robotics in space, with particular application to the proposed MSS. The main conclusion from the survey is that more accurate mathematical models and simulation procedures are needed to successfully perform prescribed robotic tasks in space.

1.3 Scope of the Proposed Study

1.3.1 Introductory comments

All the present and proposed space based manipulators are of revolute type, usually consisting of two slewing arms on a rotating and translating base, with an end-effector attached to the tip of the second link, similar to the MSS, as shown in Figure 1-2.

To carry out a typical task, such as following a desired trajectory, is a challenge even for a rigid, fixed, ground-based manipulator. In its utmost generality, a space-based MSS presents a rather formidable problem in mechanics. Dynamics and control of a flexible Space Station, supporting a flexible mobile manipulator, represents a class of problems never encountered before. Both the structural elasticity and joint compliance may adversly affect the performance in following a desired trajectory as well as the positioning and orientation of the payload.

Because of the complex nature of the space based revolute manipulator, it has been impossible to present a closed form solution, even for a simplified model, which may help gain insight into the intricate dynamics involved. To overcome some of the problems encountered with revolute type manipulators, a two arm Mobile Deployable Manipulator (MDM) system is proposed here for space application, as schematically shown in Figure 1-3. It appears to have several inherent advantages which may be classified as: software related benefits; and hardware simplification.

Software Related Advantages

- The kinematics and the inverse kinematics are less complicated in the deployable type manipulator.

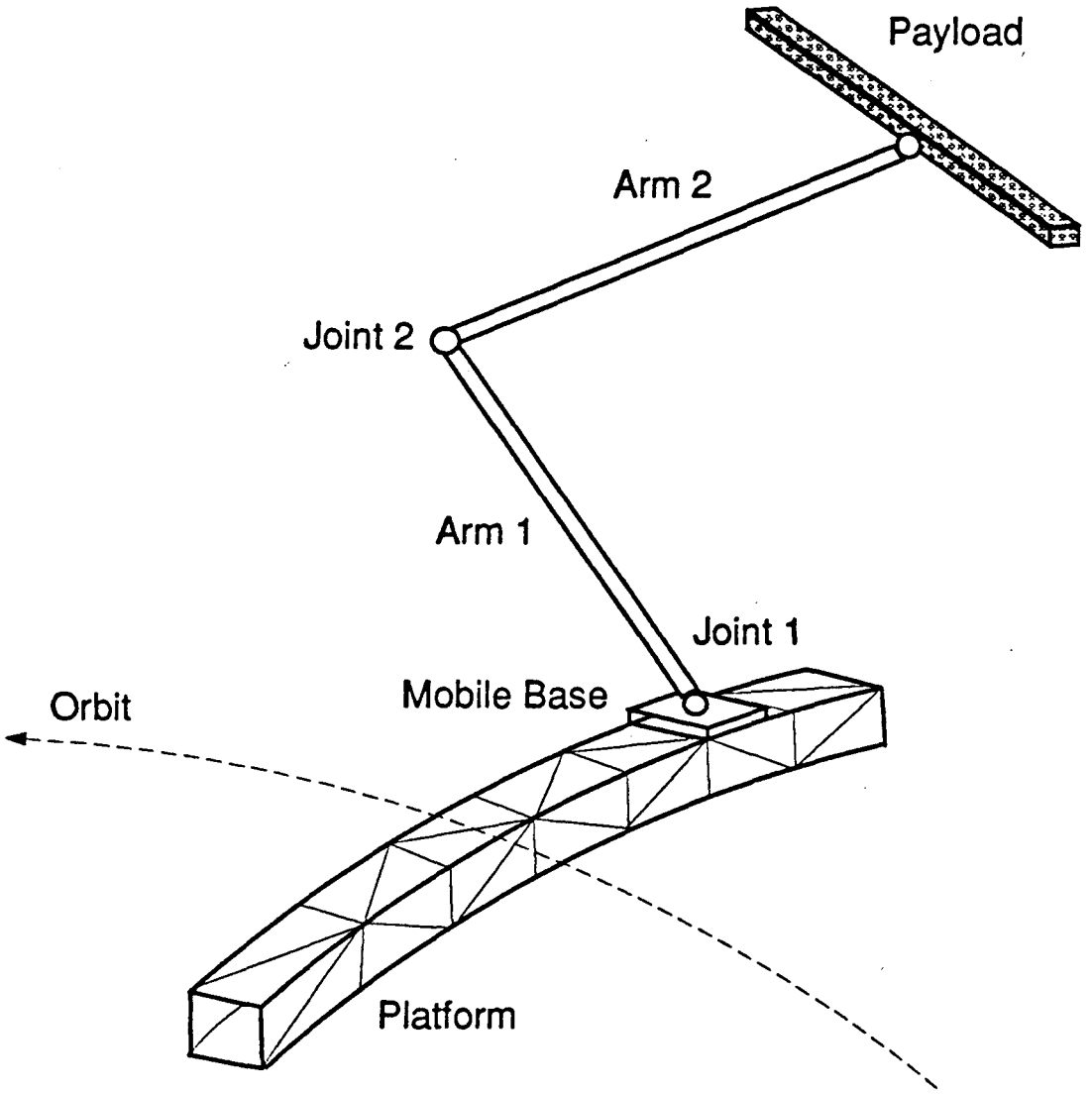

Figure 1-2 A schematic diagram of the Space Station based Mobile Servicing System (MSS).

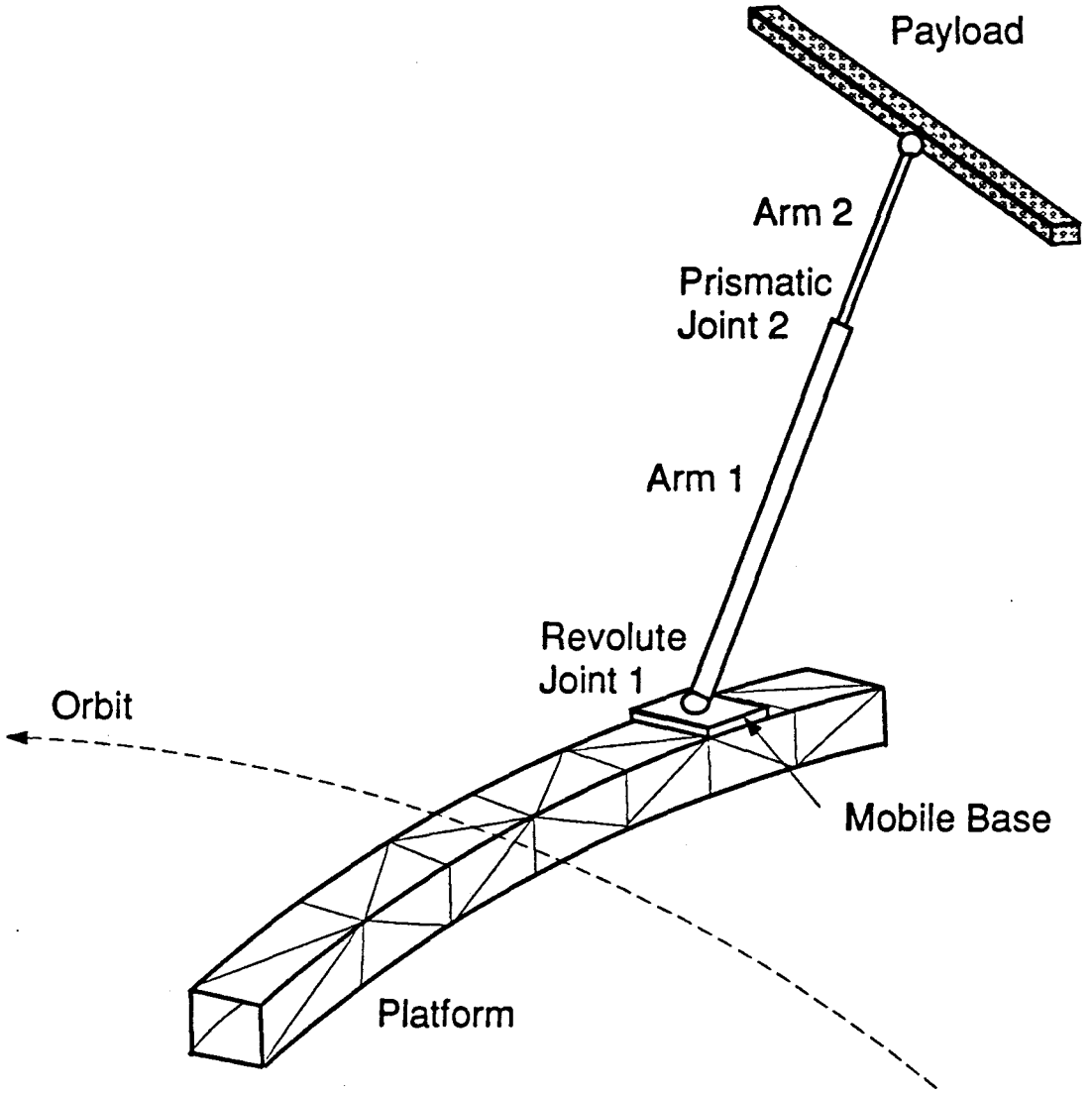

Figure 1-3 A schematic diagram of the proposed Space Station based Mobile Deployable Manipulator (MDM).

- A unique solution exists for each of the degrees of freedom which define the desired position and orientation of the payload. In revolute type manipulators, there is usually more than one possibility to attain a desired position, thus requiring a decision based optimization algorithm.
- In the system dynamics, there is no inertia coupling between the links of the deployable manipulator. This results in simpler equations of motion demanding relatively less effort in their derivation and, of course, integration.

These advantages lead to a significant decrease in the computational effort and time. Now one can obtain real time output even with a relatively small computer, thus improving the possibility of an online controller.

Hardware Advantages

- In the deployable manipulator, the actuators (including the prismatic joint) are located as one unit at the manipulator's base, thus limiting the inertia of the slewing arm only to that needed for construction and stiffness. In the revolute type manipulator, the torque motor for the second link is located at the tip of the first link thus increasing the inertia. As a result a larger torque motor is required at the base.
- In the deployable manipulator there are no singular positions, as in the revolute type when the links are 180^o apart. To compensate for the singular or close to singular position, a larger torque motor is needed.

A possible disadvantage of the MDM is the limited work space. However, this can be compensated quite readily by a moving base.

1.3.2 Present investigation

The research project aims at studying dynamics and control of a typical Space Station based MDM system as described in the following block diagram:

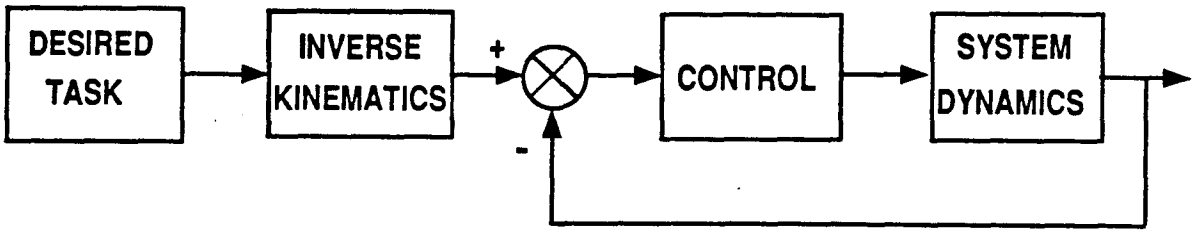

The emphasis throughout is on the development of a simulation tool, applicable to a large class of space based MDM, leading to appreciation of the system performance in the presence of structural flexibility and disturbances.

In Chapter 2 a comprehensive general formulation for studying the dynamics of this class of systems is discussed. The discretization of elastic deflections using the assumed mode method is described and the governing equations of motion obtained using the Lagrangian procedure.

The formulation is applicable to a flexible space based deployable manipulator in any desired orbit. It allows for slewing and deployment of an arbitrary payload, as well as base translation along the flexible platform, accounting for the transient system inertia and shift in the center of mass. The nonlinear, nonautonomous and coupled equations of motion are not amenable to any closed-form solution.

Chapter 3 discusses development of the numerical code for integration of the equations of motion. The emphasis is on a time efficient simulation. Validity of the formulation and the computer code is first established by checking conservation of the

system's total energy, and through comparison with results for particular configurations. A closed-form solution for a simplified case, using the variation of parameters method, not only provides better appreciation of the system behaviour but also helps in checking the numerical code. The chapter ends with a study of coupling effects between the flexible platform and the manipulator maneuvers.

In Chapter 4, the inverse kinematic approach is developed. The objective is to express the required MDM degrees of freedom in terms of the desired position and orientation of the end effector w.r.t. the chosen reference frame. To meet the requirements of both the desired position and orientation, a coordinated moving base strategy, which takes into account the local deflection and slope of the platform, is suggested.

The ultimate objective is to achieve minimum tracking error in the presence of space station maneuvers and vibrations. Conversely, to maintain position and attitude pointing within an acceptable limit, in presence of the manipulator's slewing and deployment maneuvers. With this in mind, Chapter 5 proposes a nonlinear control strategy based on the Feedback Linearization Technique (FLT), where the unknown desired values are obtained by real time numerical differentiation. To eliminate the need for real time numerical differentiation, a control approach based on variable stiffness at the joints is suggested.

The concluding chapter summarizes more important results and presents recommendations for future studies.

2. FORMULATION OF THE PROBLEM

This chapter presents the development of a relatively general formulation particularly suitable for studying dynamics and control of flexible space based deployable type manipulators.

2.1 System Modelling

A space platform based two link deployable manipulator is considered in this study. The slewing upper arm (first link), and the deployable lower arm (second link) carrying the payload, are activated through a system of motors and gears. Note, both the arms go through the same slewing maneuver, however the deployment is confined to arm 2 assembly. The manipulator is permitted to translate along the platform, orbiting around the earth.

The space platform supporting the manipulator is taken to be in an arbitrary orbit around the earth. The platform is considered to be a flexible beam type structure, and the momentum wheel(s) aboard provide the necessary control torque $\bar{T}_0$ about its principal axis. The system libration, platform vibration, as well as the manipulator's maneuvers are confined to the orbital plane.

The slewing arm is attached via a flexible and dissipative gear system, with ratio n_3, to the joint 1 torque-motor-rotor I_3, as schematicaly shown in Figure 2-1. It undergoes slewing maneuvers β_4 w.r.t. the manipulator base. The revolute joint flexibility is modelled as a torsional spring with an equivalent stiffness k_3.

The second arm assembly is deployed by an amount a_5 w.r.t. arm 1. It is connected via a flexible and dissipative linear gear assembly, with ratio n_5 and equivalent radius r_5, to a torque motor attached to the slewing arm, as shown in Figure 2-1. The prismatic joint's flexibility is modelled by a torsional spring with an equivalent

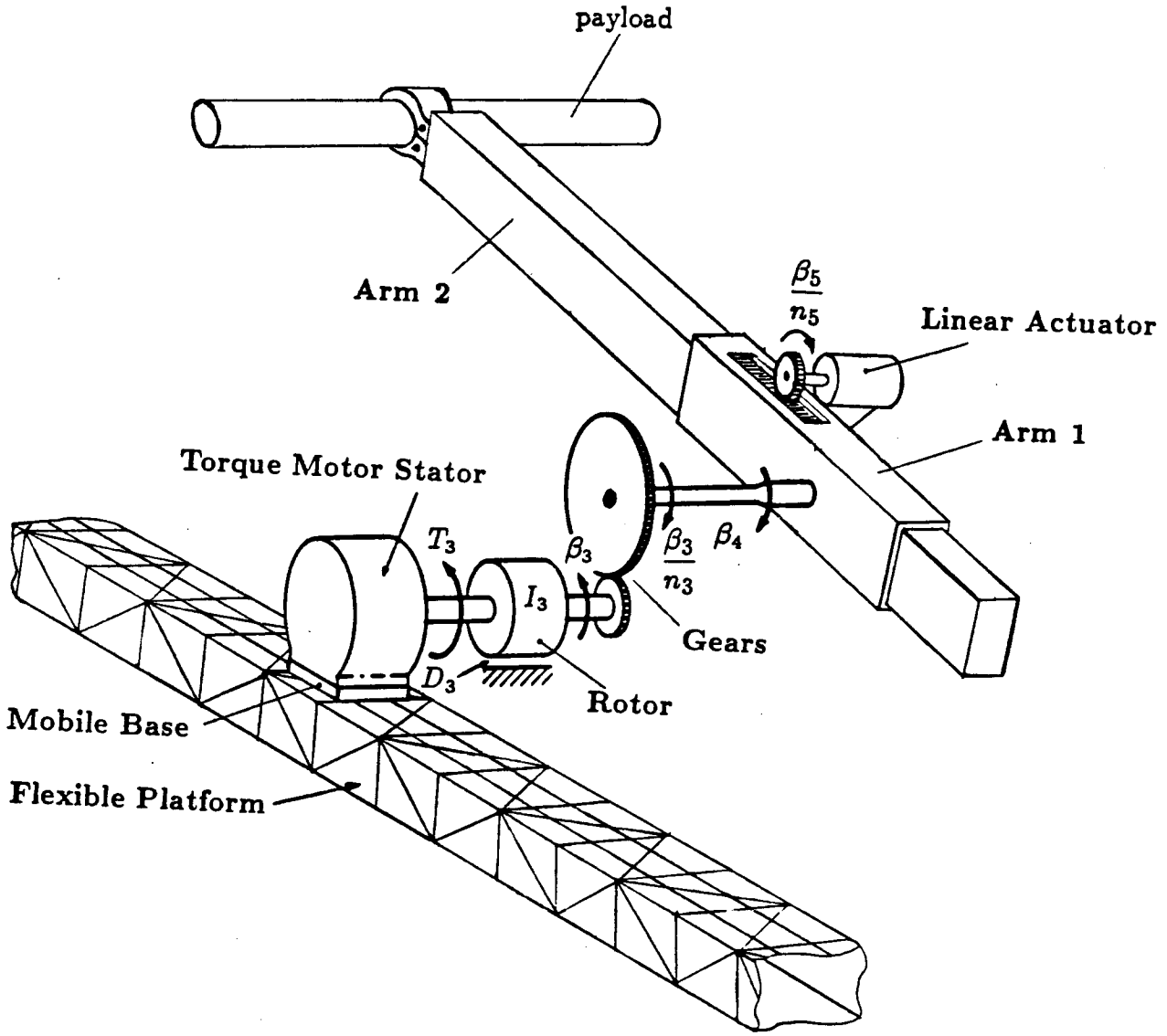

Figure 2-1 A schematic diagram showing exploded view of the motor-gear assemblies driving the arms.

stiffness of k_5. The ratio of the joint flexibility to that of the arm is considered high, i.e. the arms are taken to be rigid in this study. The end effector, with the arbitrarily shaped payload, forms an integral parts of arm 2, and is also treated as rigid.

2.2 Modal Discretization

The flexible platform is considered as a free-free Euler-Bernoulli beam with length $2l_1$ and square cross-section of dimension d_1. The platform's flexural deformation δ_1 is discretized using the admissible functions $\bar{\phi}_1(x_1)$ satisfying geometric and natural boundary conditions, in conjunction with generalized time dependent coordinates $\bar{q}_1(t)$ associated with δ_1. This procedure approximates elastic deformations by a series of spatial functions,

$$\delta_1(x,t) = \bar{\phi}_1^T(x_1)\bar{q}_1(t), \tag{2.1}$$

where $\delta_1(x,t)$ is the transverse deformation w.r.t. the platform body fixed reference frame F_1 located at the c.m. of the undeformed platform, as shown in Figure 2-2. Here x_1 is the coordinate along the longitudinal axis of the platform.

The mode shapes are obtained by applying the separation of variables method to solve the beam partial differential equation

$$\frac{\partial^2 \delta_1}{\partial t^2} + \frac{EJ}{m_p}\frac{\partial^4 \delta_1}{\partial x_1^4} = 0, \tag{2.2}$$

where:

EJ flexural rigidity of the platform;

m_p mass per unit length of the platform.

Considering the mass and inertia of the MDM to be small compared to that of the platform [12], and taking into account only the lower natural frequencies (low acceleration levels), it is possible to neglect the effect of the manipulator's inertia on

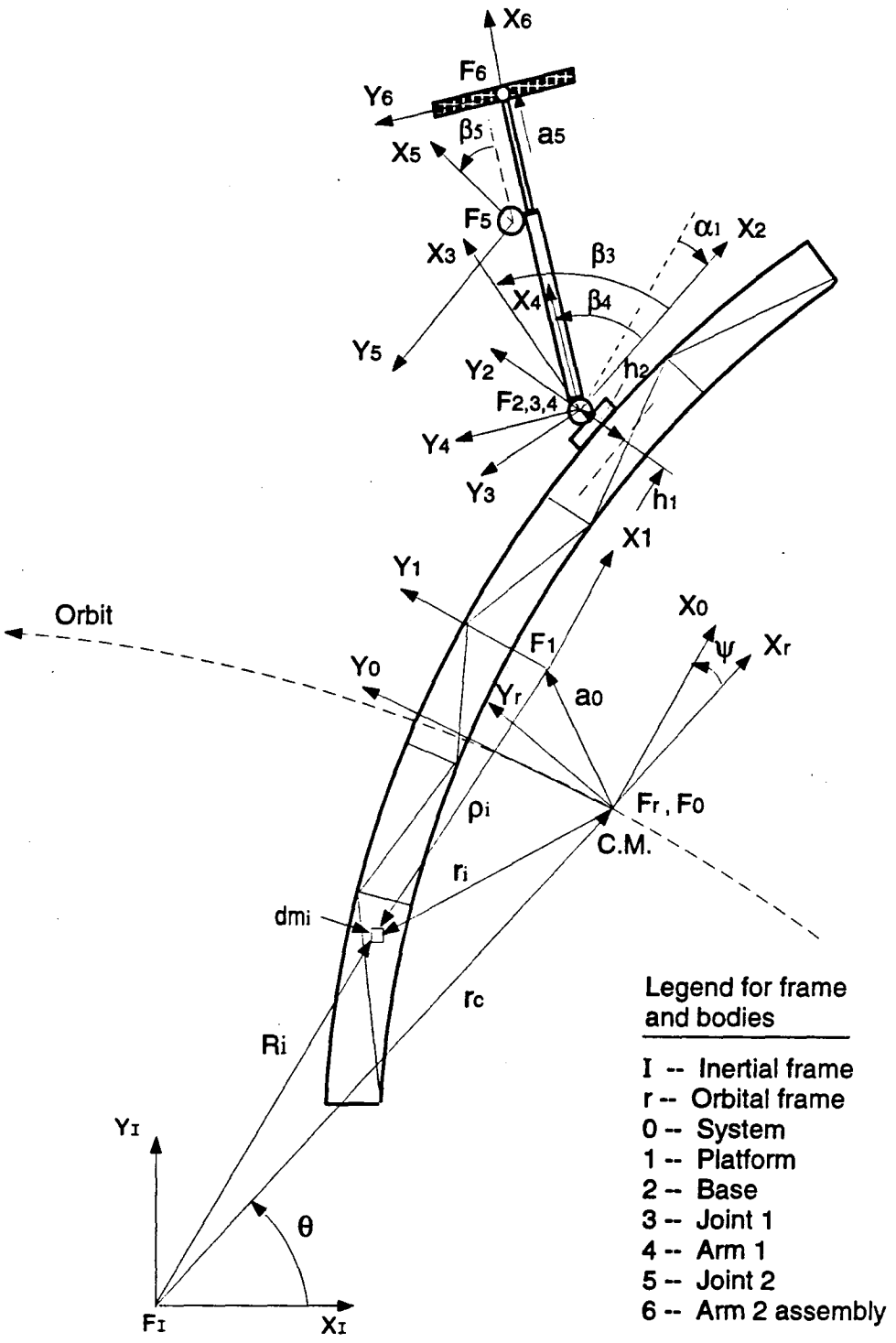

Figure 2-2 Reference frames and position vectors for the MDM system. The frames are designated as F_i (i=r,0,1,...,6).

the boundary conditions.

Introduction of the appropriate boundary conditions, i.e. zero moment and shear at the ends of the platform:

$$EJ\frac{\partial^2\delta_1(x,t)}{\partial x_1^2} = 0|_{x_1=\pm l_1}; \qquad EJ\frac{\partial^3\delta_1(x,t)}{\partial x_1^3} = 0|_{x_1=\pm l_1}; \tag{2.3}$$

yield a trancendental equation for the spatial frequency parameter 'p',

$$cos(2p_i l_1)cosh(2p_i l_1) = 1, \tag{2.4}$$

with the modes given by [46]

$$\bar{\phi}_1(x_1) = coshp_i(x_1+l_1)+cosp_i(x_1+l_1)-\sigma_i[sinhp_i(x_1+l_1)+sinp_i(x_1+l_1)]. \tag{2.5}$$

Here:

$$p_i^4 = \frac{m_p\omega_i^2}{EJ};$$

$$\sigma_i = \frac{cosh(2p_i l_1)-cos(2p_i l_1)}{sinh(2p_i l_1)-sin(2p_i l_1)};$$

where:

$2l_1$ length of the platform;

ω_i platform natural frequency associated with the i^{th} mode.

The various modes and the modal integrals are given in Appendix I.

The orientation of the MDM base w.r.t the platform, at any location h_1 from the center of the platform, is determined by the local slope,

$$tan\alpha_1 = \frac{\partial\delta_1(h_1,t)}{\partial x_1}. \tag{2.6}$$

2.3 Kinematics

Knowledge of the system kinematics is the first necessary requirement to formulate the system equations of motion.

2.3.1 Reference frames

The reference frames are carefully chosen in order to establish the state of the system at any given instant. This is necessary to undertake the kinetic study.

Consider the space platform and the MDM model as shown in Figure 2-2. The instantaneous center of mass of the system, C.M., negotiates an arbitrary orbit about the center of force coinciding with the earth's center, where the inertial reference frame F_I is located. As the system has finite dimension, i.e. it has mass as well as inertia, it is free to undergo librational (pitch) motion about its c.m. This can be defined as the rotation ψ of the system frame F_0 w.r.t. the orbital frame F_r. Here X_0, Y_0 are aligned with the principal moments of inertia directions for the entire system in its reference equilibrium configuration.

For the orbital frame, X_r coincides with the local vertical, Y_r is aligned with the local horizontal, and Z_r is along the orbit normal in accordance with the right hand rule. At any instant, the position of F_r is determined by the orbital elements ϵ, r_c and θ. Here ϵ is the eccentricity of the orbit; r_c, the distance from the center of force to F_0 (C.M.); and θ, the true anomaly of the orbit. As the dimensions of the system are negligible compared to the orbital altitude, the effect of librational, slewing and translational motions on the orbit is expected to be negligible [47,48], therefore the orbit can be represented by the classical keplerian relation,

$$r_c = \frac{h^2}{GM(1 + \epsilon cos\theta)} \quad , \tag{2.7}$$

where:

h the angular momentum per unit mass of the system about F_I, $r_c^2\dot{\theta}$;

ϵ orbit eccentricity;

θ true anomaly;

r_c radius of the orbit;

GM earth's gravitational constant.

Attached to each member of the system (platform, base, joint 1, arm 1, joint 2, arm 2 assembly) is a body coordinate system helpful in defining relative motion between the memebers. Thus F_1 is the platform body fixed reference frame located at the c.m. of the platform and taken to be parallel to the frame F_0. Here X_0 coincides with X_1, the longitudinal axis of the platform.

For the undeformed platform with the MDM, in absence of deployment (a_5=0), located at the geometric center of the platform (h_1=0), the system C.M. coincides with the platform c.m. In general there is a shift between this two centers of mass due to the MDM maneuvers.

The position and orientation of the base frame F_2 w.r.t. the platform frame F_1 is determined by the translation h_1, the platform transverse deflection $\delta_1(h_1, t)$, and the local slope α_1, as shown in Figure 2-2.

At joint 1, the rotor body fixed frame F_3 rotates by an angle β_3 about Z_2. The orientation of the slewing arm body fixed reference frame F_4 w.r.t. the base is β_4, where X_4 is pointed in the direction of the prismatic joint 2. Joint 2 rotor fixed reference frame F_5 is rotated through angle β_5 w.r.t. X_4, about Z_4. The end effector body fixed reference frame F_6 is parallel to F_4 and translates through a_5 along X_4. The centers of mass of the payload, end effector and arm 2 assembly coincide with the origin of F_6.

2.3.2 Position vectors and transformations

The system and orbital frames were defined with their origins at the system C.M. while the local body fixed reference frames were attached to the members constituting the MDM system.

The position vector $\bar{R}_i$ to the mass element dm_i in the i^{th} body, w.r.t. the inertial frame, can be expressed as (Figure 2-2)

$$\bar{R}_i = \bar{r}_c + \bar{r}_i, \tag{2.8}$$

where:

$\bar{r}_c$ position vector of the system frame F_0 in the inertial reference F_I;

$\bar{r}_i$ position vector to a mass element in the i^{th} body w.r.t. the system frame F_0.

Expanding $\bar{r}_i$ in terms of the body fixed reference frame,

$$\bar{r}_i = \bar{a}_0 + \sum_{j=1}^{i-1} \prod^{i-1} [c_j]\bar{a}_j + \prod_{j=1}^{i} [c_j]\bar{\rho}_i \qquad i = 1, ...n, \tag{2.9}$$

where:

$[c_j]$ rotation transformation matrices from the j^{th} frame to the $(j-1)^{th}$ frame;

$\bar{a}_j$ position vector locating the $(j+1)^{th}$ body fixed frame w.r.t. the j^{th} frame;

$\bar{\rho}_i$ position vector for the mass element dm_i w.r.t. the i^{th} body frame F_i;

n number of bodies in the system.

The transformation matrix for the planar case has the form

$$[c_i] = \begin{bmatrix} cos\,\psi_i & -sin\,\psi_i & 0 \\ sin\,\psi_i & cos\,\psi_i & 0 \\ 0 & 0 & 1 \end{bmatrix}, \tag{2.10}$$

where $\bar{\psi}_i$ is the rotation angle of the body fixed frame F_i w.r.t. the $F_{(i-1)}$) frame.

When dealing with a flexible body, angle ψ_i can be expressed as the sum of rigid and flexible body rotations,

$$\bar{\psi}_i = \bar{\alpha}_{i-1} + \bar{\beta}_i, \tag{2.11}$$

where:

$\bar{\alpha}_{i-1}$ rotation due to bending of the flexible body $(i-1)$;

$\bar{\beta}_i$ rigid body rotation.

The position vector which locates a mass element in the flexible beam is obtained by superposing $\bar{x}_i$ (the undeformed position) and $\bar{\delta}_i$ (the transverse deformation), neglecting the fortshortening effect,

$$\bar{\rho}_i = \bar{x}_i + \bar{\delta}_i, \tag{2.12}$$

where:

$$\bar{\delta}_i = \bar{\phi}_i^T(x)\bar{q}_i(t), \tag{2.13}$$

and the $\bar{\phi}_i(x)$ vector contains the modes of the i^{th} body (Appendix I).

The term $\bar{a}_0$ in Eq. (2.9) represents shift in the system c.m., caused by the flexibility of the platform coupled with the MDM's translational and slewing maneuvers,

$$\bar{a}_0 = -\frac{1}{m}\left[\sum^{i}(\sum_{j=i+1}^{n} m_j)(\prod_{j=1}^{i} c_j)\bar{a}_i + \sum^{i}(\prod_{j=1}^{i} c_j)\int_{m_i}\bar{\rho}_i dm_i\right], \qquad i = 1, ...n, \tag{2.14}$$

where:

m_i mass of the i^{th} body;

m total mass of the system.

Note, $\int_{m_i}\bar{\rho}_i dm_i = 0$ when the body fixed reference frame is located at the c.m. of the body.

2.4 Kinetics

Application of the Lagrangian procedure to formulate the governing equations of motion requires evaluation of the total kinetic and potential energies of the system.

2.4.1 The kinetic energy

The kinetic energy accounts for the contributions from five major components of the system: the platform; the slewing arm 1; the deployable arm 2, end effector and payload assembly; and the two torque motors at the joints:

$$T = \sum_i \frac{1}{2} \int_{m_i} \dot{\bar{R}}_i \cdot \dot{\bar{R}}_i dm_i + T_{j3} + T_{j5} \qquad i = 1, 4, 6. \tag{2.15}$$

Here T_{j3} and T_{j5} are the kinetic energies associated with the motors at joints 1 and joint 2, respectively; and $\dot{\bar{R}}_i$ is the inertial velocity of the mass element dm_i, obtained by differentiating Eqs. (2.7) and (2.9) with respect to time,

$$\dot{\bar{R}}_i = \dot{\bar{r}}_c + \bar{\Omega} \times \bar{r}_i + \frac{d\bar{r}_i}{dt}. \tag{2.16}$$

The orbital velocity of the system, $\dot{\bar{r}}_c$, is given by

$$\dot{\bar{r}}_c = \dot{r}_c \hat{i}_r + \dot{\theta} r_c \hat{j}_r, \tag{2.17}$$

and the angular velocity $\bar{\Omega}$, of the system frame F_0 due to the orbital velocity $\dot{\theta}$ and the librational rate $\dot{\psi}$ as

$$\bar{\Omega} = (\dot{\psi} + \dot{\theta}) \hat{k}_0. \tag{2.18}$$

Substituting for $\dot{\bar{R}}_i$ from Eq. (2.16), the expression for the kinetic energy can be written in the form

$$T = \frac{1}{2}\int_m (\dot{\bar{r}}_c \cdot \dot{\bar{r}}_c)dm + \frac{1}{2}\int_m (\bar{\Omega} \times \bar{r}_i) \cdot (\bar{\Omega} \times \bar{r}_i)dm + \frac{1}{2}\int_m (\dot{\bar{r}}_i \cdot \dot{\bar{r}}_i)dm$$

$$+ \int_m \dot{\bar{r}}_c \cdot (\bar{\Omega} \times \bar{r}_i)dm + \int_m (\dot{\bar{r}}_c \cdot \dot{\bar{r}}_i)dm + \int_m \dot{\bar{r}}_i \cdot (\bar{\Omega} \times \bar{r}_i)dm + T_{j3} + T_{j5}. \quad (2.19)$$

This is the general expression of the kinetic energy. By looking at each term separately, physical appreciation can be gained and some simplifications may be introduced. Note, definition of the c.m. requires $\int_m \bar{r}_i dm = 0$. Hence the terms: $\int_m \dot{\bar{r}}_c \cdot (\bar{\Omega} \times \bar{r}_i)dm$ and $\int_m (\dot{\bar{r}}_c \cdot \dot{\bar{r}}_i)dm$ vanish. The kinetic energy contributions can readily be identified with the orbital (T_O) and librational (T_L) motions; rotations with respect to the body frames (T_S); angular momentum with librational coupling (T_H); and angular velocities with respect to the body fixed reference frames (T_{j3}, T_{j5}). Thus the kinetic energy expression can be written in the form

$$T = T_O + T_L + T_S + T_H + T_{j3} + T_{j5}. \quad (2.20)$$

The kinetic energy contributions from the various sources can be expressed as follows:

$$T_O = \frac{1}{2} m \dot{\bar{r}}_c^T \cdot \dot{\bar{r}}_c; \quad (2.21)$$

$$T_L = \frac{1}{2} \bar{\Omega}^T [I] \bar{\Omega}; \quad (2.22)$$

$$T_S = \sum_{i=1}^{3} \frac{1}{2} \int_{m_i} (\dot{\bar{r}}_i^T \cdot \dot{\bar{r}}_i)dm_i; \quad (2.23)$$

$$T_H = \bar{\Omega} \cdot \sum_{i=1}^{3} \int_{m_i} (\bar{r}_i \times \dot{\bar{r}}_i)dm_i; \quad (2.24)$$

$$T_j 3 = \frac{1}{2} I_3 (\dot{\psi} + \dot{\theta} + \dot{\alpha}_1 + \dot{\beta}_3)^2; \quad (2.25)$$

$$T_j 5 = \frac{1}{2} I_5 (\dot{\psi} + \dot{\theta} + \dot{\alpha}_1 + \dot{\beta}_4 + \dot{\beta}_5)^2. \quad (2.26)$$

where:

$[I]$ matrix of instantaneous total moment of inertia about the system frame F_0 (Appendix II);

I_3 joint 1 motor rotor inertia;

I_5 joint 2 linear actuator rotor inertia;

$\dot{\alpha}$ angular velocity of the MDM base due to platform deflection;

$\dot{\beta}_3$ angular velocity of joint 1 torque-motor-rotor w.r.t. the base F_2;

$\dot{\beta}_5$ angular velocity of joint 2 linear-actuator-rotor w.r.t. the slewing arm.

$\dot{\alpha}_1$ can be expressed as the rate of change of the local slope in the flexible platform,

$$\dot{\alpha}_1 = \frac{d}{dt}\{\frac{\partial}{\partial x_1}[\bar{\phi}_1^T(h_1)\bar{q}_1(t)]\}. \tag{2.27}$$

The system inertia diadic [I] w.r.t. the system frame can be obtained from the relation

$$[I] = \sum_{i=1}^{n} \int_{m_i} [(\bar{r}_i^T \cdot \bar{r}_i)[U] - (\bar{r}_i \cdot \bar{r}_i^T)]dm_i, \tag{2.28}$$

where [U] is the unit matrix. Details of the inertia matrix are presented in Appendix II.

2.4.2 The potential energy

The potential energy contribution arises from two sources: position in the inverse gravitational field; and the strain energy.

The librational response is dominated by the gravitational potential energy U_g, while the vibrations are primarily dependent on the elastic or strain energy, stored in the flexible platform and the joints,

$$U = U_g + U_e. \tag{2.29}$$

The strain energy contributions come from three members,

$$U_e = U_1 + U_3 + U_5,$$

where:

U_1 the strain energy stored in the deflected platform;

U_3, U_5 the strain energies stored in the twisted joints 1 and 2, respectively.

Gravitational Potential Energy

The system potential energy in the gravitational field is given by

$$dU_g = -GM\frac{1}{R_i}dm. \tag{2.30}$$

Substitute R_i from Eq. (2.8) into Eq. (2.30), expanding according to the Binomial power series, and ignoring terms of order $1/r_c^4$ and higher, the expression for the potential energy can be rewritten as [49]

$$U_g = -\frac{GMm}{r_c} - \frac{GM}{2r_c^3}\{trace[I] - 3\bar{l}_{r_c}^T[I]\bar{l}_{r_c}\}, \tag{2.31}$$

where $\bar{l}_{r_c}$ is the direction cosine vector of $\bar{r}_c$ w.r.t. the system frame,

$$\bar{l}_{r_c}^T = [cos\psi \quad -sin\psi \quad 0]. \tag{2.32}$$

The first term in Eq. (2.31) represents the potential energy due to attraction between two bodies represented as point masses. In the present study this term will be eliminated, as no generalized coordinate is associated with it. The second term corresponds to the contribution due to 3-D character of the body, i.e. the inertia effect. The third term is the contribution due to the librational motion (microgravity term).

Elastic Potential Energy

The platform contribution to the strain energy comes mainly from bending deformation and can be expressed as

$$U_1 = (EJ)\int_0^{l_1}\left[\frac{d^2\bar{\phi}^T}{dx_1{}^2}\right]^2 dx_1\bar{q}_1^2(t). \tag{2.33}$$

The strain energy due to flexibility of the joints (primarily contributed by torsional deformations of the transmission shafts) can be expressed as:

$$U_3 = \frac{1}{2}k_3(\beta_4 - \frac{\beta_3}{n_3})^2; \tag{2.34}$$

$$U_5 = \frac{1}{2}k_5(\frac{a_5}{r_5} - \frac{\beta_5}{n_5})^2; \tag{2.35}$$

where:

k_3, k_5 equivalent torsional stiffnesses of joints 1 and 2, respectively;

n_3, n_5 gear ratios at joints 1 and 2, respectively;

r_5 effective linear actuator radius;

β_3 joint 1 torque motor rotation w.r.t. the MDM base;

β_4 slew angle of arm 1 w.r.t. the MDM base;

β_5 prismatic joint 2 torque motor rotation w.r.t. the slewing arms;

a_5 translation of the deployable arm w.r.t. the frame F_4.

2.5 Equations of Motion

The earlier multibody derivations were based on the Newton-Euler approach, which involves physically visualizable quantities represented by vectors. Usually less time and effort are required to arrive at a compact and explicit form of the governing equations of motion. This also makes the Newton-Euler method computationally

more attractive. However, the method is useful only when dealing with relatively simple configurations. For complex flexible mechanical systems with shifting center of mass, the Eulerian approach has limitations. On the other hand, the Lagrangian procedure automatically satisfies holonomics constraints, and nonholonomic conditions through the Lagrange multipliers. This is in sharp contrast to the Newton-Euler method which requires introduction and subsequent elimination of the constraint forces. Obviously, it would be almost impossible to achieve this in the present study due to the complex character of the system. Furthermore, Silver [50] has shown that with a proper choice of generalized coordinates, the Lagrangian formulation can be, numerically, as efficient as the Newton-Euler approach. However, the Lagrangian procedure involves considerable amount of algebra. This is especially true in the case of multibody systems where the position vectors are presented as a product of matrix and vector, and first as well as second derivatives are required.

The governing equations of motion can be obtained from

$$\frac{d}{dt}(\frac{\partial T}{\partial \dot{\bar{q}}}) - \frac{\partial T}{\partial \bar{q}} + \frac{\partial U}{\partial \bar{q}} = \overline{Q}, \tag{2.36}$$

where T and U are the kinetic and potential energies of the system, respectively; $\bar{q}$, the generalized coordinates; and $\overline{Q}$, the associated generalized forces.

The generalized coordinates and the corresponding generalized forces for the MDM system are as follows:

ψ system libration angle w.r.t. the orbital frame;

$\bar{q}_1$ generalized coordinate vector associated with platform deformation;

β_3 joint 1 motor rotation w.r.t. the MDM base frame F_2;

β_4 slew angle of arm 1 w.r.t. the MDM base frame F_2;

β_5 prismatic joint 2 motor rotation w.r.t. the slewing arms;

a_5 translation of the deployable arm w.r.t. the frame F_4;

T_0 resultant control torque acting on the platform due to momentum wheels;

T_3 electro-magnetic control torque at joint 1;

T_5 electro-magnetic control torque at joint 2 (the linear actuator torque motor);

D_0 system damping in the pitch d.o.f.;

D_1 platform damping in the vibrational d.o.f.;

D_3 damping at joint 1;

D_5 damping at joint 2;

D_4 slewing arm damping torque;

D_6 deployable arm damping force.

The total number of the generalized coordinates is $5 + nom$, where nom is the number of the modes chosen to represent the deflection of the flexible platform.

Note, the translation h_1 of the mobile base is treated as a specified coordinate, governed by the desired payload orientation, as discussed in Chapter 4. However, if required, it can easily be treated as a generalized coordinate resulting in one additional equation.

The resultant governing equations of motion can be rewritten in a compact form as

$$[M(q,t)]\ddot{\bar{q}} + \overline{N}(q,\dot{q},t) = \overline{Q}, \tag{2.37}$$

where:

[M(q,t)] non-singular symmetric mass matrix (Appendix III);

$\bar{q}$ generalized coordinates vector with elements: ψ, $\bar{q}_1$, β_3, β_4, β_5, a_5;

$\overline{N}$ nonlinear force/torque vector (Appendix III);

$\overline{Q}$ generalized force vector, evaluated using the virtual work principle.

The contributions to the generalized force vector are from the control torques and the non-conservative damping forces/torques:

$\overline{T}$ control torque vector with elements T_0, $\bar{\phi}_1'(\mathrm{x})T_0$, 0, T_3, 0, T_5, 0;

$\overline{D}$ nonconservative generalized damping vector with elements D_0,D_1,D_3,D_4,D_5,D_6.

Here, $\bar{\phi}_1'(x)$ is the value of the first derivative w.r.t. x_1 of the mode shapes at the locations of the momentum wheels.

The equations of motion are explicitly derived in a compact form in order to identify the inertia terms associated with the mass matrix and the nonlinear gyroscopic, Coriolis, centripetal and gravity related contributions. This helps in identifying incompatible terms in the formulation, if any. Of course, as can be expected, the governing equations of motion are highly nonlinear, nonautonomous, and coupled. An analytical closed-form solution is not possible unless substantial simplifications are introduced. Therfore, one is forced to resort to a numerical approach. However, search for an analytical solution is also attempted using the variation of parameter method for a particular case [43].

The validity of the governing equations of motion will have to be established through checks with similar mathematical formulations documented in the literature. Obviously, the same model has not been reported in the literature, and hence can not be compared. However, some special cases may be available for comparison. The conservation of system energy and momentum are also important avenues to follow.

As pointed out before, the equations of motion are solved numerically, after checking the integration code against a benchmark case to ensure its validity.

3. OPEN LOOP STUDY

The objective of this chapter is to study the dynamic response of the system. To that end, parametric studies with an increasing order of system complexity have been carried out. This provides better physical understanding of the system behaviour, helps establish relative significance of the various system parameters, and suggests critical combinations of parametric values which may lead to an unacceptable response.

As mentioned before, the nonlinear, nonautonomous and coupled equations of motion are not amenable to any closed-form solution and hence must be solved numerically. A FORTRAN computer code has been written in a modular form to help isolate effects of the system variables.

3.1 Numerical Approach

In order to solve the equations of motion numerically, they have to be rearanged into a set of first order ordinary differential equations. Consider Eq. (2.37), a set of $N = 5 + nom$ second order differential equations,

$$\{\ddot{\bar{q}}\} = \overline{F}(q, \dot{q}, t). \tag{3.1}$$

Here

$$\overline{F}(q, \dot{q}, t) = [M(q,t)]^{-1}\{\overline{Q}(t) - \overline{N}(q, \dot{q}, t)\}.$$

Rewriting Eq. (3.1) in the state space form gives $2N$ first order differential equations to be numerically integrated:

$$\bar{y} = \{\begin{matrix}\bar{q} \\ \dot{\bar{q}}\end{matrix}\};$$

$$\dot{\bar{y}} = \{\begin{matrix}\dot{\bar{q}} \\ \overline{F}(q, \dot{q}, t)\end{matrix}\}. \tag{3.2}$$

The subroutine IMSL (International Mathematical and Statistical Library): DGEAR was chosen for the integration procedure. The advantages of this subroutine include: automatic adjustment of the iteration step-size; two built-in integration approaches available to the user: the implicit ADAMS method and the backward differentiation procedure, also refered to as GEAR's stiff method.

The prime consideration is the stiffness of the problem, i.e. situations involving vastly different time constants. For the space station based MDM, the orbital period is about 100 minutes, while the structural vibration period can be less than 5 s.

For the reasons of efficiency and speed, the ADAMS method is used with non-stiff systems, whereas the GEAR method handles stiff configurations. For each step, the DGEAR subroutine checks for the possibility that the step-size is too large to pass the error test based on the specified tolerance. The integration step-size specified by the user (10^{-8}–10^{-12} in this study) is employed only as a starting value, and it is adjusted automatically by the subroutine.

In order to understand the program architecture, a brief background to the numerical integration methodology may be useful. Let $\bar{y}_n$ be the solution of Eq. (3.2) at the n^{th} integration interval (τ), such that $t = n\tau$. Use of the multivalue method to obtain $\bar{y}_n$ may lead to better accuracy but the execution speed is reduced. The multi-value method consists of three stages: prediction, error-test and correction as shown in the open-loop simulation flowchart of Figure 3-1.

Given $\bar{y}_{n-1}$,.....,$\bar{y}_{n-k}$, the prediction of $\bar{y}_n$, denoted by $\bar{y}_{n,0}$, is obtained by a linear interpolation. A negative result of the error-test prompts the corrector to determine a refined value $\bar{y}_{n,1}$. The error-test and the correction procedure are repeated m times until $\bar{y}_{n,m}$ satisfies the tolerance $\bar{y}_n$=$\bar{y}_{n,m}$. The error TOlerance Level (TOL) in the range of 10^{-8} to 10^{-12} used here is governed by the system under study.

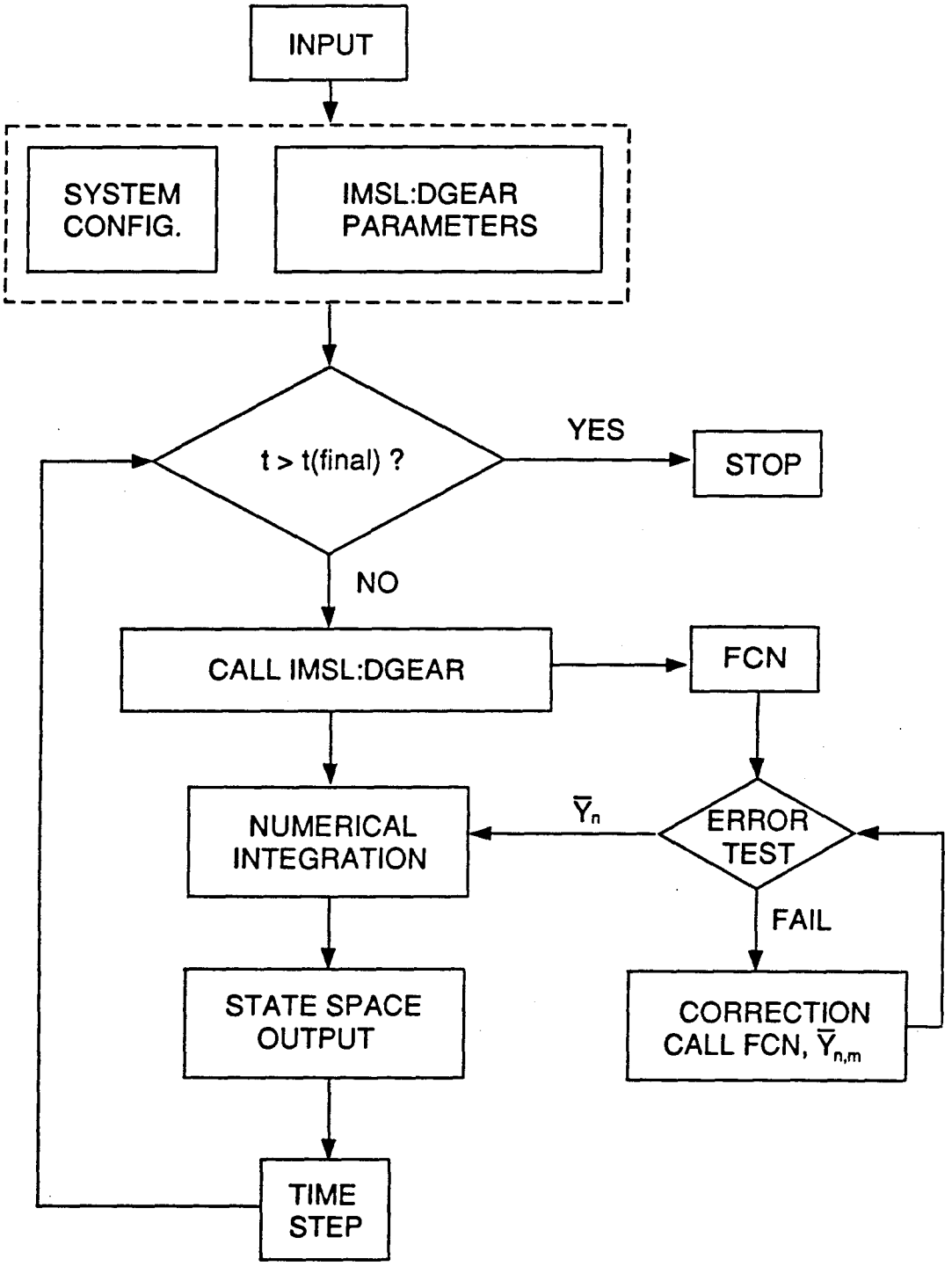

Figure 3-1 The MDM dynamic simulation flowchart.

Consider the flowchart showing computational steps for the MDM system dynamics simulation (Figure 3-1). The INPUT DATA block supplies the initial conditions, the MDM system properties (dimensions, mass, inertia, stiffness, damping, gear ratio), orbital elements and the open-loop input torques to the MAIN block where the system configuration is determined and the modal integrals of the flexible platform calculated. The numerical integration IMSL:DGEAR routine calls the FCN subroutine to assess dynamics of the system (governing equations of motion). The actual state of the system is obtained from the OUTPUT block.

3.2 Formulation and Program Verification

In modelling a complex multibody, flexible system such as the space based MDM, an obvious question concerning validity of the formulation and the computer code arises. Assessment of their accuracy presents a challenging task. In absence of a formulation for the same system, obtained independently by an other investigator and reported in the open literature, three possible avenues are available:

(i) continuouse monitoring of the system total energy to assure its conservation;

(ii) comparison with the reported particular cases obtainable from the present "general" formulation;

(iii) comparison between the numerical simulation and analytical closed-form solution results for a simplified configuration.

3.2.1 Total energy conservation

The total energy for a conservative system is constant,

$$E = T + U = constant. \tag{3.3}$$

Substituting T from Eqs. (2.21–2.26), and U from Eqs. (2.31-2.35) into Eq. (3.3),

the general expression for the system total energy is obtained as

$$E = \frac{1}{2}m\dot{\bar{r}}_c^T \cdot \dot{\bar{r}}_c + \frac{1}{2}\bar{\Omega}[I]\bar{\Omega} + \sum_{i=1}^{3}\frac{1}{2}\int_{m_i}(\dot{\bar{r}}_i^T\dot{\bar{r}}_i)dm_i + \bar{\Omega}\cdot\sum_{i=1}^{3}\int_{m_i}(\bar{r}_i \times \dot{\bar{r}}_i)dm_i$$

$$+\frac{1}{2}I_3(\dot{\psi}+\dot{\theta}+\dot{\alpha}_1+\dot{\beta}_3)^2 + \frac{1}{2}I_5(\dot{\psi}+\dot{\theta}+\dot{\alpha}_1+\dot{\beta}_4+\dot{\beta}_5)^2$$

$$-\frac{GMm}{r_c} - \frac{GM}{2r_c^3}\{trace[I] - 3\bar{l}_{r_c}^T[I]\bar{l}_{r_c}\}$$

$$+(EJ)\int_0^{l_1}\left[\frac{d^2\bar{\phi}^T}{dx_1{}^2}\right]^2 dx_1\bar{q}_1^2(t) + \frac{1}{2}k_3(\beta_4 - \frac{\beta_3}{n_3})^2 + \frac{1}{2}k_5(\frac{a_5}{r_5} - \frac{\beta_5}{n_5})^2. \qquad (3.4)$$

To facilitate the computational procedure, the total energy was monitored for the case of a system with a rigid platform in a circular orbit, neglecting the shift in the C.M. The potential and the kinetic energy terms can be presented for the simplified case as follows:

$$U = -\frac{GMm}{r_c} - \frac{GM}{2r_c^3}\{trace[I] - 3\bar{l}_{r_c}^T[I]\bar{l}_{r_c}\} + \frac{1}{2}k_3(\beta_4 - \frac{\beta_3}{n_3})^2 + \frac{1}{2}k_5(\frac{a_5}{r_5} - \frac{\beta_5}{n_5})^2; \quad (3.5)$$

$$T = \frac{1}{2}m\frac{GM}{r_c} + \frac{1}{2}\bar{\Omega}[I]\bar{\Omega} + \frac{1}{2}I_3(\dot{\psi}+\dot{\theta}+\dot{\alpha}_1+\dot{\beta}_3)^2 + \frac{1}{2}I_5(\dot{\psi}+\dot{\theta}+\dot{\alpha}_1+\dot{\beta}_4+\dot{\beta}_5)^2$$

$$+\frac{m_4}{2}\{\dot{\bar{a}}_1^T\dot{\bar{a}}_1 + \dot{\bar{a}}_1^T[\dot{c}_2]l_4 + \dot{\beta}_4^2\frac{l_4^2}{3}\} + \frac{m_3}{2}\{(\dot{\bar{a}}_1 + [\dot{c}_2]\bar{a}_5 + [c_2]\dot{\bar{a}}_5)^T(\dot{\bar{a}}_1 + \dot{c}_2\bar{a}_2 + c_2\dot{\bar{a}}_2)\} + \frac{\dot{\beta}_4^2}{2}I_{6z}$$

$$+\Omega\{m_4[\dot{\beta}_4\frac{l_4^2}{3} + \dot{\beta}_4 h_1\frac{l_4}{2}c\beta_4 - \dot{h}_1\frac{l_4}{2}s\beta_4] + m_3[(h_1 + a_5c\beta_4)(\dot{\beta}_4 a_5 c\beta_4 + \dot{a}_5 s\beta_4) -$$

$$a_5 s\beta_4(\dot{h}_1 - \dot{\beta}_4 a_5 s\beta_4 + \dot{a}_5 c\beta_4)] + \dot{\beta}_4 I_{6z}\}. \qquad (3.6)$$

The system total energy was monitored for the gravity gradient stabilized orientation where the axis of minimum inertia I_{xx} is aligened with the local vertical (in the equilibrium position), while the axis of maximum inertia is aligned with the orbit normal. The orbital energy E_o can be obtained from Eqs. (3.5), (3.6) as follows:

$$T_o = \frac{GMm}{2r_c}; \qquad U_o = \frac{-GMm}{r_c}. \qquad (3.7)$$

For a system of 120,000 kg mass in a circular orbit at 400 km altitude, the orbital energy (E_o) is around $-3.55 \cdot 10^{12}$ J with the potential energy $U_o = -7.1 \cdot 10^{12}$ J, and the kinetic energy contribution $T_o = 3.55 \cdot 10^{12}$ J. The orbital energy due to finite dimensions of the system (moments of inertia) represented by a 120 m long platform is around -180 J. The changes in the potential, kinetic and the total energies during dynamical response to initial disturbances were monitored. Both rigid as well as free joint systems were simulated for several initial conditions.

The independent variable (t) can be expressed in terms of the true anomaly (θ). This transformation is useful in studying spacecraft dynamics. The simulation was performed with respect to the orbital unit of time (orbit). The transformation between the two variables is readily accomplished using the following relations:

$$\frac{d}{dt} = \dot{\theta}\frac{d}{d\theta}; \tag{3.8a}$$

$$\frac{d^2}{dt^2} = \dot{\theta}^2\left(\frac{d^2}{d\theta^2} - \frac{2\epsilon sin\theta}{1 + \epsilon cos\theta \frac{d}{d\theta}}\right). \tag{3.8b}$$

Eq. (3.8) is derived from Eq. (2.7). For a circular orbit, $t = [orbit] \cdot \tau$,

where: $\theta = orbit \cdot 2\pi$; $\quad \tau = \sqrt{\frac{r_c^3}{GM}}$.

Figure 3-2 shows the MDM free joint response and the energy variations for an initial pitch angle of ψ_o=0.1 rad. The initial slew (β_4) and deployment (a_5) were set to zero. The mass of the deployable arm/payload assembly was taken to be 500 kg, with the mass of the 10 m long slew-arm set at 400 kg. The effective radius of the linear gear was r_5=0.1 m and the gear ratios at the two joints were $n_3 = n_5 = 1$.

As can expected, a periodic response was obtained for the librational motion, ψ, as shown in Figure 3-2(a). The maximum energy exchange of 2.8 J between the potential and the kinetic energy is the dominant feature of this response and the system's total

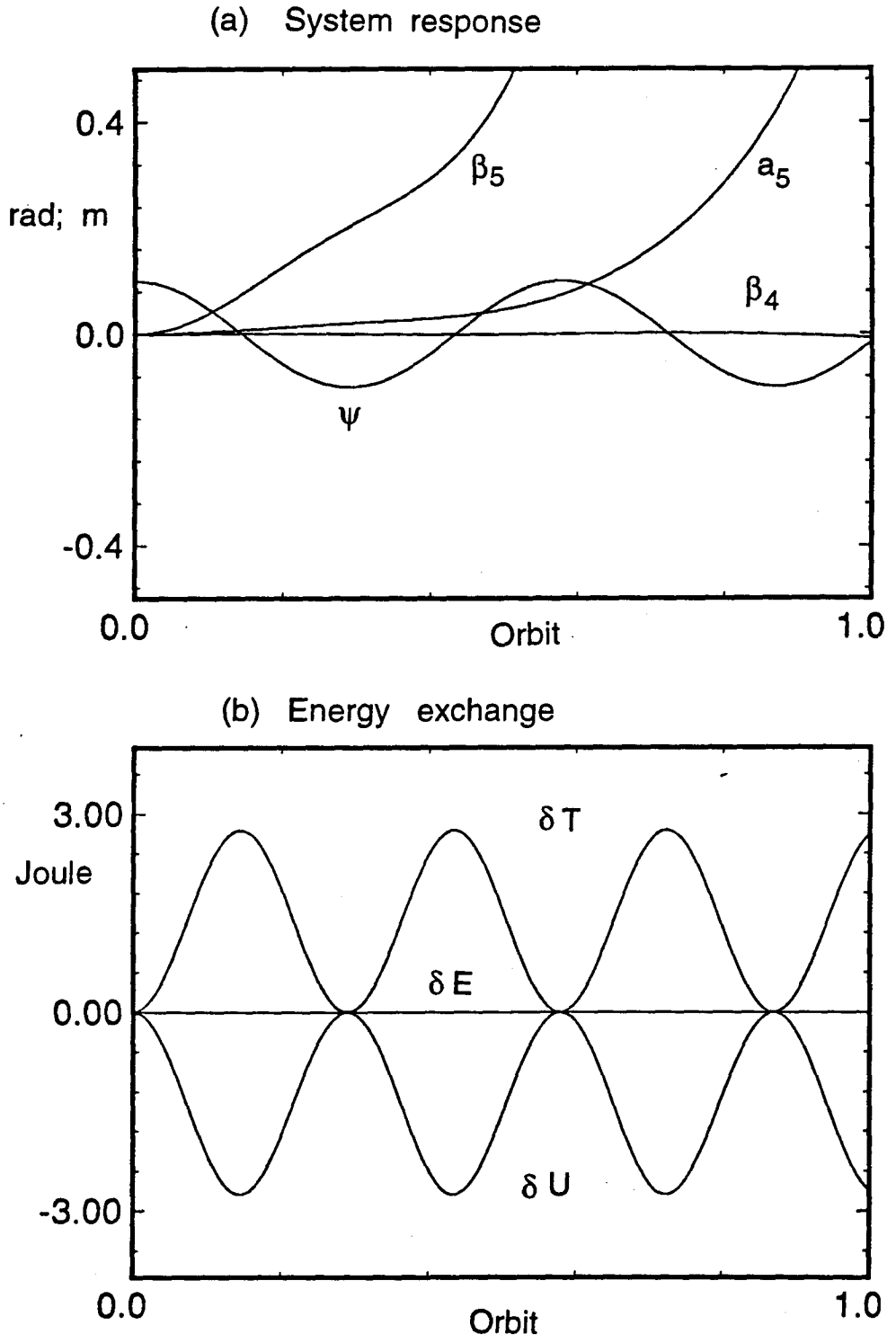

Figure 3-2 The MDM free joint response and energy exchange for a rigid platform subjected to an initial pitch disturbance of ψ=0.1 rad: (a) system response; (b) energy exchange.

energy is conserved, i.e. $\delta E = 0$ (Figure 3-2b). Note, the coupling effect leads to the slew response (β_4), as can be seen after one orbit. The linear actuator rotor (I_5) induces shift of the deployable arm (a_5) from the unstable equilibrium position (near the system c.m.), and causes the payload to deviate from the platform with an increasing acceleration, resulting in further rotation of the motor (β_5), as shown in Figure 3-2(a). The Coriolis effect induced moment, due to the deploying arm coupled with the librational and the orbital motion, affects the slew response β_4.

Figure 3-3 shows the MDM open loop response and energy variation for an initial slew arm position at β_4=0.5 rad. The system parameters are as in the previous case, and the initial conditions for the deployment and the platform pitch are zero. As before, a periodic response of the arm with a peak energy exchange of 0.008 J between the potential and the kinetic energy was obtained for about 0.6 orbit, as shown in Figure 3-3(a). As the departure of the payload (a_5) from the platform becomes significant after 0.6 orbit, a continious increase in the system energy is observed (Figure 3-3b). This is directly related to the shift in the c.m., and its rate, which were purposely neglected (although the formulation account for it), to emphasize their importance. The increase in the energy of the system is due to the contribution of the rate of the center of mass shift to the kinetic energy.

Figure 3-4 shows the MDM response and energy exchange for an initial arm position at $\beta_4 = 1.0$ rad and the payload displaced by 0.01 m (i.e. a_5=0.01 m).

In this case the payload departs from the platform with an increasing acceleration, while affecting the periodic motion of the slew d.o.f. due to the Coriolis reaction, as can be seen in Figure 3-4(a). The maximum energy exchange of 0.024 J between the potential and the kinetic energy is periodic, and is dominated by the slew motion up to around 0.8 orbit (Figure 3-4b). However, the secular increase in the energy follows

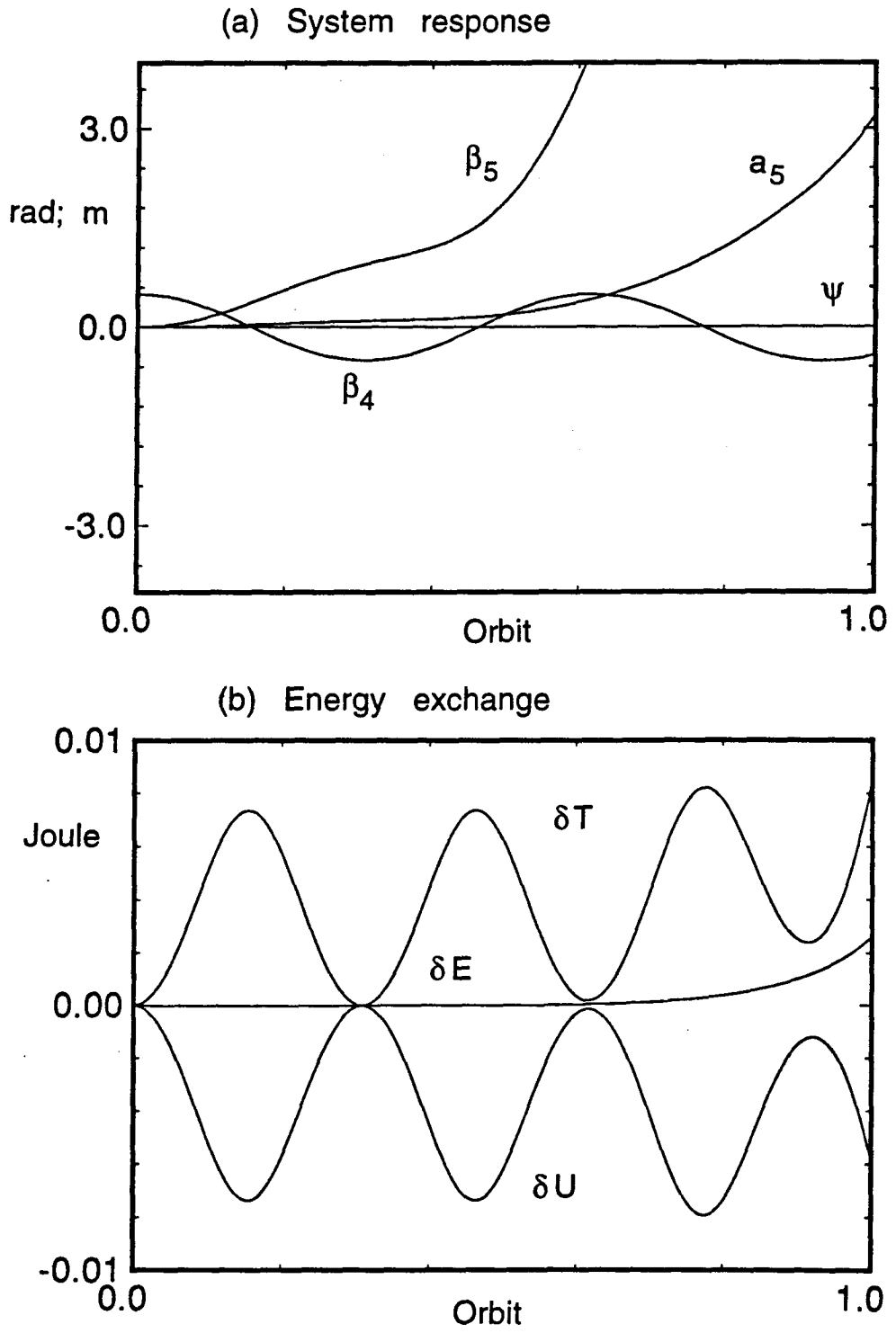

Figure 3-3 The MDM system free joint response and energy exchange for an initial slew angle β_4=0.5 rad: (a) system response; (b) energy exchange.

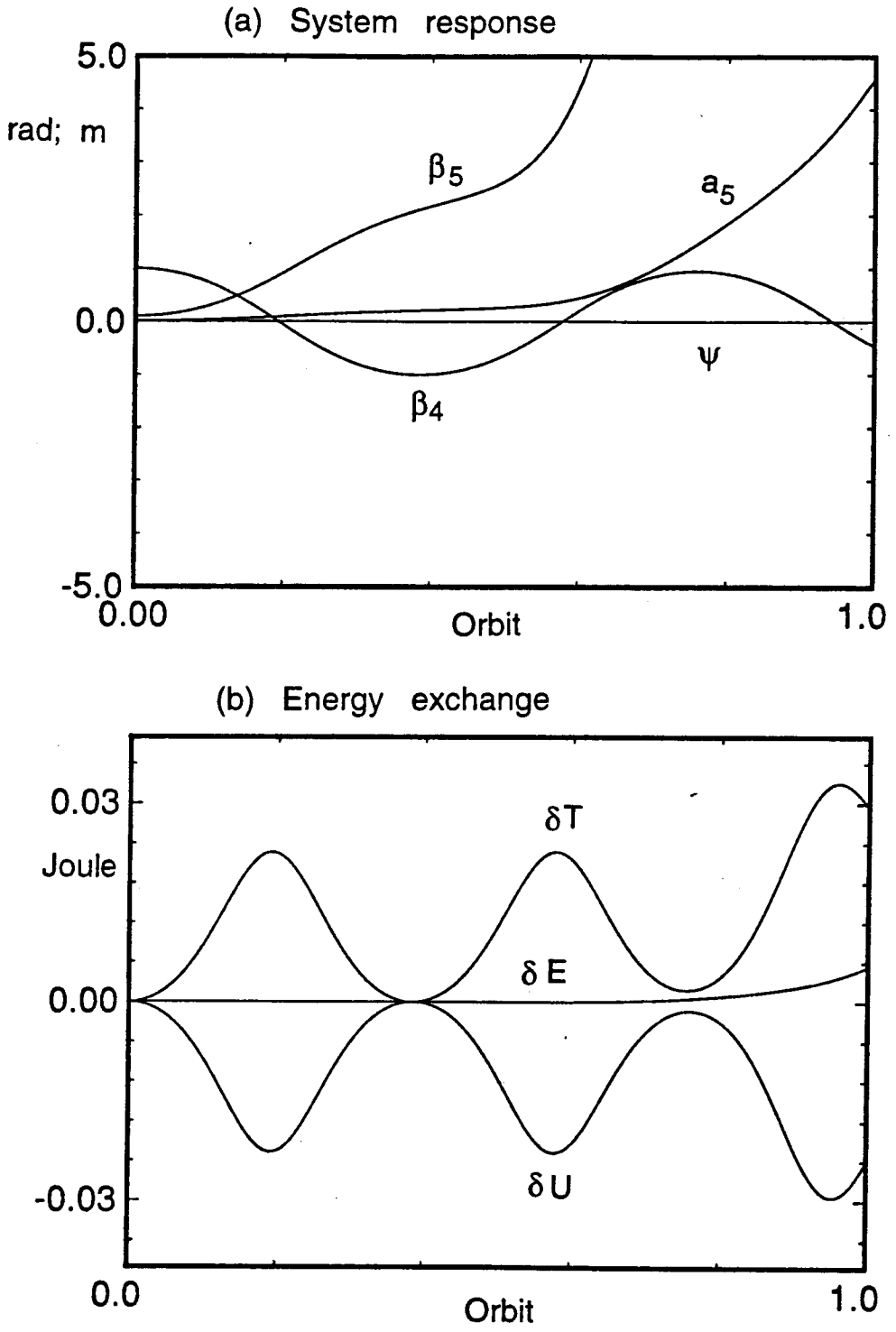

Figure 3-4 Response and energy exchange for the MDM, with free joints, when subjected to a combined initial conditions of β_4=1.0 rad, and a_5=0.01 m: (a) system response; (b) energy exchange.

due to a large and fast shift in the c.m., caused by the payload moving away from the platform, the effect neglected in the simulation as pointed out before.

In the actual practice, this would not lead to any significant inconsistancy even if the c.m. shift is neglected as the system is, generally, actively controlled. The closed-loop response will maintain displacements, accelerations, etc. within the permissible limits and restablish the operational configuration in a short specified time. Of course, as emphasized before, the formulation developed here accounts for a shift in the c.m.

3.2.2 A comparison with a particular case

A simplified system as shown in Figure 3-5 was considered for comparison with a relevant case studied by Pradhan [51]. The platform is assumed to be rigid with the MDM located 30 m from its center (C.M.).

Only one rigid joint for the slew d.o.f. (β_4) is considered here. A 500 kg point mass payload is attached at the tip of a 1000 m massless arm. The deployment d.o.f. a_5 is assumed to be frozen at that value. The configuration is similar to a rigid tethered satellite model (also a degenerated case) investigated by Pradhan. The simulation response results for several different initial conditions were found to be identical for all the generalized coordinates. This provided further confidence in the formulation and the associated computer code.

3.2.3 Closed-form solution

A closed-form solution of the problem if available, can be useful to independently check the validity of the formulation and the numerical simulation. Therefore, an attempt was made to arrive at an analytical solution of a rather simplified model of the system used in the previous Section 3.2.2.

Consider the MDM system with a rigid platform in a circular orbit around the

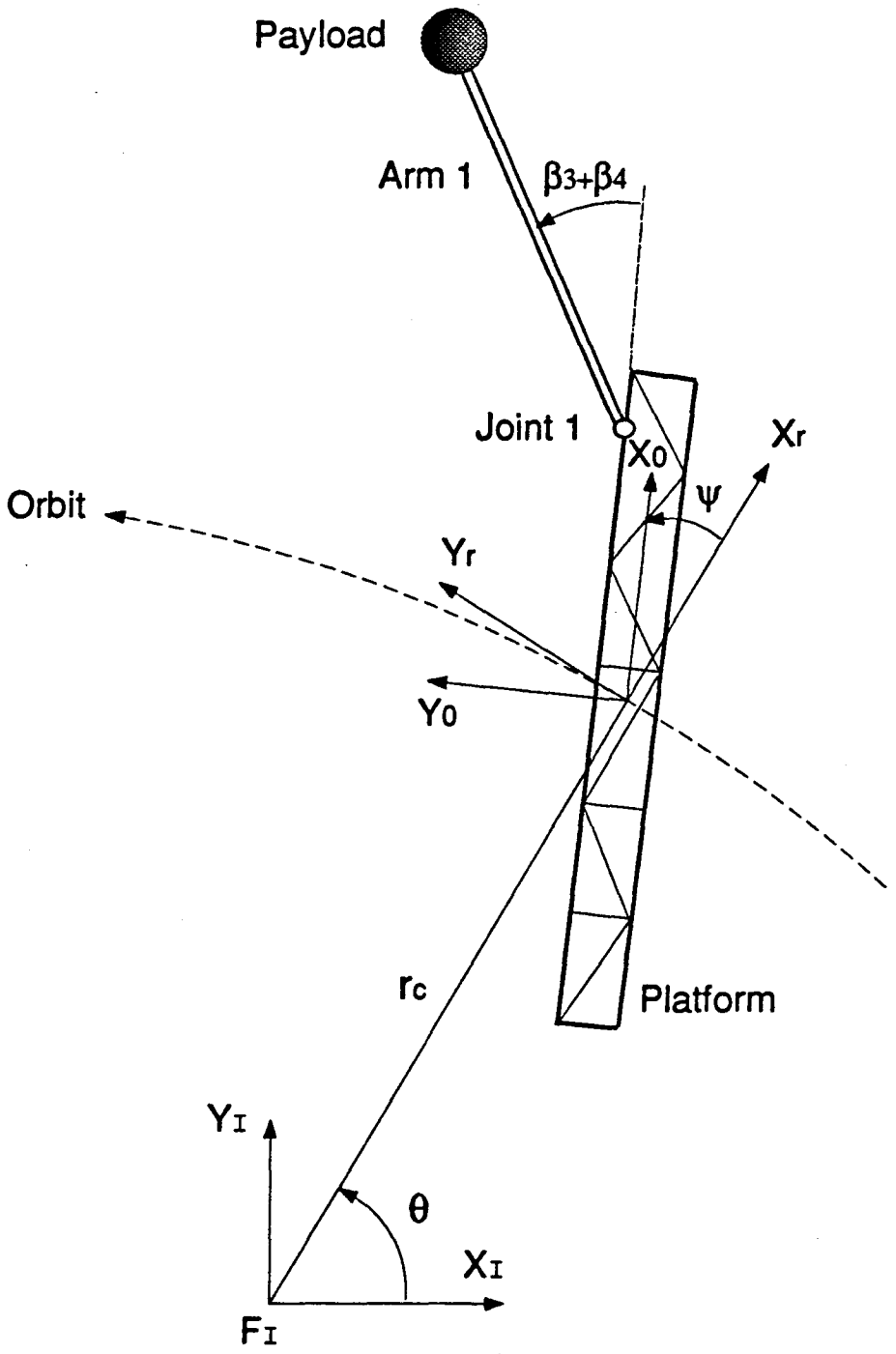

Figure 3-5 Simplified configuration of the MDM system.

earth. It supports a rigid arm carrying a point mass payload as shown in Figure 3-5. The platform and the arm are free to librate and rotate through angles ψ and β_3, respectively in the orbital plane. The model accounts for the joint's torsional flexibility by assuming that the generalized coordinate β_3, associated with the joint's rotor, is fixed in any specified position. Thus the system has two degrees of freedom ψ and β_4. For this particular case the governing equations of motion were obtained independently, and can be presented as follows:

$$
\begin{aligned}
&[m_1(\frac{d_1^2}{16}+\frac{l_1^2}{3})+(m_4+m_6)h_1^2+2(\frac{m_4}{2}+m_6)h_1l_4cos(\beta_3+\beta_4)+(\frac{m_4}{3}+m_6)l_4^2]\ddot{\psi}\\
&+[(\frac{m_4}{2}+m_6)h_1l_4cos(\beta_3+\beta_4)+(\frac{m_4}{3}+m_6)l_4^2]\ddot{\beta}_4\\
&-(\frac{m_4}{2}+m_6)h_1l_4sin(\beta_3+\beta_4)\dot{\beta}_4(2\dot{\psi}+2\dot{\theta}+\dot{\beta}_4)\\
&+3(\frac{m_4}{2}+m_6)h_1l_4sin(2\psi+\beta_3+\beta_4)\dot{\theta}^2+\frac{3}{2}(\frac{m_4}{3}+m_6)l_4^2sin2(\psi+\beta_3+\beta_4)\dot{\theta}^2\\
&+\frac{3}{2}[(m_4+m_6)h_1^2+m_1(\frac{l_1^2}{3}-\frac{d_1^2}{16})]sin2\psi\dot{\theta}^2=-C_0\dot{\psi};
\end{aligned}
\tag{3.9a}
$$

$$
\begin{aligned}
&[(\frac{m_4}{3}+m_6)l_4^2]\ddot{\beta}_4+[(\frac{m_4}{2}+m_6)h_1l_4cos(\beta_3+\beta_4)+(\frac{m_4}{3}+m_6)l_4^2]\ddot{\psi}\\
&+(\frac{m_4}{3}+m_6)h_1l_4sin(\beta_3+\beta_4)(\dot{\psi}+\dot{\theta})^2+\frac{3}{2}(\frac{m_4}{3}+m_6)l_4^2sin2(\psi+\beta_3+\beta_4)\dot{\theta}^2\\
&+(\frac{m_4}{2}+m_6)h_1l_4[sin(2\psi+\beta_3+\beta_4)+cos\psi sin(\psi+\beta_3+\beta_4)]\dot{\theta}^2\\
&+k_3\beta_4=-C_4\dot{\beta}_4.
\end{aligned}
\tag{3.9b}
$$

Here: $\dot{\theta}=\sqrt{\frac{GM}{r_c^3}}$; C_0 and C_4 are the viscous damping coefficients in ψ and β_4 d.o.f., respectively.

To make these highly nonlinear and coupled set of equations of motion amenable to known analytical procedures, it is necessary to introduce, rather judiciously, some simplifications while retaining the significant dynamics of the system. To that end, transcedental terms were expanded in series, and third and higher degree terms neglected. In the present case, the nominal operating point considered is $\beta_3 = 0$, i.e.

the arm is initially aligned with the platform. With this approximation the equations of motion reduce to:

$$\ddot{\psi} + A_1\ddot{\beta}_4 + B_1\beta_4 + n_1^2\psi = \mu_1(\beta_4\dot{\beta}_4) + \mu_3\dot{\psi}; \tag{3.10a}$$

$$\ddot{\beta}_4 + A_2\ddot{\psi} + B_2\psi + n_2^2\beta_4 = \mu_2(\beta_4\dot{\psi}) + \mu_4\dot{\beta}_4; \tag{3.10b}$$

where:

$$A_1 = \frac{B+C}{E}; \qquad B_1 = 3\dot{\theta^2}\frac{B+C}{E}; \qquad n_1^2 = 3\dot{\theta^2}\frac{E-2D}{E};$$

$$A_2 = \frac{B+C}{C}; \qquad B_2 = 3\dot{\theta^2}\frac{B+C}{C}; \qquad n_2^2 = 3\dot{\theta^2}\frac{B+C+k_3}{C};$$

$$\mu_1 = \frac{2\dot{\theta}B}{E}; \qquad \mu_2 = \frac{-2\dot{\theta}B}{C}; \qquad \mu_3 = \frac{-C_0}{E}; \qquad \mu_4 = \frac{-C_4}{C};$$

$$A = m_1\frac{l_1^2}{3} + h_1^2(m_4 + m_6); \qquad B = h_1 l_4(\frac{m_4}{2} + m_6);$$

$$C = l_4^2(\frac{m_4}{3} + m_6); \qquad D = m_1\frac{d_1^2}{16};$$

$$E = A + 2B + C + D.$$

The set of Eq. (3.10) though simplified, are still coupled and nonlinear. The variation of parameter method as proposed by Butenin [45] is applied to obtain a closed-form solution. Casting into a form similar to that discussed by Butenin:

$$\ddot{\psi} + A_1\ddot{\beta}_4 + B_1\beta_4 + n_1^2\psi = \mu f(\beta_4, \dot{\beta}_4, \dot{\psi}); \tag{3.11a}$$

$$\ddot{\beta}_4 + A_2\ddot{\psi} + B_2\psi + n_2^2\beta_4 = \mu g(\beta_4, \dot{\beta}_4, \dot{\psi}); \tag{3.11b}$$

where μ is a small dimensionless parameter indicating the degree of nonlinearity, and f, g are nonlinear functions. By continuity, solution of the nonlinear system may be expected to have approximately the same form as that of the linear homogeneous system obtained for $\mu = 0$:

$$\psi = asin(\omega_1 t + \Phi_1) + bsin(\omega_2 t + \Phi_2); \tag{3.12a}$$

$$\beta_4 = \alpha_1 a sin(\omega_1 t + \Phi_1) + \alpha_2 b sin(\omega_2 t + \Phi_2); \qquad (3.12b)$$

where ω_1 and ω_2 are the natural frequencies of the system obtained from the characteristic equation,

$$(1 - A_1 A_2)\omega^4 - (n_1^2 + n_2^2 - A_1 B_2 - A_2 B_1)\omega^2 + n_1^2 n_2^2 - B_1 B_2 = 0. \qquad (3.13)$$

Here a, b, Φ_1, Φ_2 are integration constants obtained from the initial conditions and α_1, α_2 are:

$$\alpha_1 = \frac{A_2\omega_1^2 - B_2}{n_2^2 - \omega_1^2}; \qquad \alpha_2 = \frac{A_2\omega_2^2 - B_2}{n_2^2 - \omega_2^2}. \qquad (3.14)$$

The solution of the nonlinear Eqs. (3.11a) and (3.11b) has the same form as Eq. (3.12) where a, b, Φ_1, Φ_2 are considered to be slowly varying parameters. Imposing the constraint conditions such that the derivatives of ψ and β_4 are the same as when the parameters are treated as constants:

$$\dot{\psi} = a\omega_1 cos(\omega_1 t + \Phi_1) + b\omega_2 cos(\omega_2 t + \Phi_2); \qquad (3.15a)$$

$$\dot{\beta}_4 = \alpha_1 a\omega_1 cos(\omega_1 t + \Phi_1) + \alpha_2 b\omega_2 cos(\omega_2 t + \Phi_2). \qquad (3.15b)$$

The remaining terms are set equal to zero and yield the first two of the four simultaneous equations for $\dot{a}, \dot{b}, \dot{\Phi}_1, \dot{\Phi}_2$:

$$\dot{a}sin(\omega_1 t + \Phi_1) + \dot{b}sin(\omega_2 t + \Phi_2) + a\dot{\Phi}_1 cos(\omega_1 t + \Phi_1) + b\dot{\Phi}_2 cos(\omega_2 t + \Phi_2) = 0; \quad (3.16a)$$

$$\alpha_1 \dot{a}sin(\omega_1 t + \Phi_1) + \alpha_2 \dot{b}sin(\omega_2 t + \Phi_2) + \alpha_1 a\dot{\Phi}_1 cos(\omega_1 t + \Phi_1) +$$

$$\alpha_2 b\dot{\Phi}_2 cos(\omega_2 t + \Phi_2) = 0. \qquad (3.16b)$$

The remaining two equations are found by substituting $\ddot{\psi}$ and $\ddot{\beta}_4$ into Eq. (3.11):

$$\dot{a}\omega_1(1 + \alpha_1 A_1)cos(\omega_1 t + \Phi_1) + \dot{b}\omega_2(1 + \alpha_2 A_1)cos(\omega_2 t + \Phi_2) - \omega_1 a\dot{\Phi}_1(1 + \alpha_1 A_1)$$

$$sin(\omega_1 t + \Phi_1) - \omega_2 b\dot{\Phi}_2(1 + \alpha_2 A_1)sin(\omega_2 t + \Phi_2) = \mu f(\beta_4, \dot{\beta}_4, \dot{\psi}); \qquad (3.16c)$$

$$\dot{a}\omega_1(\alpha_1 + A_1)cos(\omega_1 t + \Phi_1) + \dot{b}\omega_2(\alpha_2 + A_2)cos(\omega_2 t + \Phi_2) - \omega_1 a\dot{\Phi}_1(\alpha_1 + A_2)$$

$$sin(\omega_1 t + \Phi_1) - \omega_2 b\dot{\Phi}_2(\alpha_2 + A_2)sin(\omega_2 t + \Phi_2) = \mu g(\beta_4, \dot{\beta}_4, \dot{\psi}). \qquad (3.16d)$$

The above four equations can be solved simultaneously to obtain the following four relations for $\dot{a}, \dot{b}, \dot{\Phi}_1 and \dot{\Phi}_2$:

$$\dot{a} = \frac{\mu}{\omega_1\sigma(\omega_2^2 - \omega_1^2)}[\frac{A_2\omega_1^2 - B_2}{\alpha_1}f + (A_1\omega_1^2 - B_1)g]cos\zeta; \qquad (3.17a)$$

$$\dot{b} = \frac{-\mu}{\omega_2\sigma(\omega_2^2 - \omega_1^2)}[\frac{A_2\omega_2^2 - B_2}{\alpha_2}f + (A_1\omega_2^2 - B_1)g]cos\eta; \qquad (3.17b)$$

$$\dot{\Phi}_1 = \frac{-\mu}{\omega_1 a\sigma(\omega_2^2 - \omega_1^2)}[\frac{A_2\omega_1^2 - B_2}{\alpha_1}f + (A_1\omega_2^2 - B_1)g]sin\zeta; \qquad (3.17c)$$

$$\dot{\Phi}_2 = \frac{\mu}{\omega_2 b\sigma(\omega_2^2 - \omega_1^2)}[\frac{A_2\omega_2^2 - B_2}{\alpha_2}f + (A_1\omega_2^2 - B_1)g]sin\eta. \qquad (3.17d)$$

Here: $\sigma = 1 - A_1A_2; \quad \zeta = \omega_1 t + \Phi_1; \quad$ and $\quad \eta = \omega_2 t + \Phi_2.$

Eqs. (3.17) represent a transformation of the system (3.11) to a set of new variables. It can be seen that for sufficiently small μ the derivatives $\dot{a}, \dot{b}, \dot{\Phi}_1, \dot{\Phi}_2$ are also small, consequently a, b, Φ_1 and Φ_2 are slowly changing functions of time. For small variations compared to the oscillations in the resulting dynamic system, the approximate equations for a, b, Φ_1, Φ_2 can be obtained by averaging the r.h.s. of equations (3.17) over the periods $\frac{2\pi}{\omega_1}$ and $\frac{2\pi}{\omega_2}$ thus giving:

$$\dot{a} = \frac{\mu}{\omega_1\sigma(\omega_2^2 - \omega_1^2)}[\frac{A_2\omega_1^2 - B_2}{\alpha_1}F_1 + (A_1\omega_1^2 - B_1)G_1]; \qquad (3.18a)$$

$$\dot{b} = \frac{-\mu}{\omega_2\sigma(\omega_2^2 - \omega_1^2)}[\frac{A_2\omega_2^2 - B_2}{\alpha_2}F_2 + (A_1\omega_2^2 - B_1)G_2]; \qquad (3.18b)$$

$$\dot{\Phi}_1 = \frac{-\mu}{a\omega_1\sigma(\omega_2^2 - \omega_1^2)}[\frac{A_2\omega_1^2 - B_2}{\alpha_1}F_3 + (A_1\omega_1^2 - B_1)G_3]; \qquad (3.18c)$$

$$\dot{\Phi}_2 = \frac{\mu}{b\omega_2\sigma(\omega_2^2 - \omega_1^2)}[\frac{A_2\omega_2^2 - B_2}{\alpha_2}F_4 + (A_1\omega_2^2 - B_1)G_4]; \qquad (3.18d)$$

where:

$$F_1 = \frac{1}{4\pi^2}\int_0^{2\pi}\int_0^{2\pi} f cos\zeta d\zeta d\eta; \qquad G_1 = \frac{1}{4\pi^2}\int_0^{2\pi}\int_0^{2\pi} g cos\zeta d\zeta d\eta;$$

$$F_2 = \frac{1}{4\pi^2}\int_0^{2\pi}\int_0^{2\pi} f cos\eta d\zeta d\eta; \qquad G_2 = \frac{1}{4\pi^2}\int_0^{2\pi}\int_0^{2\pi} g cos\eta d\zeta d\eta;$$

$$F_3 = \frac{1}{4\pi^2}\int_0^{2\pi}\int_0^{2\pi} f sin\zeta d\zeta d\eta; \qquad G_3 = \frac{1}{4\pi^2}\int_0^{2\pi}\int_0^{2\pi} g sin\zeta d\zeta d\eta;$$

$$F_4 = \frac{1}{4\pi^2}\int_0^{2\pi}\int_0^{2\pi} f sin\eta d\zeta d\eta; \qquad G_4 = \frac{1}{4\pi^2}\int_0^{2\pi}\int_0^{2\pi} g sin\eta d\zeta d\eta. \quad (3.19)$$

Equations (3.18a) and (3.18b) are independent of Φ_1 and Φ_2. Therefore, one can solve them quite readily for a and b. Substiuting the results in equations (3.18c), (3.18d), and integrating, yields Φ_1 and Φ_2.

Substituting for f and g, the averaging integrals (3.19) can be evaluated as:

$$\mu F_1 = \frac{\mu_3 a\omega_1}{2}; \qquad \mu G_1 = \frac{\mu_4\alpha_1 a\omega_1}{2};$$

$$\mu F_2 = \frac{\mu_3 b\omega_2}{2}; \qquad \mu G_2 = \frac{\mu_4\alpha_2 b\omega_2}{2};$$

$$F_3 = 0; \qquad G_3 = 0;$$

$$F_4 = 0; \qquad G_4 = 0. \quad (3.20)$$

Introducing the expressions from Eq. (3.20) into Eq. (3.18) results in:

$$\dot{a} = \frac{1}{2\omega_1\sigma(\omega_2^2-\omega_1^2)}[\frac{(A_2\omega_1^2 - B_2)}{\alpha_1}\mu_3 a\omega_1 + (A_1\omega_1^2 - B_1)\mu_4\alpha_1 a\omega_1]; \quad (3.21a)$$

$$\dot{b} = \frac{-1}{2\omega_2\sigma(\omega_2^2-\omega_1^2)}[\frac{(A_2\omega_2^2 - B_2)}{\alpha_2}\mu_3 b\omega_2 + (A_1\omega_2^2 - B_1)\mu_4\alpha_2 b\omega_2]; \quad (3.21b)$$

$$\dot{\Phi}_1 = 0; \quad (3.21c)$$

$$\dot{\Phi}_2 = 0. \quad (3.21d)$$

The amplitude and phase angles can now be evaluated from equations

(3.21a), (3.21b):

$$a = a_0 e^{H_1 t}; \tag{3.22a}$$

$$b = b_0 e^{-H_2 t}. \tag{3.22b}$$

Here a_0 and b_0 are functions of the initial condition and

$$H_1 = \frac{1}{2\sigma(\omega_2^2 - \omega_1^2)}[\frac{\mu_3}{\alpha_1}(A_2\omega_1^2 - B_2) + \mu_4\alpha_1(A_1\omega_1^2 - B_1)]; \tag{3.23}$$

$$H_2 = \frac{1}{2\sigma(\omega_2^2 - \omega_1^2)}[\frac{\mu_3}{\alpha_2}(A_2\omega_2^2 - B_2) + \mu_4\alpha_2(A_1\omega_2^2 - B_1)]. \tag{3.24}$$

The amplitude parameters a and b exhibit exponential decay governed by the damping at the joints and that of the platform. Φ_1 and Φ_2 are constants determined by the initial conditions.

Substituting $a(t), b(t)$ from eqations (22) into Eqs. (12) yields the final form of the analytic solution:

$$\psi = a_0 e^{H_1 t} sin(\omega_1 t + \Phi_1) + b_0 e^{-H_2 t} sin(\omega_2 t + \Phi_2); \tag{3.25a}$$

$$\beta_4 = \alpha_1 a_0 e^{H_1 t} sin(\omega_1 t + \Phi_1) + \alpha_2 b_0 e^{-H_2 t} sin(\omega_2 t + \Phi_2). \tag{3.25b}$$

The amplitudes and the phase angles can be evaluated from the

following initial conditions:

$$\psi_0 = a_0 sin\Phi_1 + b_0 sin\Phi_2; \tag{3.26a}$$

$$\beta_{4,0} = \alpha_1 a_0 sin\Phi_1 + \alpha_2 b_0 sin\Phi_2; \tag{3.26b}$$

$$\dot{\psi}_0 = a_0 H_1 sin\Phi_1 + a_0\omega_1 cos\Phi_1 - b_0 H_2 sin\Phi_2 + b_0\omega_2 cos\Phi_2; \tag{3.27a}$$

$$\dot{\beta}_{4,0} = \alpha_1(a_0 H_1 sin\Phi_1 + a_0\omega_1 cos\Phi_1) - \alpha_2(b_0 H_2 sin\Phi_2 - b_0\omega_2 cos\Phi_2). \tag{3.27b}$$

The nonlinear analytical solution in Eq. (3.25) has the same form as that for the linear homogeneous case given in Eq. (3.12), except for the time varying amplitudes

$a(t), b(t)$. Note, for this particular case, where the third and higher degrees of non-linearities were neglected, the nonlinear system oscillates at the same frequencies as the linear homogeneous case.

Results and Discussion

The response results obtained using the approximate closed form solution were compared with those given by numerical integration of the original nonlinear Eq. (3.9). The following initial conditions were used: $\psi_{t=0} = \psi_0$, $\dot{\psi}_{t=0} = 0$, $\beta_{4,(t=0)} = \beta_{4,0}$; $\dot{\beta}_{4,(t=0)} = 0$. Substituting the initial conditions into equations (3.26) and (3.27), the amplitudes and the phase angles are obtained as:

$$\Phi_1 = sin^{-1}\left(\frac{\omega_1}{\sqrt{H_1^2 + \omega_1^2}}\right); \qquad \Phi_2 = sin^{-1}\left(\frac{\omega_2}{\sqrt{H_2^2 + \omega_2^2}}\right);$$

$$a_0 = \frac{\beta_{4,0} - \alpha_2\psi_0}{sin\Phi_1(\alpha_1 - \alpha_2)}; \qquad b_0 = \frac{\beta_{4,0} - \alpha_1\psi_0}{sin\Phi_2(\alpha_2 - \alpha_1)}. \tag{3.28}$$

The numerical values used in the simulation are as follows:

System Parameters:

m_1=120,000 kg; m_4=900 kg; m_6=5000 kg; l_1=60 m; l_4=17 m;

d_1=5 m; C_4=100 Nms/rad; $C_0 = 1 \times 10^3$ Nms/rad; k_3=10 Nm/rad.

Orbital Parameters:

$\epsilon = 0$, $\tau = 6 \times 10^3 s$

Specified Coordinates Values:

$\beta_3 = 0$, $h_1 = 30$ m

Initial conditions:

$\psi_0 = 0.1$ rad, $\dot{\psi}_0 = 0$, $\beta_{4,0} = 0.2$ rad, $\dot{\beta}_{4,0} = 0$

The response results are compared in Figure 3-6. As can be seen from the platform and the link responses, the numerical simulation results are quite close to the analytical solution of the equations of motion. It is important to point out that a small phase error observed in the link response does not accumulate over more than one cycle of the platform pitch.

With these three independent approaches suggesting the right-trend, thus substantiating validity of the governing equations of motion and the numerical integration code, it was decided to undertake a parametric response study of the uncontrolled system.

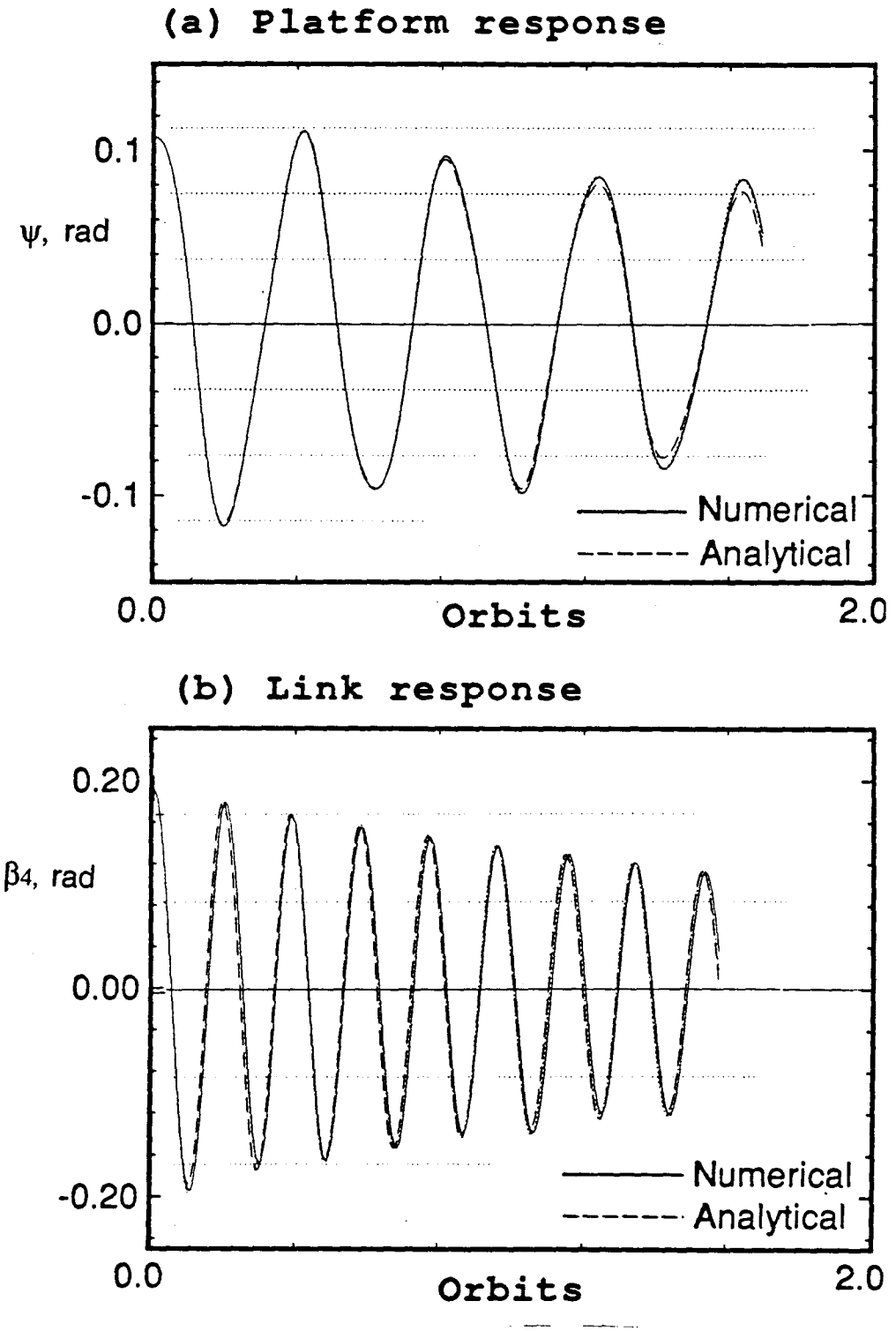

Figure 3-6 A comparison between the numerical and analytical solutions for damped response of the simplified MDM system: (a) platform response; (b) link response.

3.3 Open Loop System Dynamics

An extensive study of the MDM open loop dynamic response was undertaken. For better appreciation of the system performance, it was analyzed in an increasing order of complexity: it starts with a parametric study of the MDM, with free joints (free motion), supported by a rigid platform; this is followed by an assessment of the effects of damping and platform flexbility; and finally a parametric study of the flexible system with open loop torques.

The investigation provided better physical undrstanding of the system behavior. It helped establish relative significance of the various system parameters. Furthermore, it gave critical combinations of system parameters and disturbances leading to an unacceptable response, thus setting the stage for a control analysis.

The amount of information obtained through a planned variation of the system parameters and initial conditions is rather extensive. For conciseness, only typical results useful in establishing trends are presented here.

3.3.1 Numerical data used in the simulation

In order to focus attention on the complex interactions between the system flexibility (joints, platform); base translation; slewing and deployment maneuvers; librational motion of the entire system; etc. the study is purposely confined to the orbital plane with the platform in the gravity gradient orientation. Circular orbit of 400 km altitude (orbital period=5550 s) is considered for the parametric study. The earth gravitation constant is taken as GM=3.986005×10^{14} m^3/s^2.

The shift in the system c.m. significantly complicates the problem and increases the computational time, especially for flexible systems. Fortunately, it has relatively little effect on the system dynamics, even in the presence of flexibility and slew maneu-

vers, as shown by Chan [3]. Hence the shift in c.m. was neglected in the parametric study. However, it should be emphasized that the formulation accounts for the shift in c.m. and its effect can be assessed quite readily if required.

The system parameters as specified in NASA's space station *Freedom* reference configuration manual [52] were used in the simulation. Mass of the torque motors and the mobile base being relatively small is neglected. The equivalent linear actuator radius (r_5) is chosen to be 0.1m in this study. Typical numerical values for the system parameters are presented in Table 3-1, in Meter, Kg, Sec. (M.K.S.) units.

Table 3-1 Typical numerical values for the MDM system parameters.

parameter	system	platform	joint 1	arm 1	joint 2	arm 2
gen.co.(d.o.f.)	ψ	$\bar{q}_1$	β_3	β_4	β_5	a_5
dimension [m]		d_1=3 l_1=60		l_4=7		
mass [kg]	m^*	$m_1 =$ 120000	$m_3 = 0$	$m_4 =$ 500	$m_5 = 0$	$m_6 = 10^3$
inertia [kgm^2]		I_1^*	$I_3 = 10$	I_4^*	$I_5 = 10$	$I_{6x} = 100$ $I_{6y} = 100$ $I_{6z} = 100$
stiffness [kgm^2/s^2rad] [kgm^3/s^2]		EJ= $0.55 \cdot 10^9$	$k_3 =$ 1000		$k_5 =$ 1000	
damping ratio	$\xi_0 =$ 10^{-5}	$\xi_1 =$ 0.01	$\xi_3 =$ 0.005	$\xi_4 = 0$	$\xi_5 =$ 0.005	$\xi_6 =$ 0.005
damping coefficient [kgm^2/s/rad]	$C_0 = 5.6$	$C_1 = 22$	$C_3 = 10$	$C_4 = 0$	$C_5 = 10$	$C_6 = 10$ [kg/s]
gear ratio			$n_3 = 1$		$n_5 = 1$	

* calculated during the simulation.

3.3.2 MDM undamped response for the rigid platform case

The purpose of studying this relatively simple configuration is to have some insight into the intricate dynamics and gain better physical understanding of the system behavior. To this end the system was subjected to a variety of initial conditions

representing a wide spectrum of disturbances.

There are several equilibrium positions for the MDM system, however the stable equilibrium configuration corresponds to the platform in the gravity gradient orientation with $\beta_4 = h_1 = h_2 = a_5 = 0$, i.e. the arm is aligned with the platform, and the c.m. of arm 2 assembly is assumed to coincide with the center of mass of the system. The unstable equilibrium position is obtained when the platform axis of the minimum moment of inertia coincides with the local horizontal, and the slew angle $\beta_4 = \pm\frac{\pi}{2}$. In all the simulations, the stable equilibrium position is considered as reference. The geometry and the common initial conditions are summarized in Table 3-2.

Table 3-2 MDM configuration and typical initial conditions

i.c. of	system	platform	base	joint 1	arm 1	joint 2	arm 2
position [rad], [m]	$\psi = 0.1$	$\bar{q}_1 = 0.1$	$h_1 = 60$	$\beta_3 = n_3\beta_4$	$\beta_4 = 0.1$	$\beta_5 = a_5 n_5 / r_5$	$a_5 = 10$
velocity [rad/s], [m/s]	$\dot{\psi} = 0$	$\dot{\bar{q}}_1 = 0$	$\dot{h}_1 = 0.1$	$\dot{\beta}_3 = n_3\dot{\beta}_4$	$\dot{\beta}_4 = 0$	$\dot{\beta}_5 = \dot{a}_5 n_5 / r_5$	$\dot{a}_5 = 0$
acceleration $[m/s^2]$			$\ddot{h}_1 = 0$				
torque $[Kgm^2/s^2]$		$\bar{T}_1 = 0$		$\bar{T}_3 = 0$		$\bar{T}_5 = 0$	

Figure 3-7 shows undamped response of the system when the manipulator base (F_2) is located at the center of the platform (h_1=0). The arms are completely free, i.e. unconstrained, to swing and translate. Figure 3-7(a) shows the MDM response over one orbit when the initial slew of β_4=0.1 rad. is imparted, i.e. the arm 1 is rotated through 0.1 rad and released. The arm starts to oscillate with the initial period of 0.6 orbit. The arm, being connected through the shaft to the rotor at joint

1, causes it to follow the arm's motion as shown by the β_3 response. As can be seen, the linear actuator inertia I_5 causes the rotor at joint 2 to rotate through an angle β_5 w.r.t. the slewing arm and, as a consequence, the deployable arm with the payload assembly, originaly located in the unstable equilibrium position (on the orbit), starts to deviate (a_5) with increasing acceleration. The rotor (I_5) is finally constrained by the motion of the deployable arm and rotates according to the effective radius and gear ratio (r_5, n_5). As the velocity of the payload w.r.t. the slewing link increases, the Coriolis reaction moment starts to dominate the link oscilations which is apparent after 0.8 orbit. The platform pitch response ψ is not excited as the base is located at the c.m. of the platform.

Figure 3-7(b) shows the MDM response for an initial deployement of 0.5 m, i.e. the payload, originally located at the system c.m., is displaced through 0.5 m. As can be expected, the payload starts to move outwards (away from the c.m.) with an increasing acceleration. The rotor I_5 of the linear actuator follows the deployment according to the linear transmission $r_5 = 0.1$ m as shown by the β_5 response. The Coriolis reaction moment exerted by the deploying arm 2 causes the arm 1 (initially located in the stable equilibrium position with $\beta_4 = 0$) to rotate through $\beta_4 = -1$ rad where the gravity gradient moment balances the Coriolis torque. The rotor at joint 1, being connected to the arm, is forced to rotate (β_3). As before, the platform pitch ψ is not exited.

Figure 3-7(c) shows the MDM response over one orbit for an initial pitch disturbance of ψ=0.1 rad. As can be expected the platform starts to oscillate about the local vertical (the equilibrium position) with a period of approximatly 0.6 orbit. Up to 0.2 orbit, arm 1 (β_4) and the torque motor rotor (β_3) follow the platform with the same oscillation frequency. As arm 1 starts to oscillate with the platform, the inertia

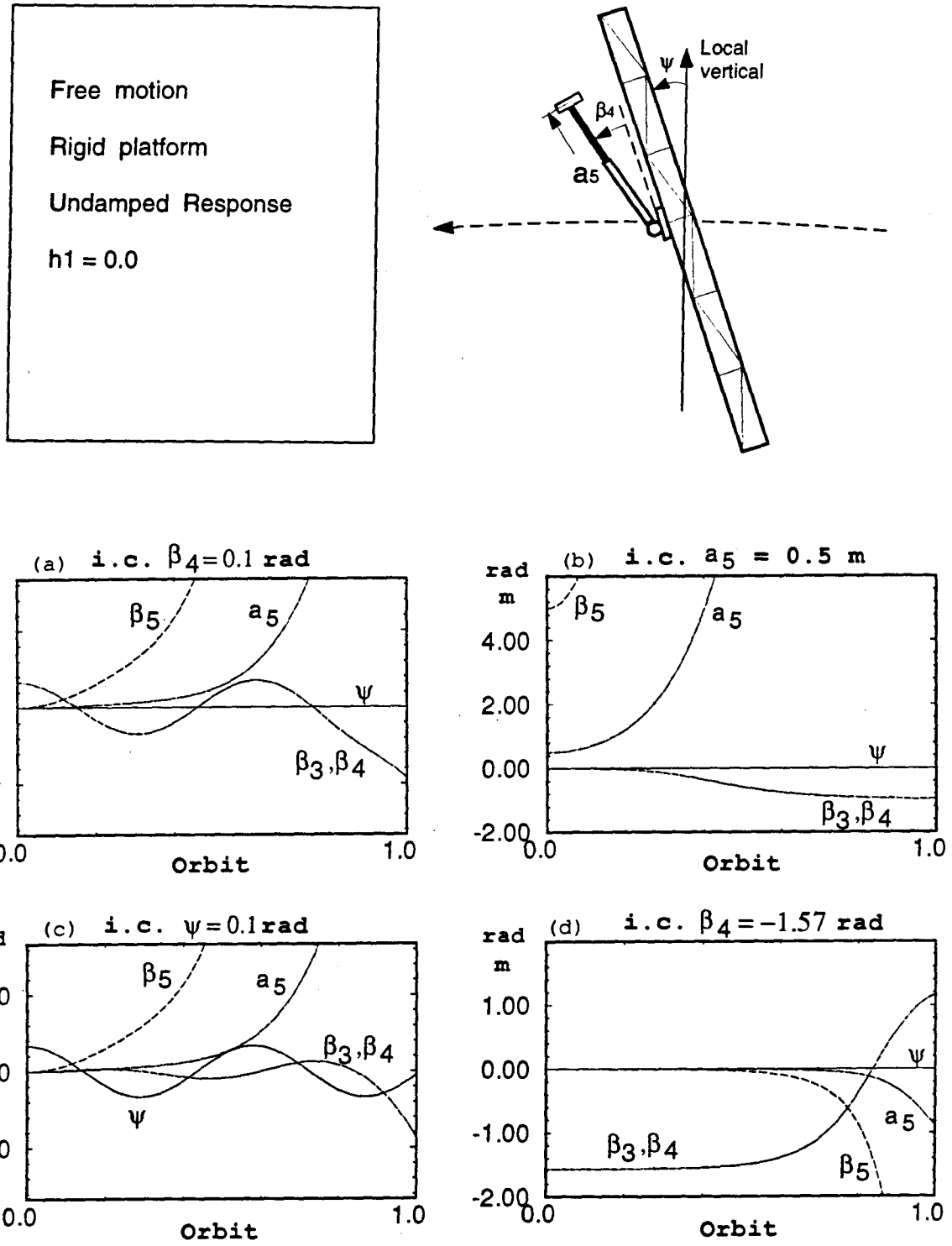

Figure 3-7 MDM free joints undamped response when supported by a rigid platform and subjected to various initial conditions: (a) $\beta_4 = 0.1$ rad; (b) a_5=0.5 m; (c) $\psi = 0.1$ rad; (d) $\beta_4 = -1.57$ rad.

I_5 causes the linear actuator to rotate w.r.t. the slewing arm and, as a consequence, shifts the deployable arm with the payload away from the unstable equilibrium position. The payload deployment (a_5) begins and gradually gains acceleration which is reflected in the rotation of the linear actuator rotor β_5. As the velocity of the deployable arm increases, the Coriolis reaction starts to dominate the motion of the slewing arm and the torque motor rotor attached to it.

Figure 3-7(d) shows the MDM response for an initial slew angle $\beta_4 = -1.57$ rad. In this case both the slewing and the deployable arms are initially in the unstable equilibrium position; i.e. aligned with the local horizontal. Because of the arms' and payload's inertias and the small gravitational moment, the angular acceleration of the slewing arm is relatively small in the begining (up to around 0.5 orbit). As the slew angle increases the payload starts to accelerate.

From the dynamic response of the MDM described in Figure 3-7, it can be concluded that, even for a relatively simple system represented by a rigid platform, undamped and in absence of external torques applied at the joints, the behaviour of the system is rather complex and sometimes unpredictable. Hence a thorough dynamic simulation study is necessary for a reliable design of the manipulator and its control system.

Figure 3-8 shows the undamped dynamical response of the system, in absence of external torques, with a variety of initial conditions when the manipulator base is located at h_1=30 m from the center of the platform.

Figure 3-8(a) presents the system behaviour, over one orbit, when the arm slews through 0.1 rad in 0.05 orbit in a sinusoidal fashion. Note, the arm starts to oscillate and the torque motor rotor follows the arm (β_3). The deployable arm and payload originally located approximatly 30m from the equilibrium position, deviates from

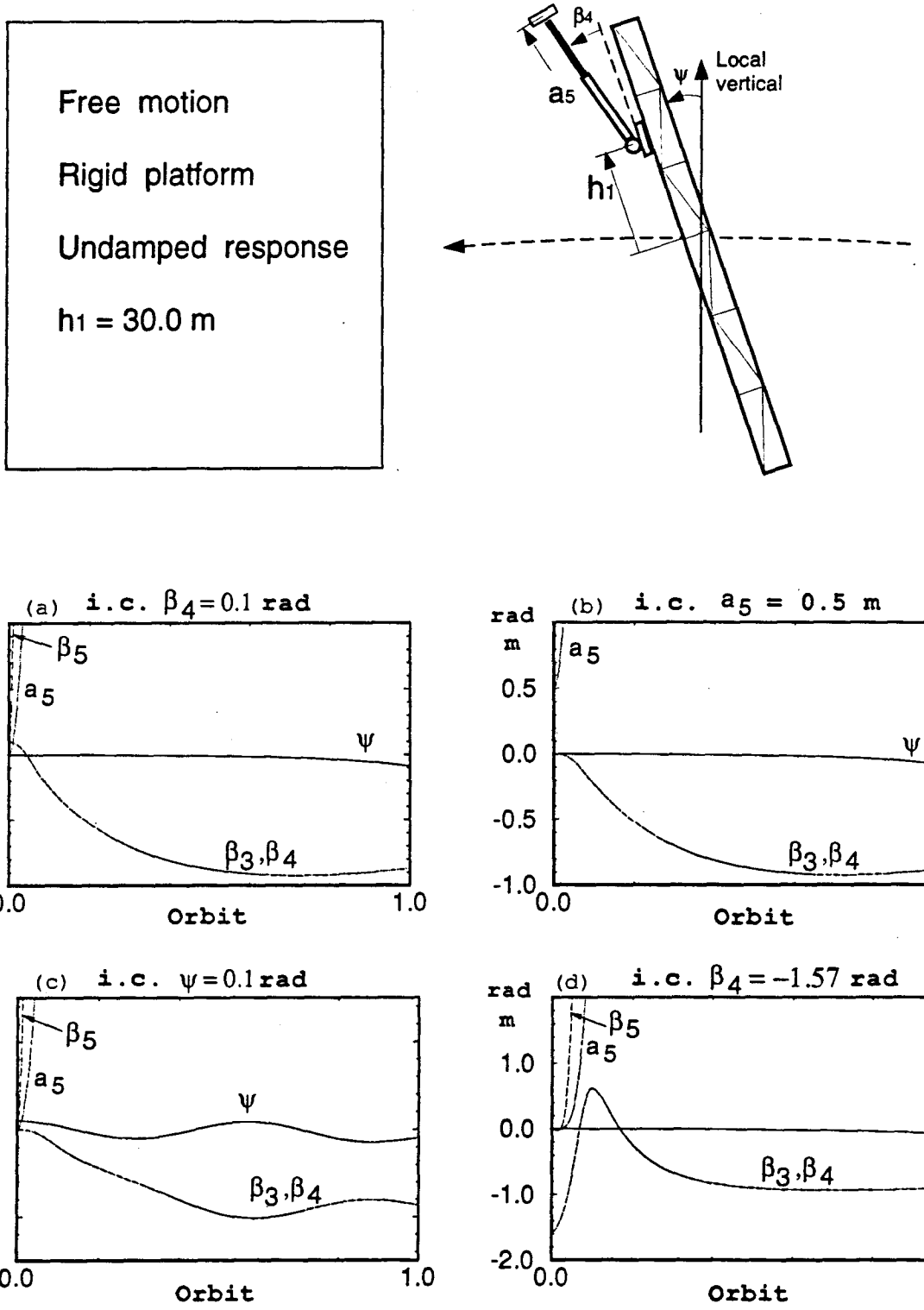

Figure 3-8 Undamped response of the MDM, with free joints and supported by a rigid platform, when the base is located at h_1=30 m from the platform c.m. The initial conditions are: (a) $\beta_4 = 0.1$ rad; (b) a_5=0.5 m; (c) $\psi = 0.1$ rad; (d) $\beta_4 = -1.57$ rad.

this location with a relatively high velocity right from the beginning. The Coriolis reaction moment on the slewing arm dominates its motion. As can be seen, the gravity moment balances the Coriolis reaction moment on the arm at $\beta_4 = -0.9$ rad. The reaction on the base, due to the centripetal and Coriolis accelerations, induce moment on the platform and a relatively small pitch motion (ψ) ensues.

Figure 3-8(b) considers a case similar to that studied in Figure 3-8(a) with an initial condition of a_5=0.5 m. It is apparent that $\beta_4 = -0.9$ rad is the equilibrium position governed by the moments exerted at joint 1 due to the gravity field and the Coriolis reaction. The latter arises due to the rate of the deployment ($\dot{a}_5$) coupled with the rotating system (Ω). The reactions on the base, located 30m from the center of mass of the platform, excites the pitch motion ψ as before.

Figure 3-8(c) shows the system response for an initial disturbance of 0.1 rad in pitch. As can be expected, the effect of the reaction forces at the base on the pitch motion is relatively small, due to the large platform inertia. As in the case of Figure 3-8(b), the slew response (β_4) of arm 1 is affected by the deployed payload. The gravity induced moment balances the Coriolis reaction moment as the arm reaches -0.9 rad from the local vertical. It may be pointed out that β_4 is measured w.r.t. the platform.

Figure 3-8(d) shows the system behaviour when arm 1 is originally located at $\beta_4 = -1.57$ rad. As in the previous cases, the slew motion is strongly affected by the deployable d.o.f.

From the dynamical response study in Figure 3-8 it can be concluded that the coupling among all the system degrees of freedom is significant and cannot be neglected.

Figure 3-9 shows the undamped free system response when the MDM base,

initially located at the c.m. of the platform, continuously translates with a constant velocity of 0.01 m/s along the platform and the deployment d.o.f. is frozen at a_5=10 m.

Figure 3-9(a) shows the system response for a slew initial condition of β_4=0.1 rad. As can be observed, the oscillation amplitude of the arm is amplified 8 times compared to the initial disturbance of 0.1 rad, and the equilibrium is shifted from zero to -0.4 rad. As the MDM base moves away from the c.m. of the platform, the frequency of oscillations increases and the equilibrium position is shifted. The magnified view of the platform pitch response also shows a shift in the equilibrium position from zero to -0.0015 rad after one orbit. The response is governed mainly by the Coriolis reaction due to the base translation $\dot{h}_1$ coupled with the rotation of the system, $\overline{\Omega}$.

Figure 3-9(b) shows the effect of simultaneous slew ($\beta_4 = -0.1$ rad.) and pitch (ψ =0.1 rad) disturbances. As in the previous case, the Coriolis reaction excites the slew motion with a shift in the equilibrium position and an increase in the oscillation frequency as the base moves away from the c.m. of the platform. It may be re-emphasized that the slew d.o.f. β_4 is measured from the platform.

Figures 3-9(c) and 3-9(d) show the system response for two other combinations of initial disturbances. The responses are similar to those observed in Figures 3-9(a) and 3-9(b).

The main conclusion from the system response described in Figure 3-9 is that the velocity of the base dominates the dynamic response of the slew d.o.f. and the platform pitch irrespective of the initial condition of the arm. The significant features of the response are: a shift in the equilibrium position; and increase in the amplitude and frequency of the arm's oscillations.

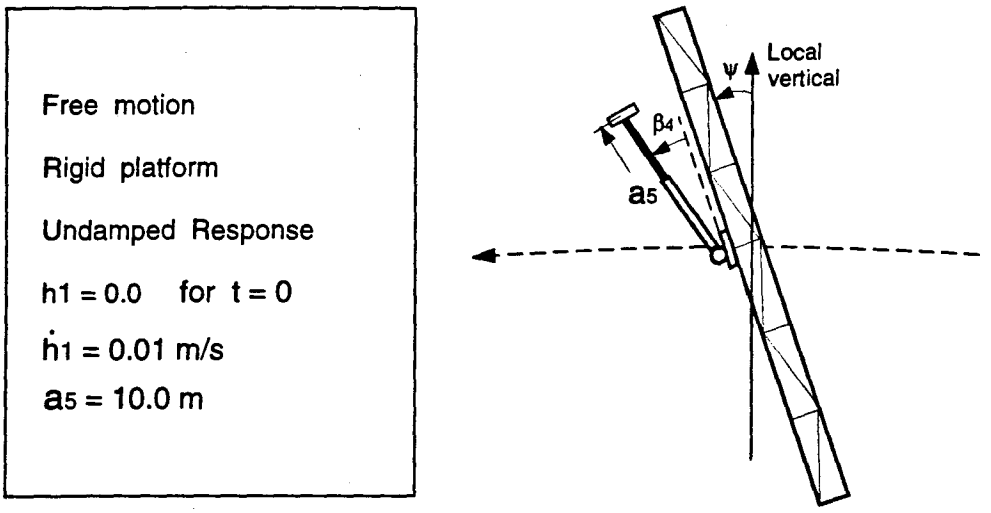

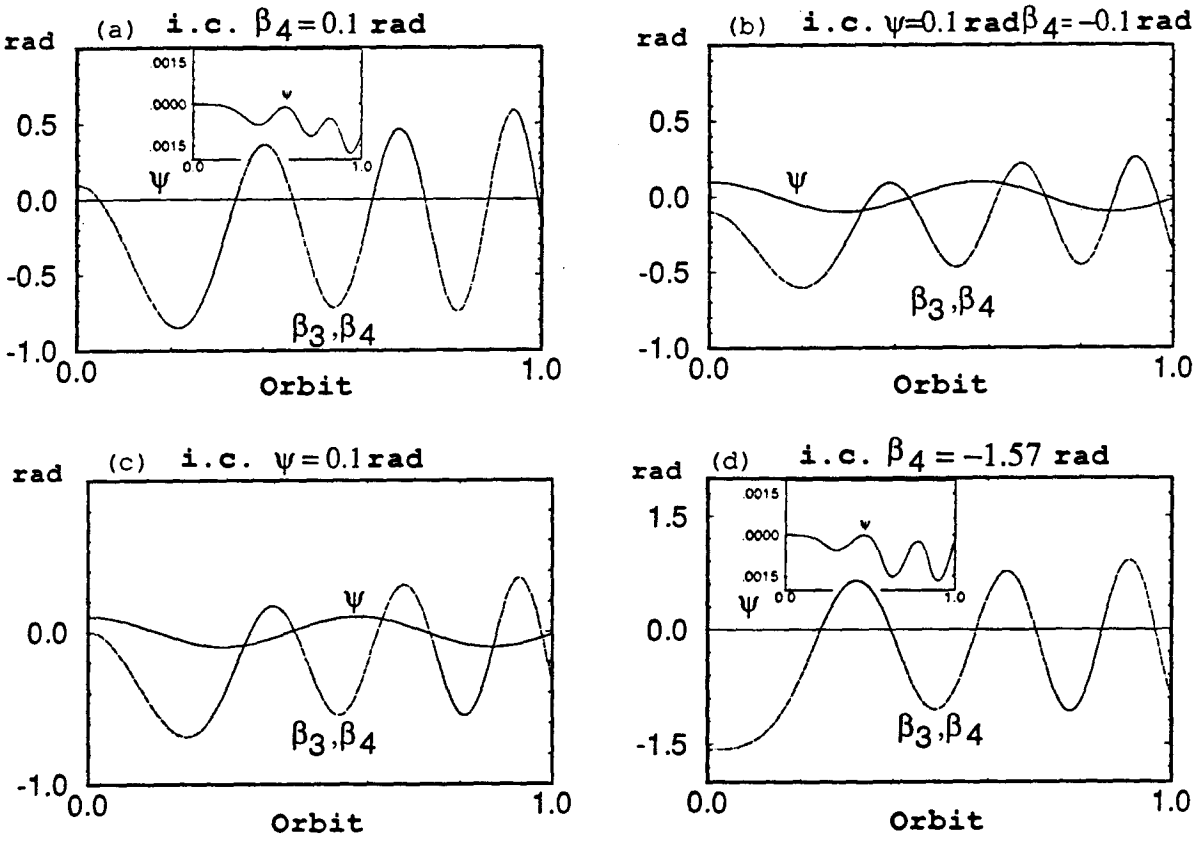

Figure 3-9 Undamped free response of the system during translational maneuver from $h_1 = 0$ at a constant velocity of 0.01 $\frac{m}{s}$. The deployable arm is held fixed at $a_5 = 10$ m. Initial conditions are: (a) $\beta_4 = 0.1$ rad; (b) ψ=0.1 rad, $\beta_4 = -0.1$ rad; (c) $\psi = 0.1$ rad; (d) $\beta_4 = -1.57$ rad.

3.3.3 MDM on a flexible platform

Objective here is to assess the effect of platform flexibility on the dynamical response of the MDM. The platform flexibility is represented, in this case, by only the first mode, which is symmetric [46]. As in the previous section, a parametric study has been carried out for the undamped system, subjected to various initial conditions, in an increasing order of complexity. The system parameters were shown in Table 3-1, and typical initial conditions used in Table 3-2.

It is of interest to point out that a wide spectrum of initial conditions chosen for the study is not aimed at mere generation of response data. Rather it provides information as to the possible critical system behaviour under diverse circumstances which is considered essential to its design and operation under a variety of contingencies. Past experience suggests that slewing and deployment failures are not uncommon, and freeing of a locked member often demands a variety of maneuvers as shown by GEOTAIL, ANIK, GALILEO and other spacecraft.

Figure 3-10 presents the free system undamped response when the flexibility of the platform is represented by only the first mode. The payload was initially located at the c.m. of the platform in the unstable equilibrium position, a_5=0, and the initial slew angle was set at $\beta_4 = 0.1$ rad.

Figure 3-10(a) shows the slew response over one orbit. As can be expected, a periodic motion of around 0.7 orbit (3000 s) and 0.1 rad amplitude is observed for the slewing arm.

Figure 3-10(b) shows the flexible platform response, excited by the slewing arm and coupling with the payload dynamics. The platform behaviour is characterized by the deflection δ_1 at the MDM base. In this particular case, $h_1 = 0$ (i.e. the deflection takes place at the c.m. of the platform). Due to a relatively small mass of the arm and

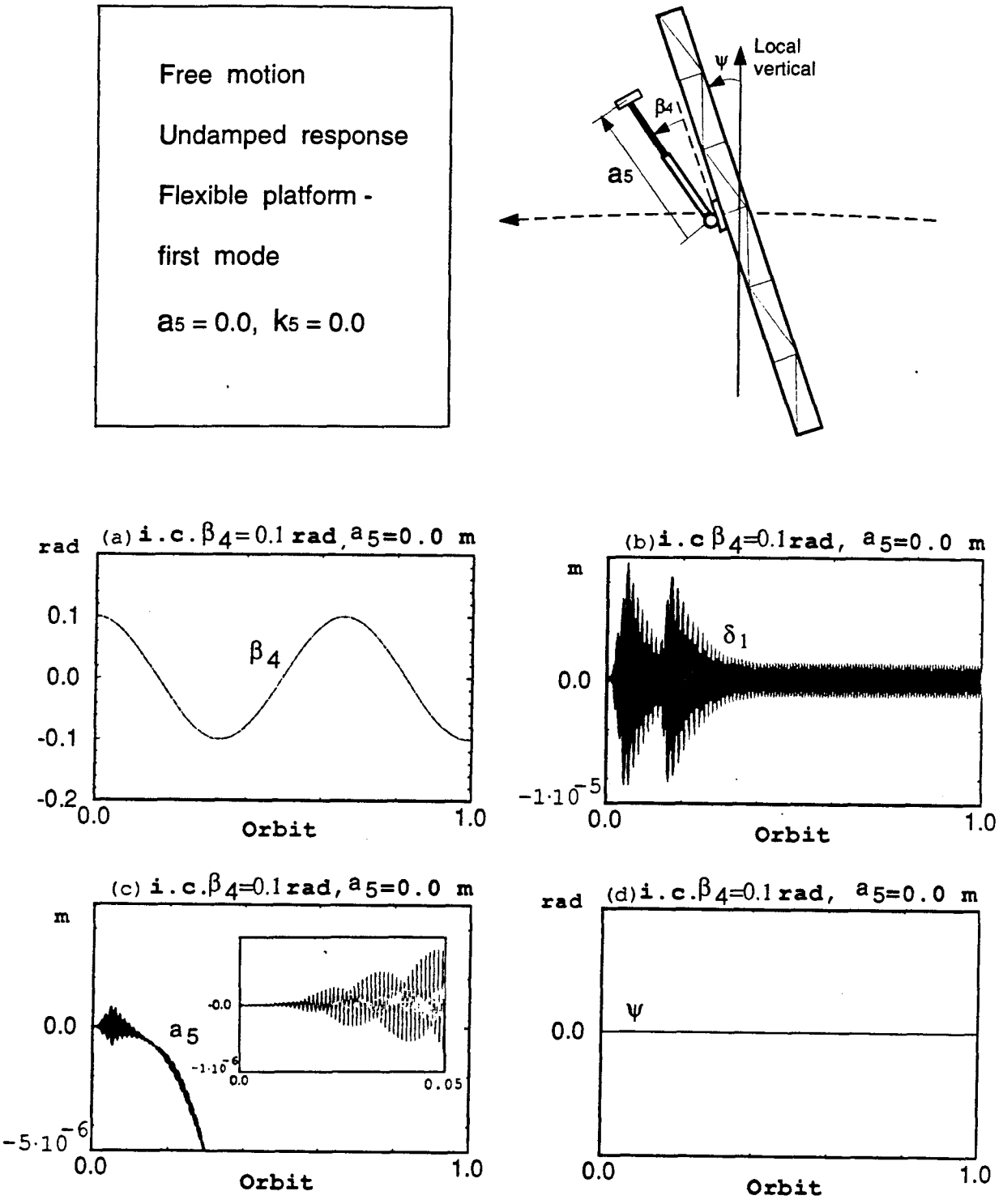

Figure 3-10 Effect of the platform flexibility on the free undamped system response. The payload is initially located at $a_5 = 0$ and disconnected from the linear actuator gear ($k_5 = 0$). The slewing arm is initially oriented at $\beta_4 = 0.1$ rad.

the weak initial condition, the maximum displacement during the transient response is only 10^{-5} m. The enlarged view of the δ_1 response is characterized by the natural frequency of 0.18 Hz, associated with the platform first mode.

Figure 3-10(c) presents time history of the deployment degree of freedom (a_5) associated with arm 2, initially located in the unstable equilibrium position at the c.m. of the platform. The platform vibrations, excited by the slewing arm, force the deployable arm-payload assembly to move and gain acceleration due to the gravitational force. The direction of the deployment towards the center of force (the earth) in this case, is determined by the platform displacement δ_1 and the slew motion, as the payload motion along the slewing arm is unconstrained ($k_5 = 0$). Of course, the deploying arm rotates with the slewing arm. From the enlarged view in Figure 3-10(c) it is apparent that the deployment is coupled with the platform vibrations at 0.18 Hz.

Figure 3-10(d) suggests that the angular pitch librational motion is not excited by the slewing maneuver of the arm, at least within the accuracy of the numerical simulation and duration.

From the response results in Figure 3-10 it can be concluded that the flexible and rigid d.o.f. are coupled. Flexibility of the platform changes the dynamic response of the system quite significantly and hence must be accounted for.

Figure 3-11 presents free undamped response of the system, over one orbit, with the platform flexibility represented by the first mode. The deployable arm is held fixed at a_5=10 m, and the MDM base is located at h_1=0, i.e. the manipulator is located at the mid-point of the platform. The initial slew angle is 1.5 rad (86 deg.) and the platform initial condition is $q_1 = 0.01$, i.e. the platform is initially deformed in the 1^{st} mode with a midpoint deflection of 0.012 m.

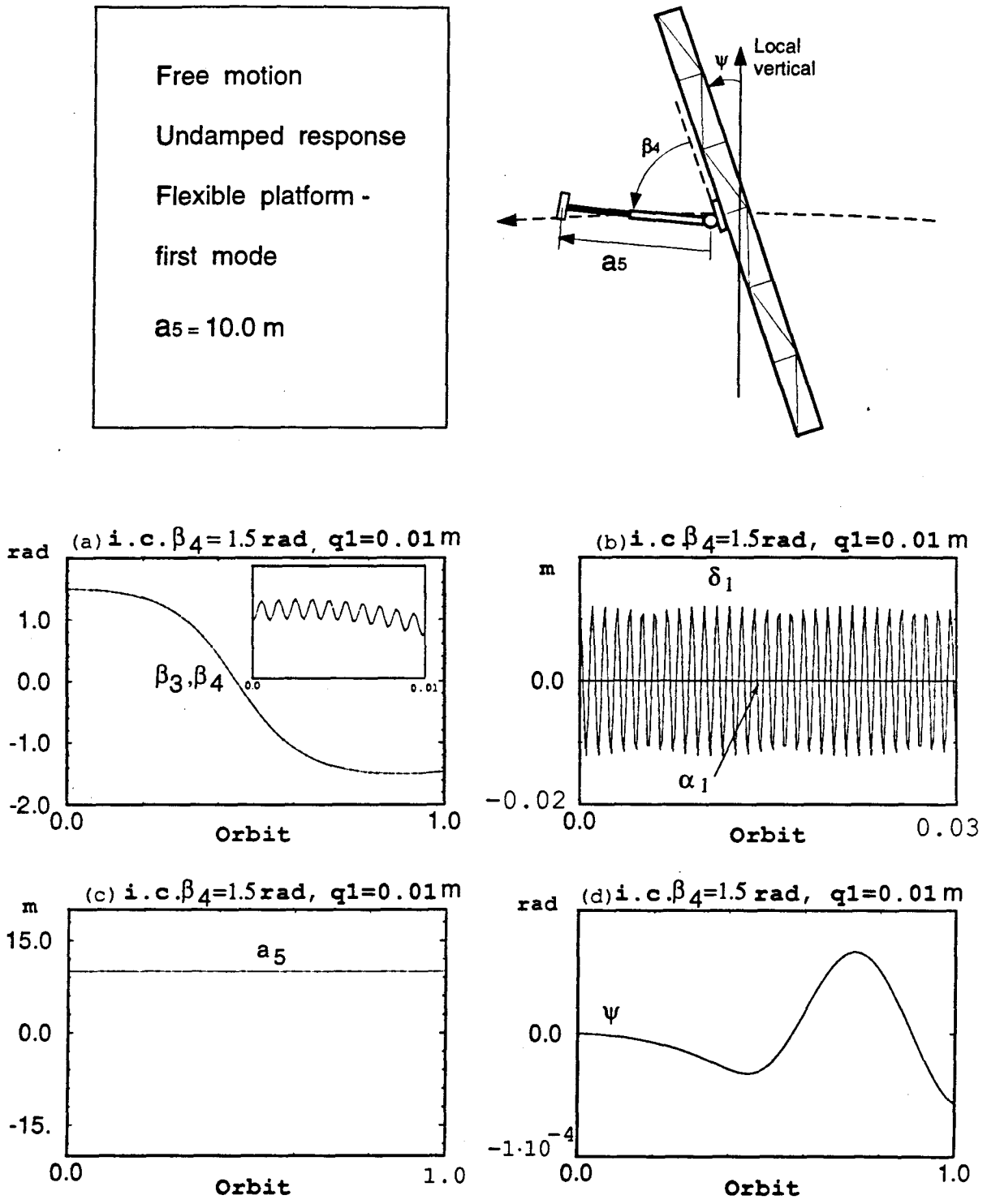

Figure 3-11 Effect of the platform excitation on the system response. The deployable arm is held fixed at a_5=10 m. The initial conditions are $\beta_4 = 1.5$ rad and q_1=0.01 m.

Figure 3-11(a) shows the slew response, i.e. angular motion of the arm in pitch. The relatively low frequency of the slew motion is due to the platform vibrations that induce a pseudo-gravitational field in the local horizontal direction. The oscillation period is about 1.8 orbit compared to 0.7 orbit in the undisturbed motion. As can be seen from the enlarged view of the β_4 response, the rotational motion is modulated at a frequency of 0.18 Hz due to the platform vibrations. The amplitude of the modulations is a function of the base displacement of 0.012 m, in this particular case, where the MDM base is located at the center of the platform and only the first flexural mode is taken into account for the platform lateral vibrations. It also depends on the distance between the common c.m. of the slew arm, the deployable arm assembly and joint 1, and the slew arm position β_4.

Figure 3-11(b) shows the displacment and the slope of the flexible platform at the base. As can be expected, with only the first mode, the slope at the center of the platform where the base is located is zero.

Figure 3-11(d) presents the platform pitch response. Note, although joint 1 is located at the center of mass of the platform and the slew arm is free to respond without any constraint, the pitch d.o.f. is excited. The gravitational and the centrifugal forces coupled with the platform displacment induce torque about the c.m. of the platform causing it to oscillate with a relatively large amplitude. The results suggest that presence of even small platform vibrations, through the coupling dynamics, can cause the system to become unstable.

Figure 3-12 shows response of the system (same as in Figure 3-11) but under an increased disturbance corresponding to the flexible degree of freedom of $q_1 = 0.1$m. The arms continue to slew through 1 rad as before. Note, a rather unexpected response of the slew arm (β_4).

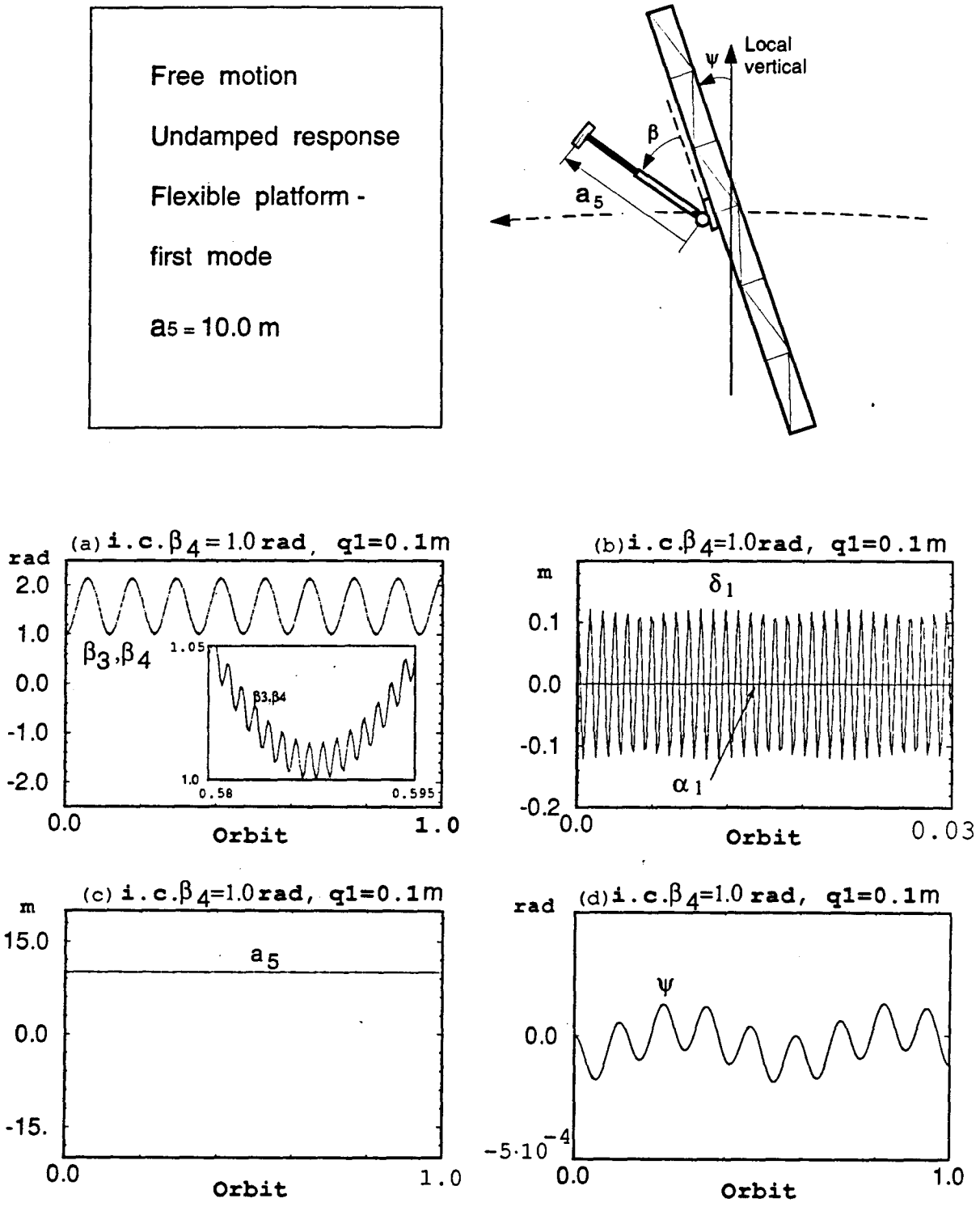

Figure 3-12 Effect of a larger platform excitation of $q_1 = 0.1$ m on the free, undamped response of the system. The deployable arm is held fixed at $a_5 = 10$ m, while the slewing arm is initially oriented at $\beta_4 = 1.0$ rad.

The equilibrium position shifts from zero to 1.57 rad (90 deg.) and the period of the oscillations is 0.12 orbit compared to 0.65 orbit in the rigid platform case (Figure 3-12a). The relatively large platform amplitude at the MDM base, creates a force field perpendicular to the earth gravitational field causing the arms to oscillate about the local horizontal. The frequency of oscillations is a function of the vibration amplitude of the MDM base. It is apparent from the expanded view that the arm response β_4 is modulated, at the higher frequency of 0.18 Hz, due to the coupling with the platform vibrations as shown in Figure 3-12(b).

Figure 3-12(d) presents the pitch response excited by the oscillating arm and its coupling with the platform vibrations. The basic pitch response, with a period of 0.6 orbit, is modulated due to the arm oscillations at a period of 0.12 orbit.

Corresponding results for the slew arm, initially at 1.5 rad ($\beta_4 = 1.5$ rad instead of 1 rad in Figure 3-12), are presented in Figure 3-13.

Note, the equilibrium position for the slew arm is shifted to 90 deg as shown in Figure 3-13(a). The amplitude of the pitch response and its high frequency modulations are functions of the slew arm oscillation amplitude about the local horizontal. The pitch modulation virtually disappears and the librational amplitude decreases as the initial slew angle is set close to the new equilibrium position (Figure 3-14).

Figure 3-15 presents the dynamic response of the system, similar to that described in Figure 3-14, with the slewing arm initially set at $\beta_4 = 0$. As can be seen in Figure 3-15(a), the arm swings between the two unstable equilibrium positions β_4=0 and 2π (local vertical). The arm response is coupled with the platform vibrations as shown in the expanded view of the β_4 time history. The platform pitch response (Figure 3-15d) is strongly affected by the slewing arm dynamics, and a significant librational amplitude of 0.001 rad is observed. Note, no torque is applied to the

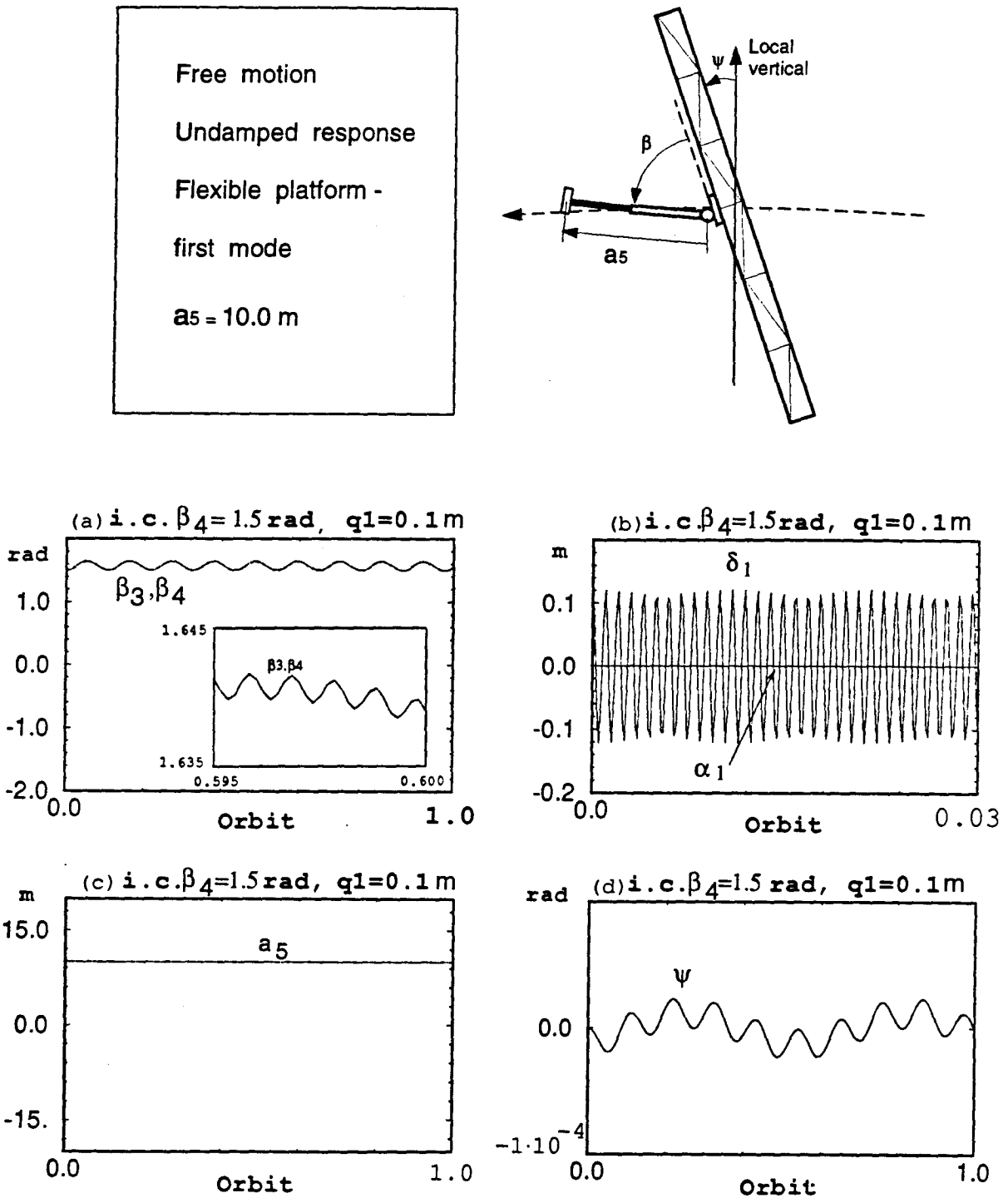

Figure 3-13 Free undamped response of the system with the deployable d.o.f. frozen at a_5=10 m. Initially $\beta_4 = 1.5$ rad and q_1=0.1 m.

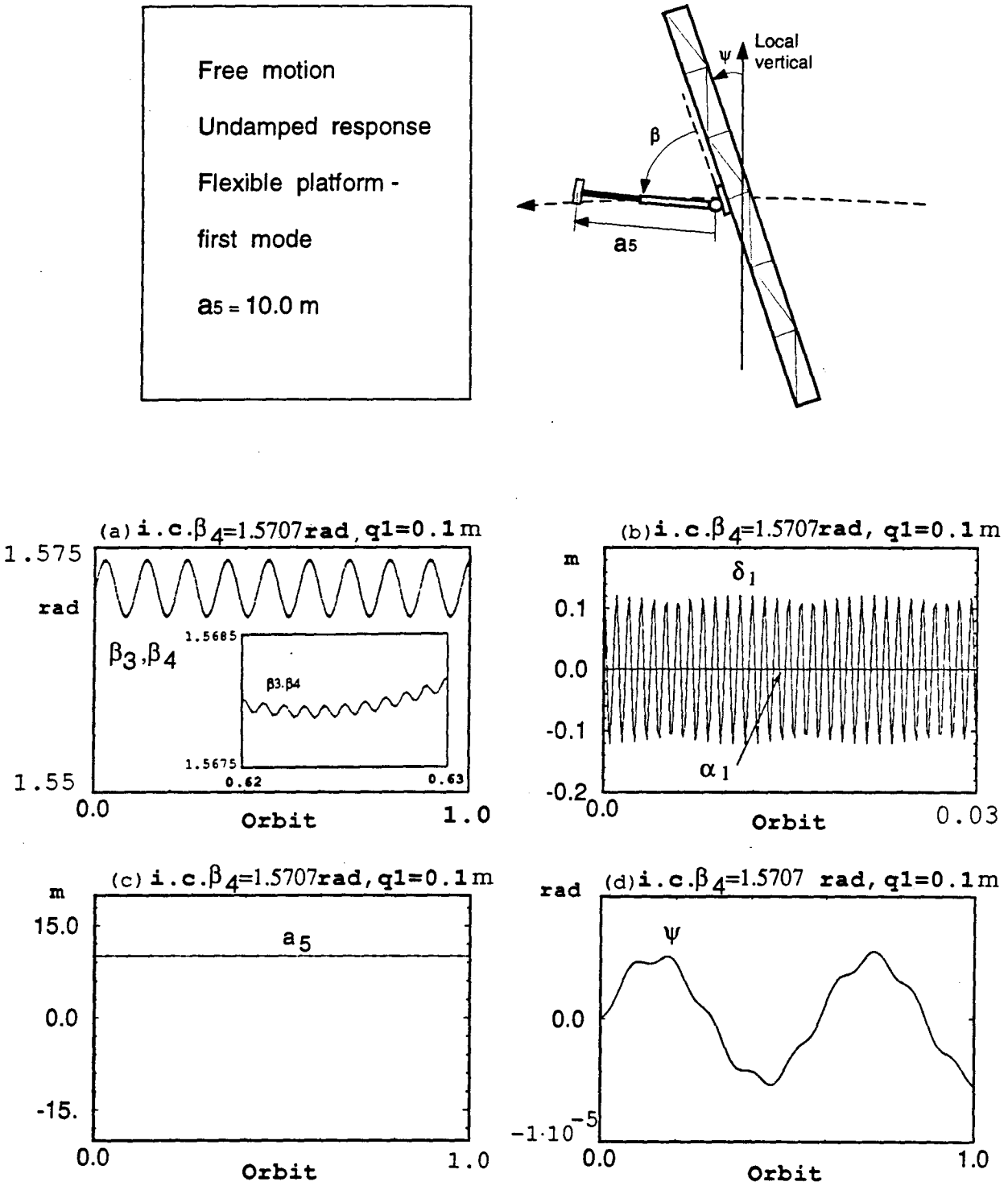

Figure 3-14 Free undamped system response with the deployable arm held fixed at a_5=10 m. Initial orientation of the slewing arm is β_4 = 1.5707 rad. The platform is excited in the first mode with q_1=0.1 m.

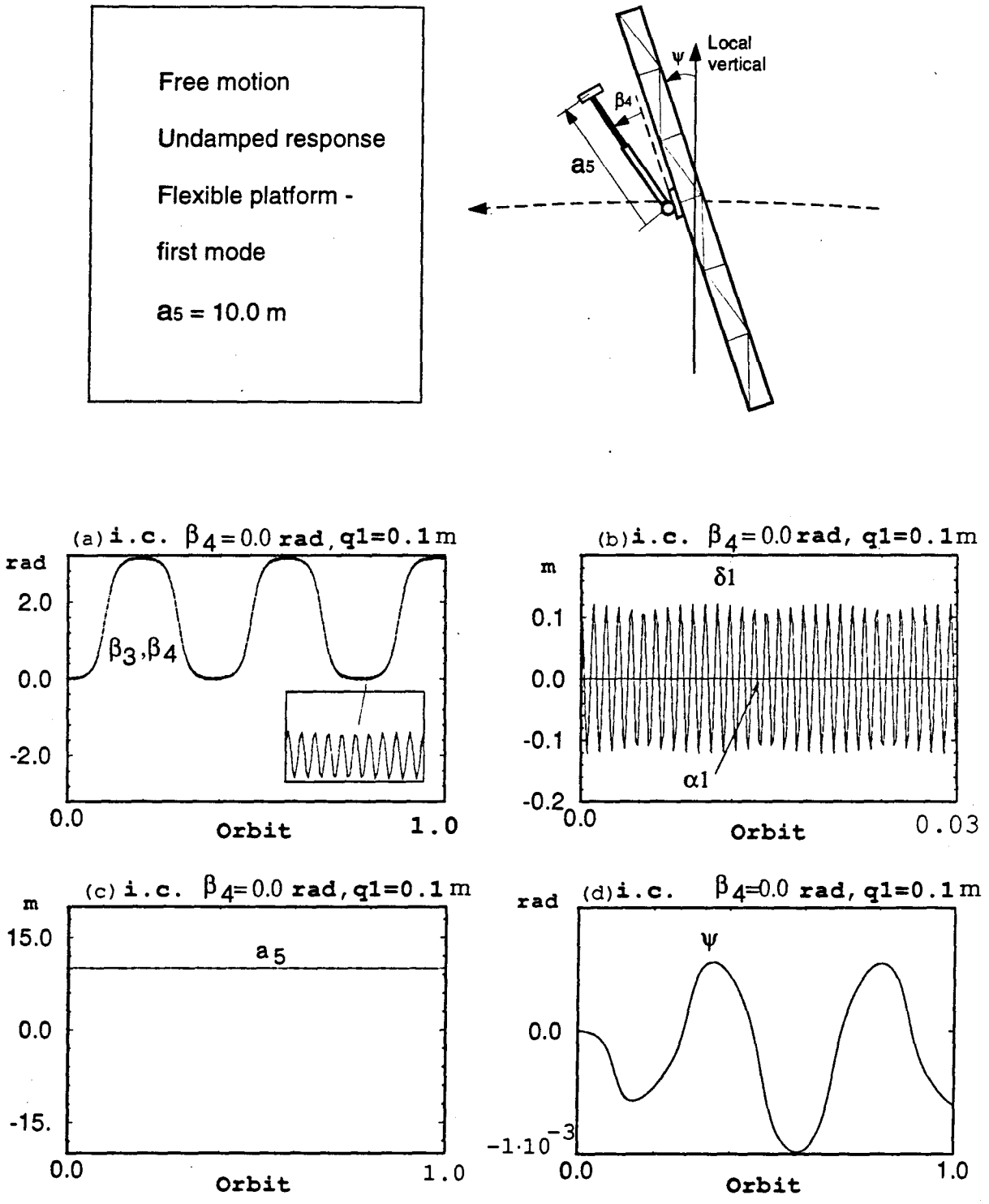

Figure 3-15 Effect of the initial orientation of the slewing arm on the system response with the deployable arm fixed at a_5=10 m. Initially $\beta_4 = 0$ and q_1=0.1 m.

motors and pitch response is the result of the platform vibrations.

From the parametric study for the system configurations and the initial conditions as desribed in Figures 3-11 to 3-15 it is apparent that even a relativly small disturbance applied to the platform can adversly affect the dynamics. This can excite significant slew and pitch responses which affect the performance of the MDM and the space station. Development of a presice and reliable dynamical simulation procedure is necessary to predict unexpected system behaviour.

3.3.4 Damped response for the flexible MDM

The parametric study carried out so far was for the undamped system with free joints. As in real life there are no ideal systems, so in the next phase of the parametric study viscous damping is introduced in all the d.o.f. The damping coefficient considered is realistic and accounts for the frequency spectrum associated with the individual generalized coordinate. The numerical values for the damping coefficient are presented in Table 3-1. In general, damped systems have an inherent tendency to be more stable.

Figure 3-16 presents damped response of the system having free joints and the flexible platform represented by the first free-mode. The deployable arm is held fixed at $a_5 = 10$ m while the slewing arm is initially oriented at $\beta_4 = 0$. The flexible platform is initially disturbed, in the first mode, so that q_1=0.1 m.

It is apparent from Figure 3-16(a) that introduction of the damping changes the slewing arm response substantially. Now the arm rotates in the positive direction (counterclockwise) about joint 1, as against the oscillatory motion in the undamped case. The damping torque of the rotor I_3, together with the inertia force field due to platform vibrations, force the arm to the monotonic response. The arm's rotational

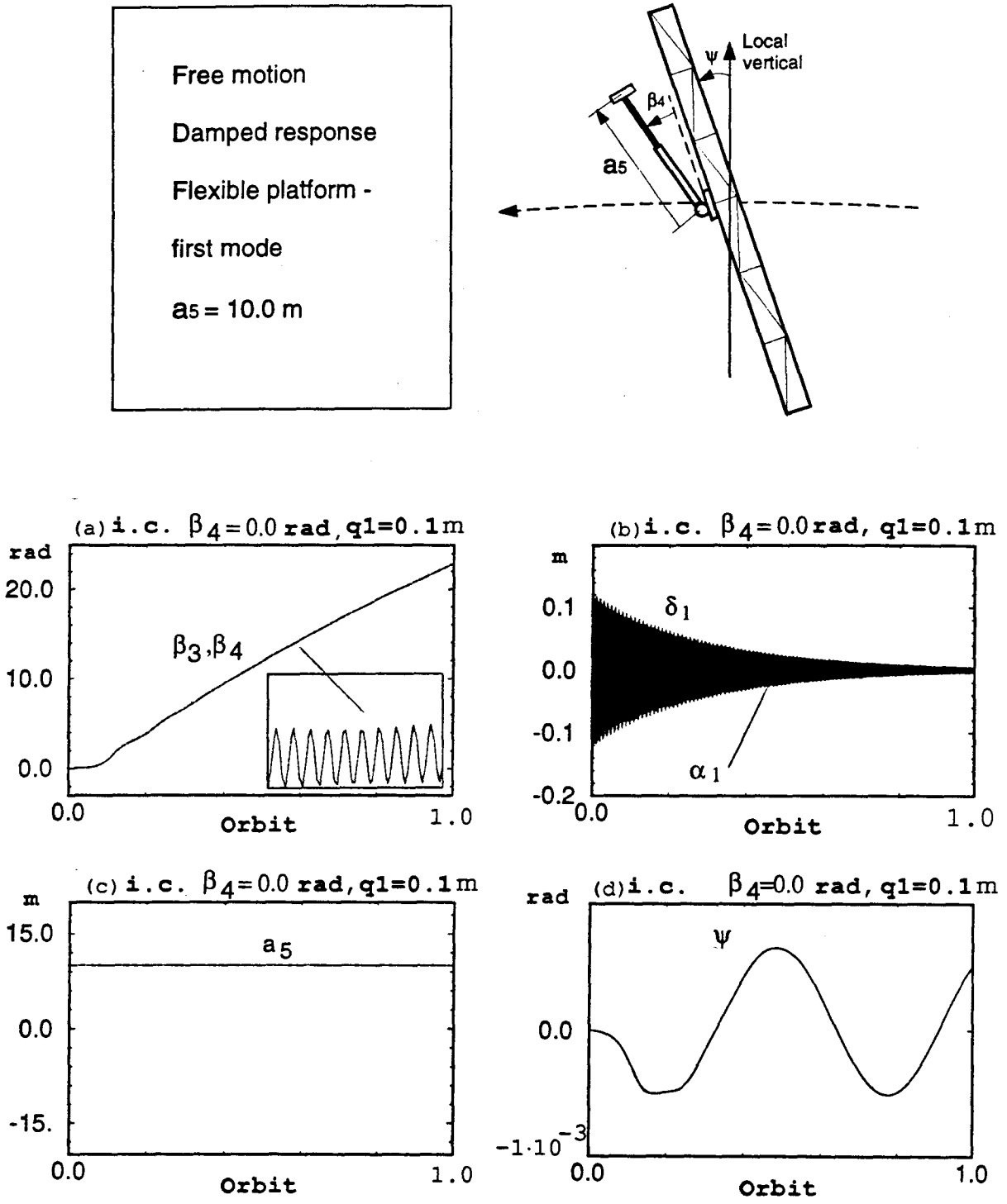

Figure 3-16 System open loop damped response, with the deployable d.o.f. frozen at $a_5 = 10$ m. The platform is initially excited in the first-mode with $q_1 = 0.1$ m.

rate decreased as the vibration amplitude decayed due to the structural damping of the platform truss (Figure 3-16b). The pitch amplitude also showed a slight decrease and the period of oscilation, as expected, approached $\sqrt{3}$(orbital period) as shown in Figure 3-16(d).

To accentuate the response, the MDM base was placed at the tip of the platform, i.e. h_1=60 m. The response results for this case are presented in Figure 3-17.

When the platform vibrations are relatively large (0.1 - 0.2 m) the slew-arm equilibrium position is shifted from $\beta_4 = 0$ to 1.5707 rad (90 deg). As the vibration amplitude decays the slew-arm starts to oscillate about $\beta_4 = 0$ with the amplitude decreasing due to the damping of the platform truss and the torque motor (Figure. 3-17a). The MDM base, being at the tip of the platform, experiences local rotation as indicated in Figure 3-18(c).

The reaction on the MDM base due to the arm oscillations, coupled with the platform vibrations, exert a relatively large moment about the center mass of the platform, especially when the MDM is located at the tip of the platform. The moment induce pitch oscillations of 0.01 rad (0.5 deg) as shown in Figure 3-17(d). The pitch and arm responses are modulated at a higher frequency of 0.18 Hz due to the platform vibrations as shown by the expanded view of ψ and β_4 time histories.

Based on the results, it can be concluded that introdution of damping affects the system dynamics directly through changes in the moments at the joints, and indirectly by reducing the magnitude of the response.

The MDM base can have a specified translation rate ($\dot{h}_1$) along the platform. A resonable base velocity is 0.02 m/s. In that case, the MDM base translates along the entire length of the platform in approximatly one orbit. As apparent from Figure 3-18(b), the base motion excites the platform vibrations at the beginning of the

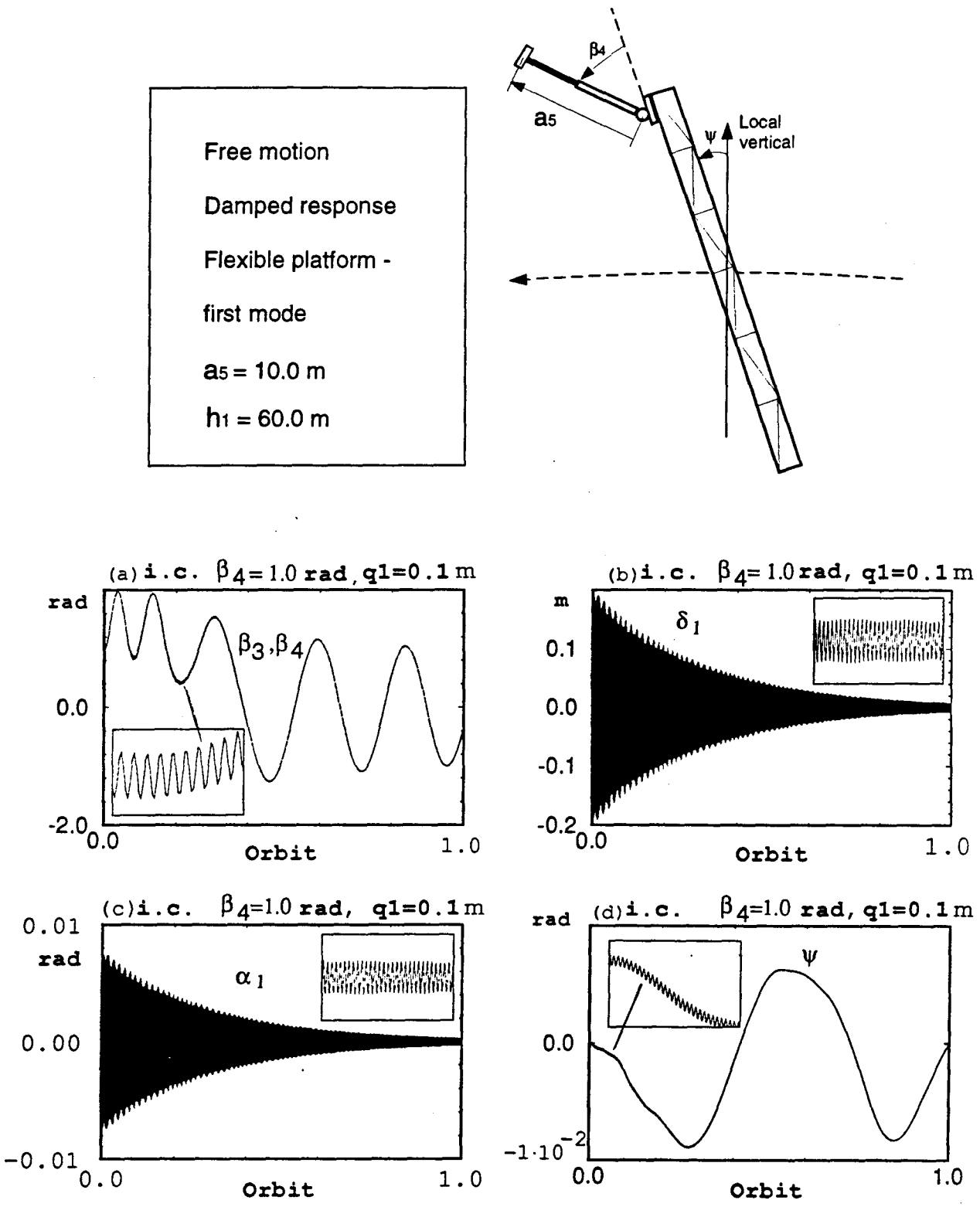

Figure 3-17 Damped response of the system with the deployable arm fixed at $a_5 = 10$ m, the MDM base held at $h_1 = 60$ m, and the slewing arm initially located at $\beta_4 = 1.0$ rad. The platform is set vibrating with an initial disturbance of $q_1 = 0.1$ m.

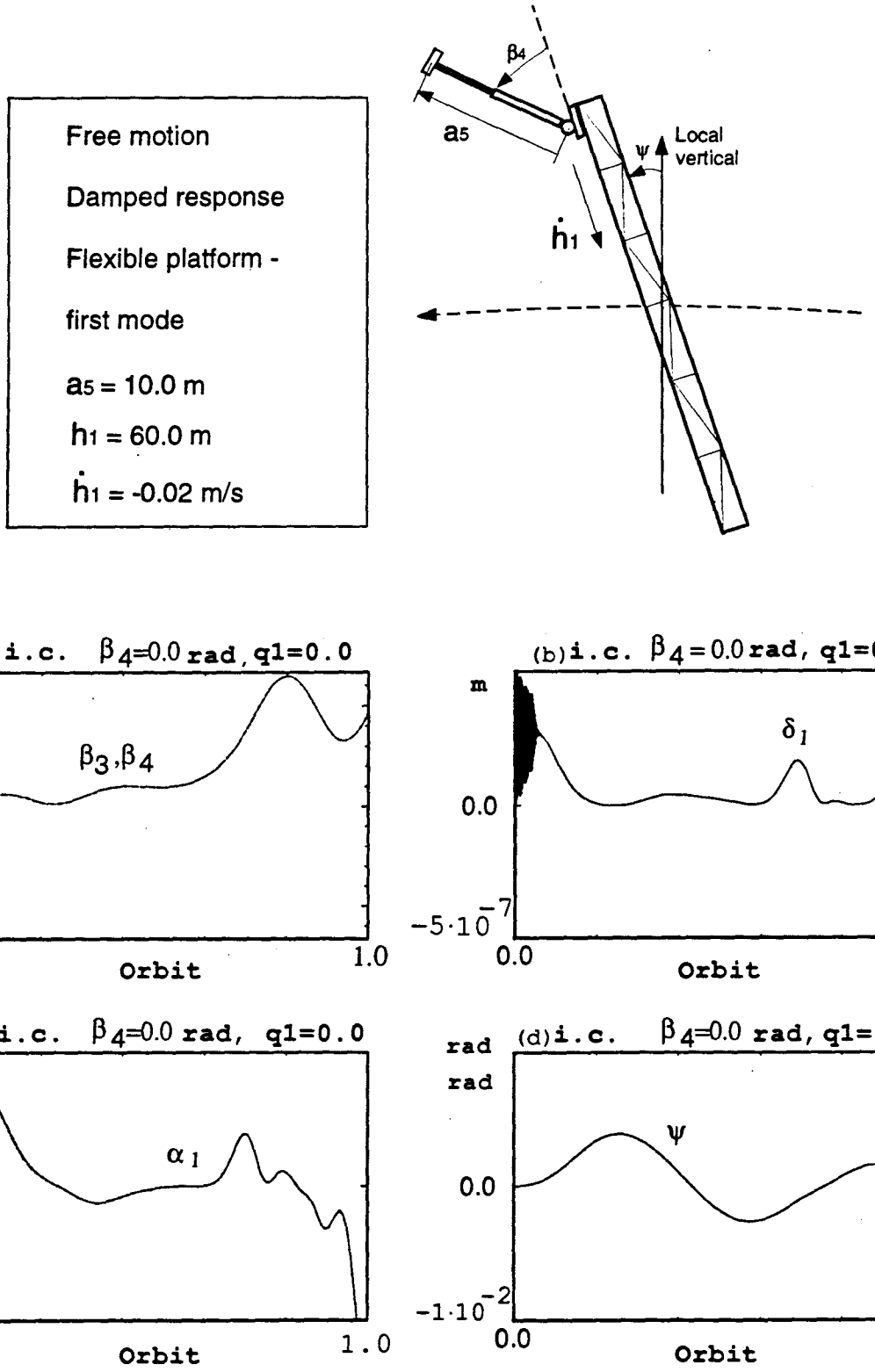

Figure 3-18 Effect of the MDM's translational maneuver, at $-0.02\ \frac{m}{s}$ on the flexible platform, from the initial location of $h_1 = 60$ m. The deployable arm is fixed at $a_5 = 10$ m. The initial conditions are: $\beta_4 = 0$; $q_1 = 0.1$ m.

translational maneuver; but the oscillations decay as the base advances along the platform. The movement of the reaction point along the vibrating platform, and the fact that the direction of the reaction on the flexible platform remains the same (as concluded from the slew arm response shown in Figure 3-18a), cause the vibrations to decay and the platform deflects according to the reaction moment.

The Coriolis and the gravitation moments about joint 1 cause the slew arm to rotate to the second equilibrium position when the resultant c.m. of the payload and the slew arm cross the orbital trajectory. In other words, the base is located 50 m from the second tip of the platform as can be seen in Figure 3-18(a). The reaction at the base excites the pitch motion as shown in Figure 3-18(d).

The free vibration analysis results suggest that the system response can be unpredictable and the instability may result under certain combinations of configuration and initial disturbances. Lateral inertia force field due to the vibrating platform can be used to orient the slewing arm in a predefined position.

3.3.5 Flexible system response to open loop torques

The next logical step is to introduce generalized forces and represent the platform flexibility more precisely through the necessary number of modes that would converge to the right response.

The MDM system is simulated with open loop torques applied through the motors located at the joints. The system parameters and configuration are according to the data in Tables 3-1 and 3-2, respectively. To start with, a constant torque of $T_3 = 1$ Nm is applied at joint 1, when joint 2 is locked with arm 2 deployed to 10 m. The system response is presented in Figure 3-19. In this reference case, the MDM is located at the center of the platform ($h_1 = 0$) and the flexibility is still represented

by the first mode. The initial conditions for all the d.o.f. are zero.

The applied torque causes the rotor I_3 and arm 1 to rotate through angle β_3 and β_4, respectively (Figure 3-19a). From the expanded view, it can be seen that the rotation of I_3 deviates by 0.001 rad w.r.t. the slew arm and oscillates at its natural frequency of 9.6 rad/s (1.5 Hz). The natural frequency is detemined by the inertia of the rotor and the joint stiffness, taking into account the gear ratio $n_3 = 1$ in this case. The relative rotation $(\beta_3 - \beta_4)$ is the actual twist of the torsional shaft due to the joint flexibility. The damped response of β_3 is due to the dissipation at the joint.

The rotation of the arm excites the flexible platform, with increasing frequency and amplitude, according to the rate of the slew (Figure 3-19b). From the expanded view it is apparent that the response is modulated at a frequency of 0.18 Hz associated with the first mode. As the MDM base is located at the geometric center of the platform, and only the first free-free mode is taken into account, the local slope α_1 is zero (Figure 3-19c). This, of course, does not reflect the reality as the applied torque must deform the platform asymmetrically.

The rotation of the arm, together with the platform vibrations, excite the pitch d.o.f. by a small amount as the MDM is located at the c.m. of the platform (Figure 3-19d). Note, the oscillations are about the new equilibrium position of $-1.6 \cdot 10^{-5}$ rad.

More general case is presented in Figure 3-20, where the MDM base is located at the tip of the platform ($h_1 = 60$ m), and the slewing arm's initial condition is $\beta_4 = 1.0$ rad.

The input torque to joint 1 balances the gravitational torque at $\beta_4 = 0.4$ rad, about which the slew arm is oscillating (Figure 3-20a). The deflection of the platform is affected at the begining by the torque motor oscillations, and later by the oscilla-

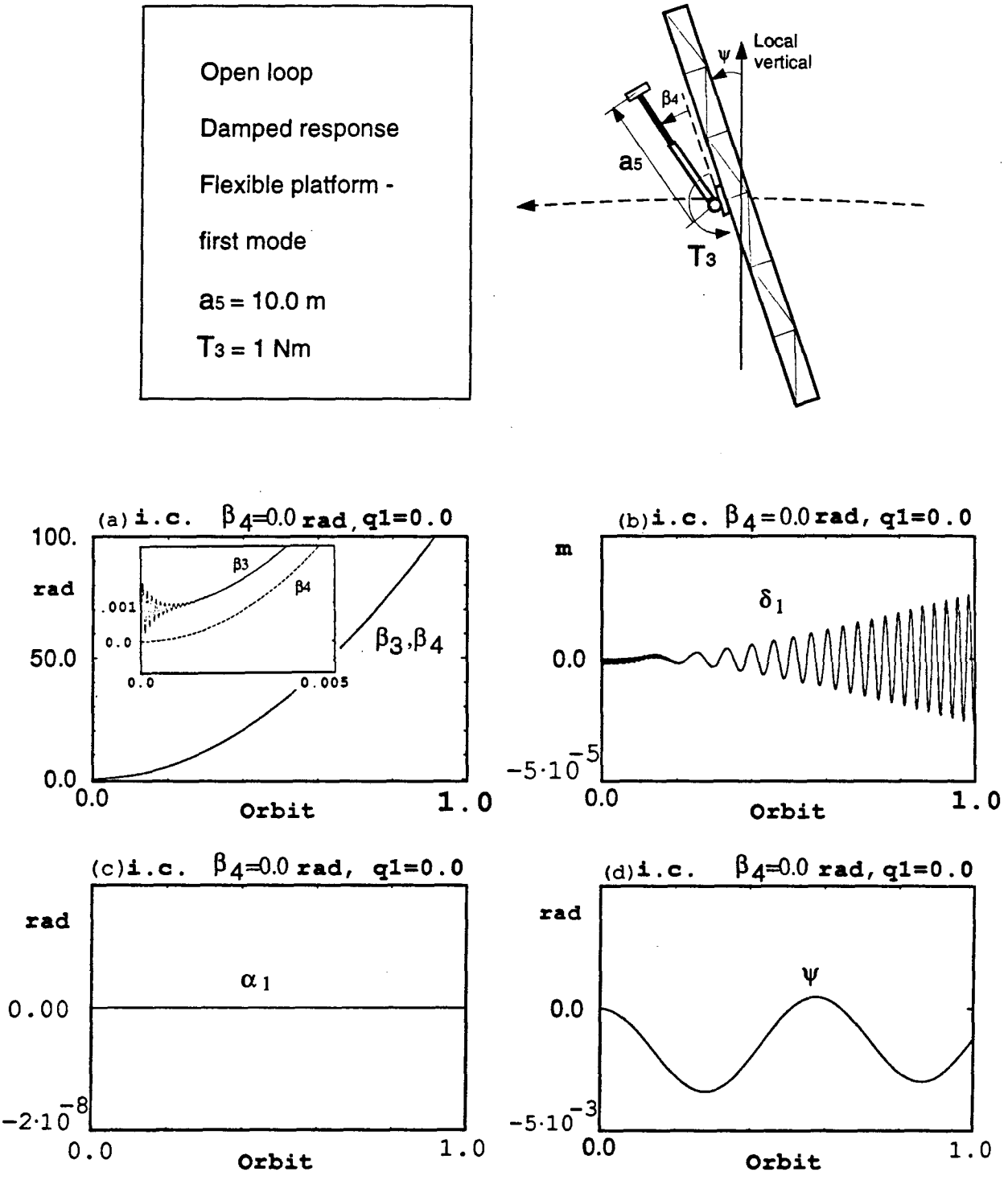

Figure 3-19 Response of the MDM system to a constant torque of 1 Nm applied at joint 1. The deployable d.o.f. is frozen at $a_5 = 10$ m, the manipulator is located at the midpoint of the flexible platform ($h_1 = 0$). The platform flexibility is represented by the first mode.

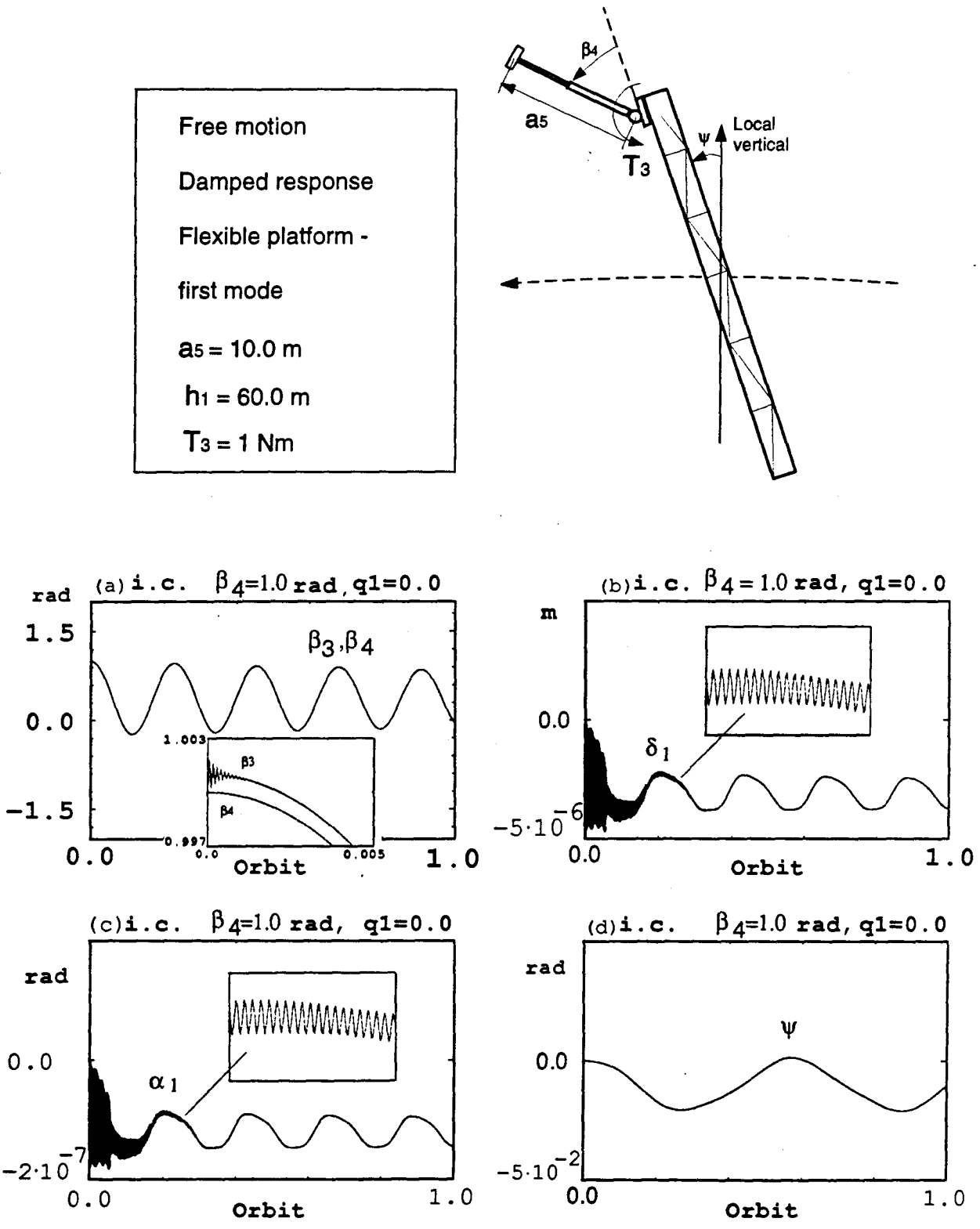

Figure 3-20 Open loop response of the MDM with a constant torque $T_3 = 1$ Nm applied at joint 1. The deployable d.o.f. is frozen at $a_5 = 10$ m. The base is located at $h_1 = 60$ m and the platform flexibility is represented by the first mode. The initial arm position is $\beta_4 = 1.0$ rad.

tions of the arm as shown in Figure 3-20(b). The time history of the local slope at $h_1 = 60$ m is presented in Figure 3-20(c). Both the platform deflection as well as rotation (libration) remain quite small.

Next, to better model the system, the platform flexibilty was represented by the first two modes. For the present case, the natural frequency of the first (symmetric) mode is 1.13 rad/s (0.18 hz) and the second (antisymmetric) mode is 3.11 rad/s (0.5 Hz). The corresponding simulation results are presented in Figure 3-21. System configuration and parameter values are the same as those for the case discussed in Figure 3-19.

Comparing the response results in Figures 3-21(b), 3-21(c) with those in Figure 3-19, clearly reveals the discrepancies. The local slope α_1 is the result of the reaction torque $-T_3$ acting on the platform at $h_1 = 0$. The expanded view in Figure 3-21(c) clearly shows, that the slope is modulated at a higher frequency of 0.5 Hz, which corresponds to the second mode. Obviously, it can be concluded that one mode is not enough to represent the flexible platform.

To progress further towards a more realistic simulation of the system behaviour, open loop torques $T_3 = 1$ Nm and $T_5 = -1$ Nm were applied to joints 1 and 2, respectively. The MDM base was located at the tip of the platform, $h_1 = 60$ m, and the initial conditions of $\beta_4 = 1.0$ rad and $a_5 = 10$ m for the slew and deployable arms, respectively, were applied. The platform flexibility was simulated with an increasing number of modes to assess the effect on the dynamical response. This set of results are presented in Figures 3-22 to 3-26.

The response of joint 1, the slew-arm and the deployable-arm, as represented by the generalized coordinates β_3, β_4 and a_5, respectively, is presented in Figures 3-22(a) to 3-26(a). The deployable-arm is retrived as a result of T_5, where the small

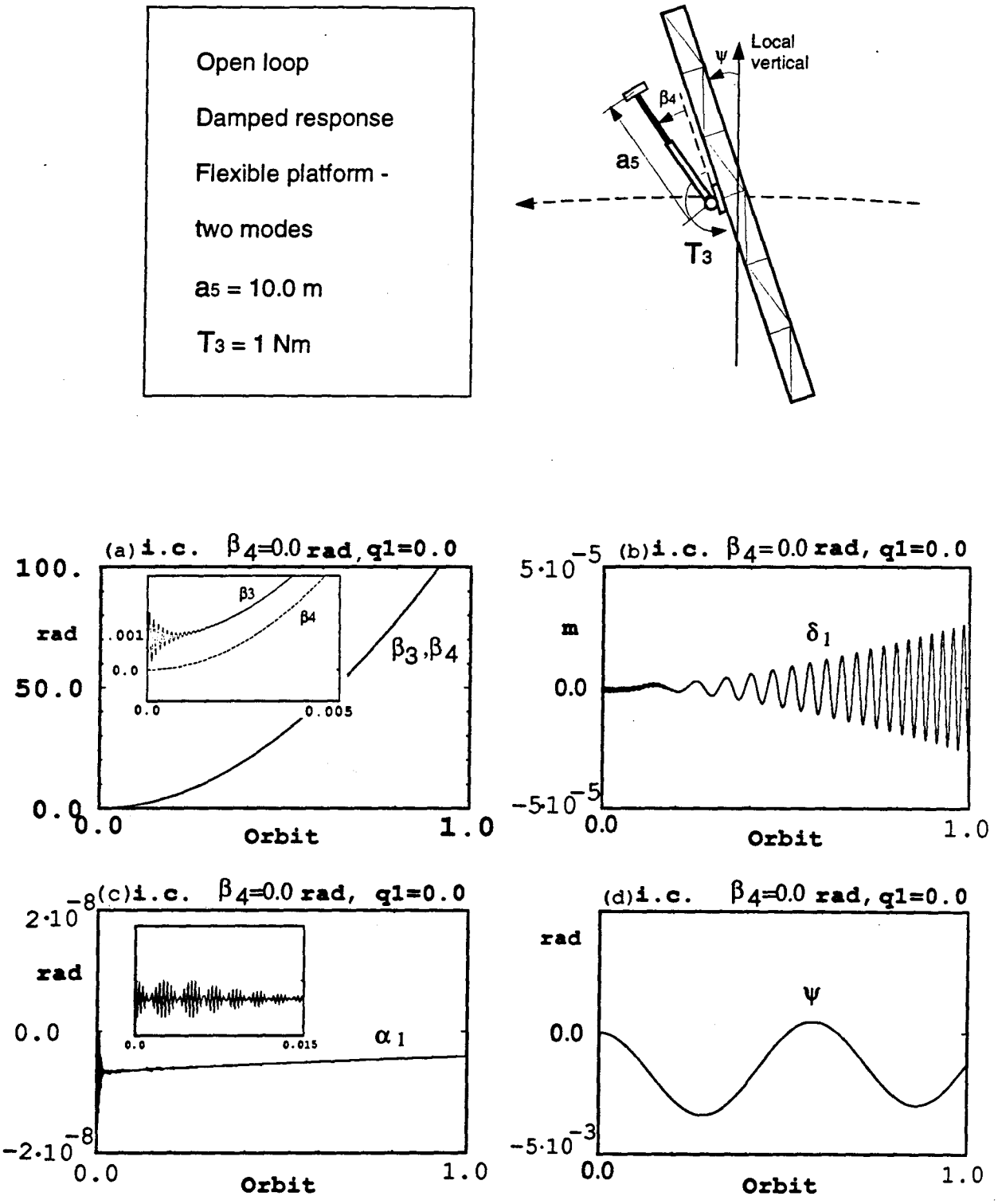

Figure 3-21 System response to a constant torque $T_3 = 1$ Nm applied at joint 1. The deployable arm is held at $a_5 = 10$ m. The manipulator is located at the midpoint of the platform and the platform flexibility is represented by the first two modes.

fluctuations are due to coupling with the slew arm oscillations. As can be seen, the equilibrium position is shifted as a result of a decrease in the gravity moment (payload approaches the joint). In general, the system response remains virtually unchanged due to inclusion of the second mode (Figure 3-23). However, the platform deflection δ_1 and local slope α_1 do show some sensitivity to the number of modes (Figures 3-23, 3-24 and 3-25). Now the joints oscillations at 9.6 rad/s (1.5 Hz) exite the third and the forth flexible modes with natural frequencies of 1 Hz and 1.6 Hz, respectively. Adding the fifth mode with a natural frequency of 15 rad/sec (2.4 Hz), the platform becomes less sensitive to the oscillations of the joints, as apparent in Figure 3-26.

The main conclusion based on the last parametric study may be stated as follows: For flexible systems with multiple degrees of freedom (flexible and rigid), the coupling effects are considerable. For the cases demanding extreme accuracy, it is necessary to take in account additional modes beyond the fundamental, to accurately model the platform deflection and slope. However, in most situations, representation of the flexibility by a single mode may be adequate. In the present study, the accuracy is dictated by the desired tracking performance of the MDM and the system attitude. For tracking of a specified trajectory with the end effector, an accuracy of 0.01 m is considered adequate. On the other hand, for the antenna pointing and stationkeeping the librational control with an accuracy of 0.001 rad (0.05 deg) is an accepted standard. Most of the elastic energy contribution comes from the first mode. In the subsequent closed loop study, the first two modes representing the symmetric and antisymetric character of the system are used to model flexibility of the platform.

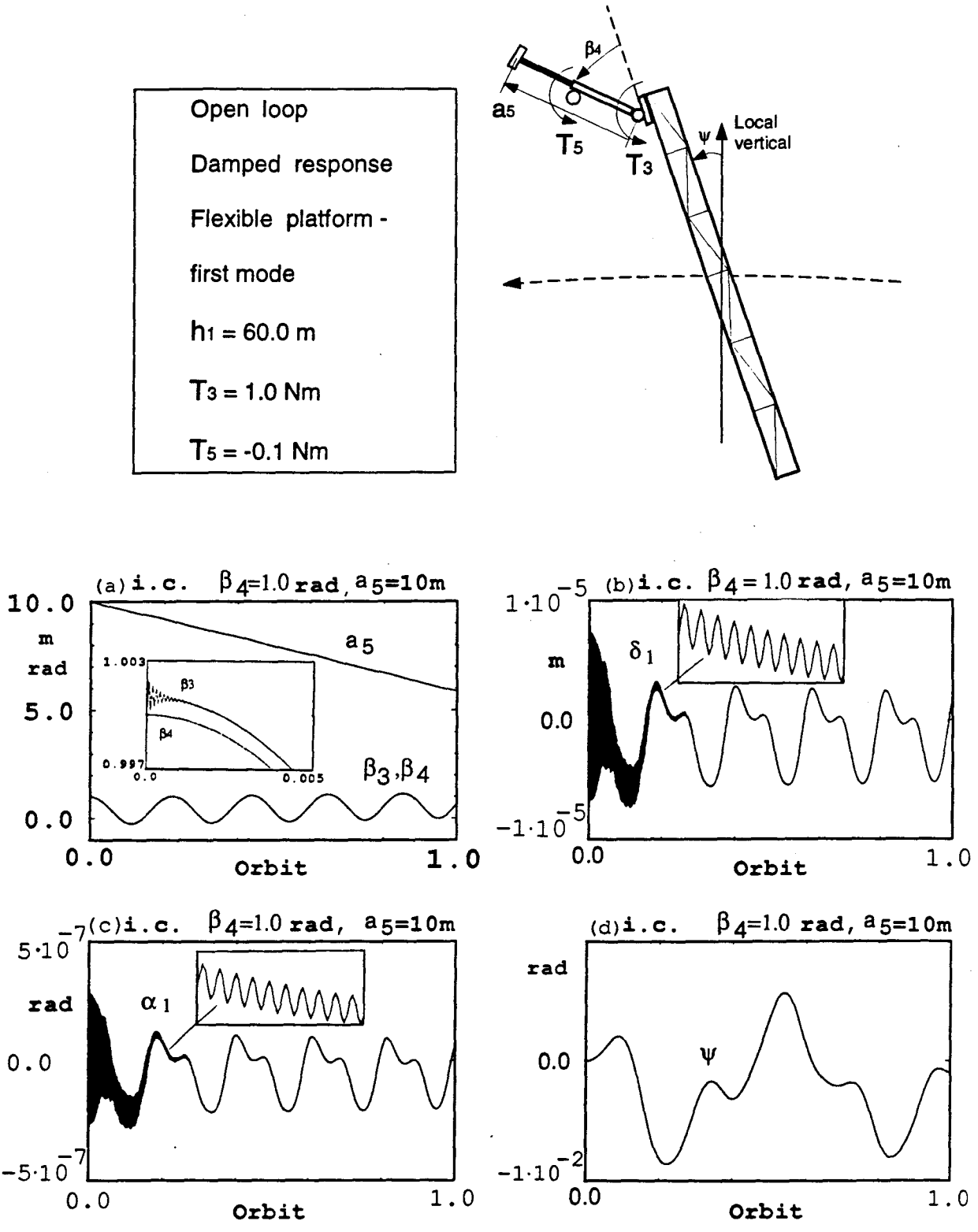

Figure 3-22 System response to open loop torques $T_3 = 1$ Nm, $T_5 = -1$ Nm, assuming one flexible mode. The MDM base is located at $h_1 = 60$ m. The initial conditions are: $\beta_4 = 1$ rad; $a_5 = 10$ m.

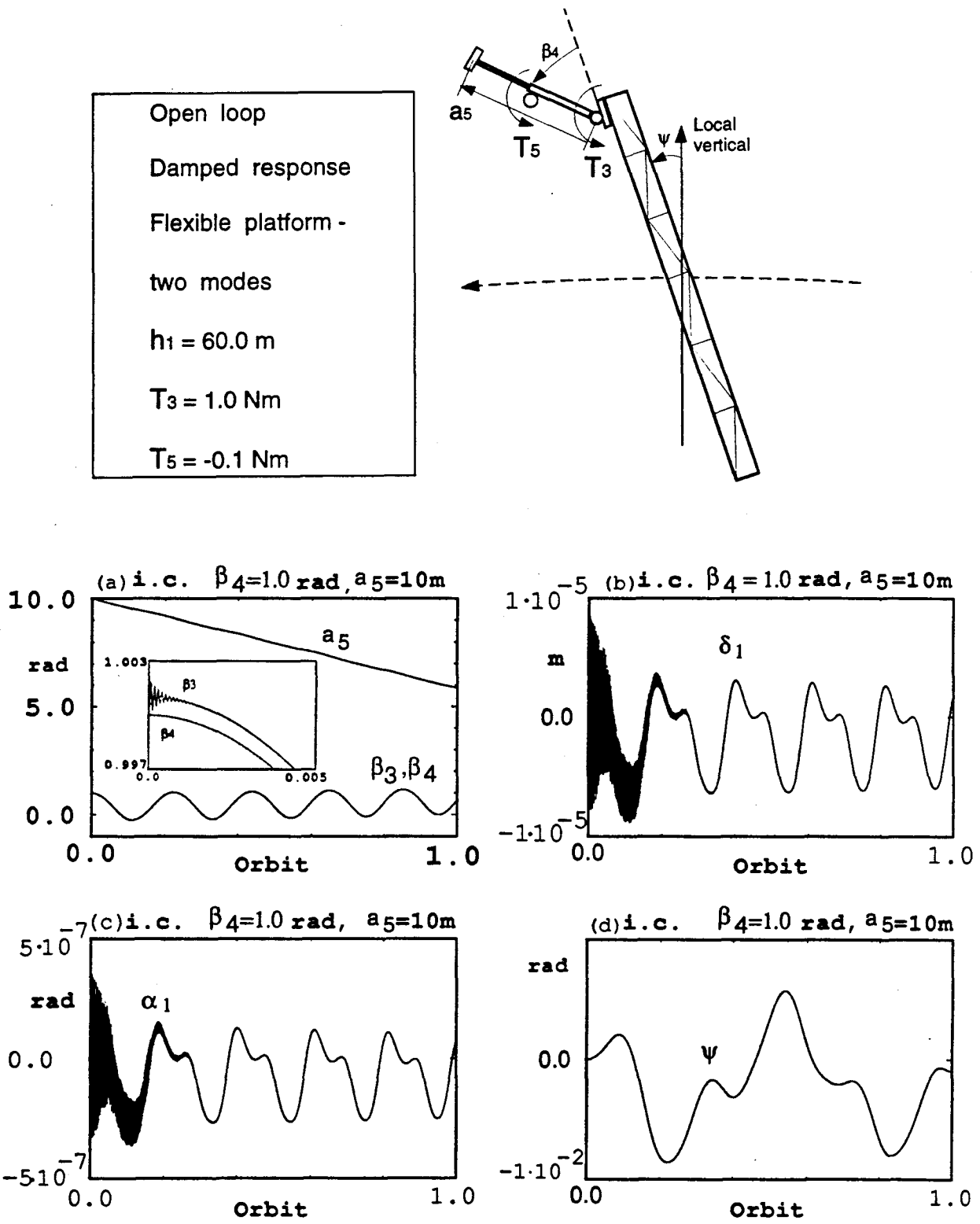

Figure 3-23 System response to open loop torques $T_3 = 1$ Nm, $T_5 = -1$ Nm, assuming two flexible modes. The MDM base is located at $h_1 = 60$ m. The initial conditions are: $\beta_4 = 1$ rad; $a_5 = 10$ m.

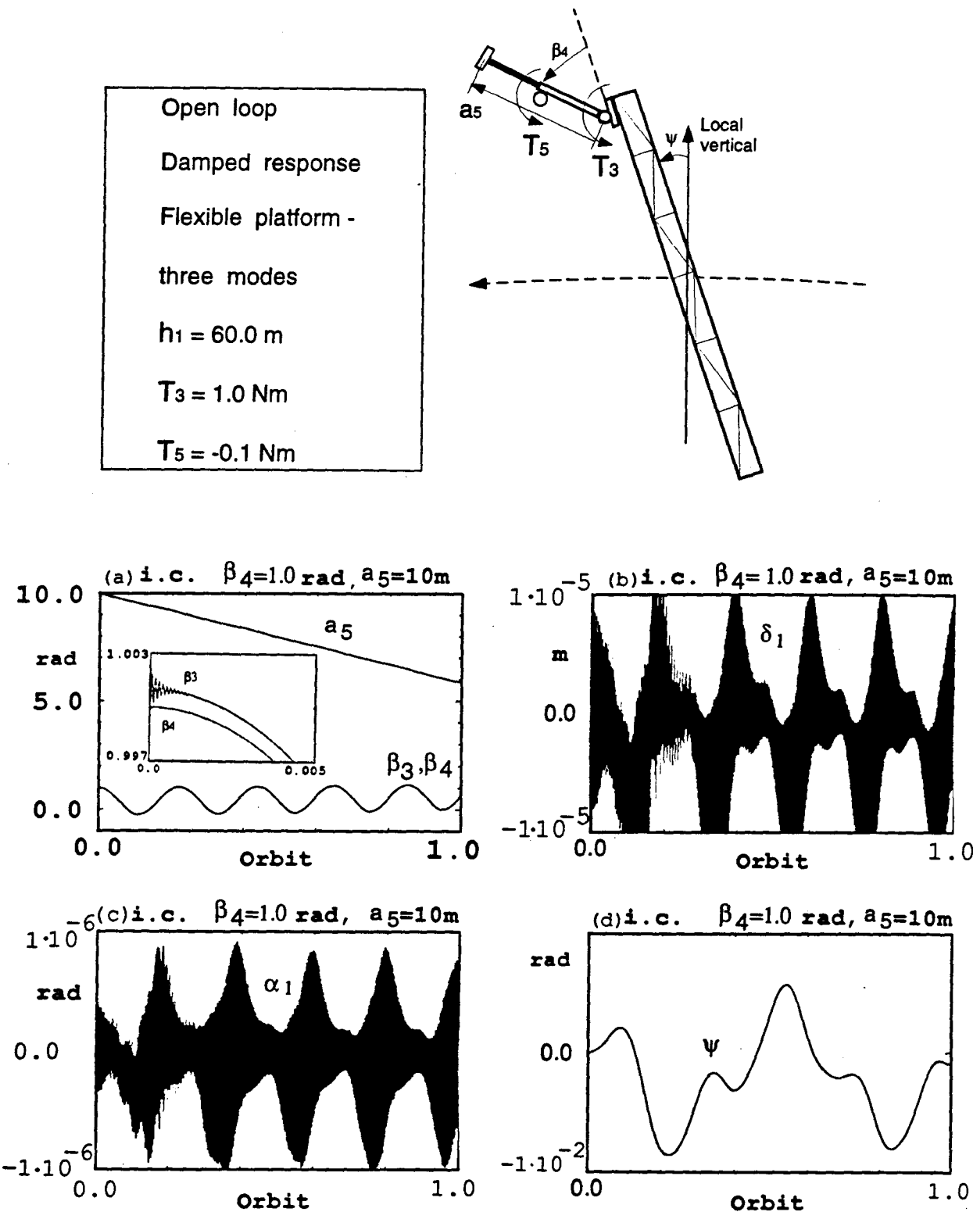

Figure 3-24 System response to open loop torques $T_3 = 1$ Nm, $T_5 = -1$ Nm, assuming three flexible modes. The MDM base is located at $h_1 = 60$ m with the system initial conditions as: $\beta_4 = 1$ rad; $a_5 = 10$ m.

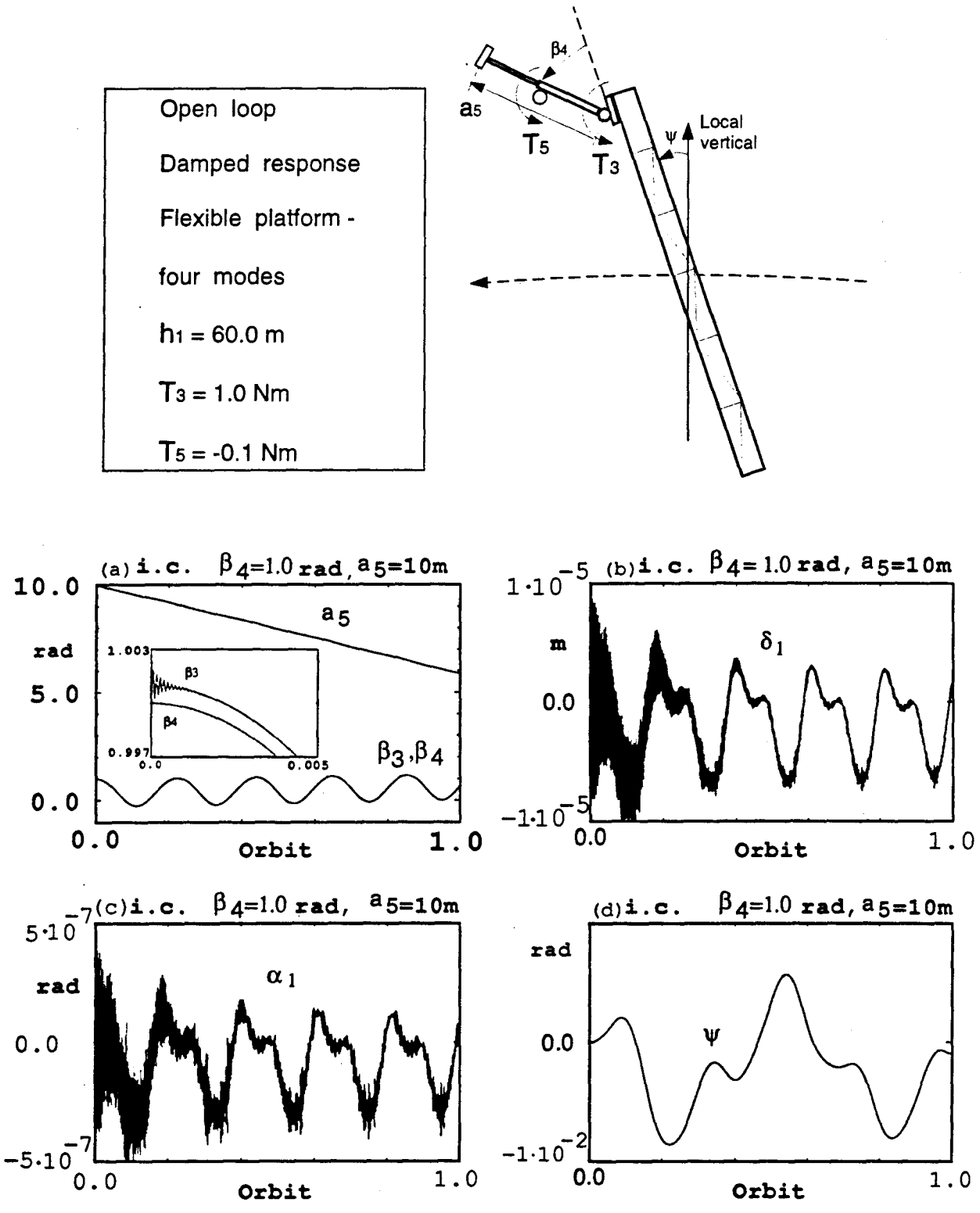

Figure 3-25 System response to open loop torques $T_3 = 1$ Nm, $T_5 = -1$ Nm, assuming four flexible modes. The MDM base is located at $h_1 = 60$ m and the initial conditions are: $\beta_4 = 1$ rad; $a_5 = 10$ m.

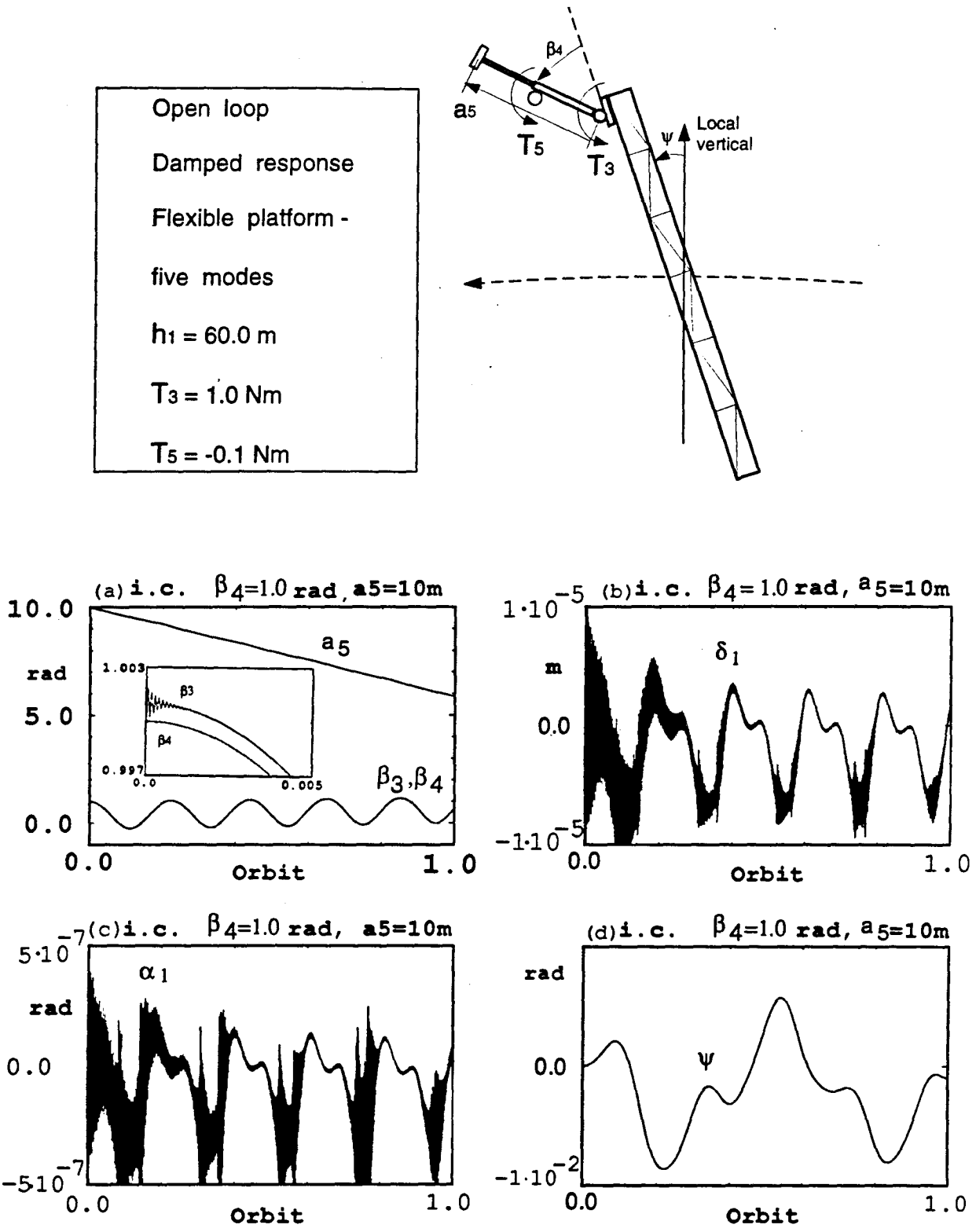

Figure 3-26 System response to open loop torques $T_3 = 1$ Nm, $T_5 = -1$ Nm, assuming five flexible modes. The MDM base is located at $h_1 = 60$ m and the initial conditions are: $\beta_4 = 1$ rad; $a_5 = 10$ m.

3.4 Summary

The chapter focused on the open loop dynamics of the MDM system using a versatile simulation tool. In general, derivation of the equations of motion and development of a computer code demand considerable amount of effort. In the present study it was minimized by structuring the equations judiciously to make the programming process more efficient. Furthermore, the computer code is structured in a modular form, thus facilitating the debugging procedure and the parametric study.

The validity of the formulation and the computer code have been established through: comparison with particular cases; checking the conservation of system energy; and by comparison with the analytical closed-form solution of a particular case.

An extensive parametric study, with an increasing order of complexity, provided insight into the complex and, at times, unexpected behaviour of the system. It helped assess the effects of platform and joints flexibilities, damping and generalized forces on the system dynamics.

From the open loop study it can be concluded that, for the space based manipulators, control of the generalized coordinates is a necessity imposed by the complex nonlinear, nonautonomous and coupled dynamics, extreme flexibility, and demanding accuracy. Compared with the conventional ground based robots, it is not possible to rely even on the so called 'stable' equilibrium position.

Description of the desired tasks and their realization through control are the issues addressed in the following chapters.

4. DESIRED TASK DEFINITION

As concluded in Chapter 3, a controlled MDM system is required in order to accomplish a predefined task. In the case of the proposed space station the manipulator will perform tasks usually w.r.t. the platform or the platform based modules.

The MDM as described in Chapter 2 operates in the joint-variables space. On the other hand, tasks to be performed, such as the space station assembly, operation, and maintenance, are usually expressed in the space station fixed coordinate system. In some cases, tasks are defined w.r.t. the orbital or the earth based coordinate system, e.g. aiming of an accurate instrumantation such a telescope and a communications antenna, transfer of payload from the space station to the shuttle, etc.

In order to control the position and orientation of the MDM's end effector so that it can perform the desired tasks, the inverse kinematics solution is more important. In other words, given the desired position and orientation of the end effector w.r.t. the selected reference coordinate system (station based, orbital or inertial frame) and the MDM parameters, it is necessary to find the corresponding MDM d.o.f. ψ, β_4 and a_5, so that the end effector can be positioned as desired. Thus, it is necessary to find the required controlled variable ψ_d, β_{4d}, a_{5d} in order to close the loop.

A number of methods are available to tackle an inverse kinematic problem. They include inverse transform, quaternion, iterative and geometric approaches, and others. Paul et al. [1] have presented an inverse transform technique using the 4×4 homogeneous transformation matrices to solve the kinematic problem. This approach is adopted in the present study to define the required MDM d.o.f. for performing the desired tasks.

4.1 MDM Kinematic Equations

In this section the homogeneous transformation, that represents the position and orientation of the end effector coordinate frame F_6 with respect to the chosen station based coordinate frame, has been developed.

The MDM is treated as a two degrees of freedom robot, on a translating and rotating base, with revolute and prismatic flexible joints as shown in Figure 4-1.

The position and orientation of the end effector frame F_6 with respect to a reference coordinate frame (i.e. the station or the orbital frame in the present case) is described by the homogeneous transformation matrix [H],

$$[H] = [B] \cdot [T_2] \cdot [E]. \tag{4.1}$$

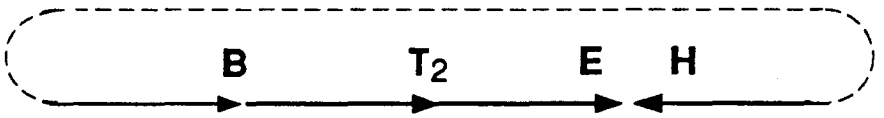

here:

[B] homogeneouse transformation matrix relating the manipulator base frame F_2 to the reference frame;

[T_2] homogeneouse transformation matrix relating the manipulator end frame F_6 to the base frame F_2;

[E] homogeneous transformation matrix relating the end effector to the manipulator end. This, in the present case, is a unit matrix as a separate end effector is not considered.

[T_2] can be expressed as a product of the arms' transformation matrices,

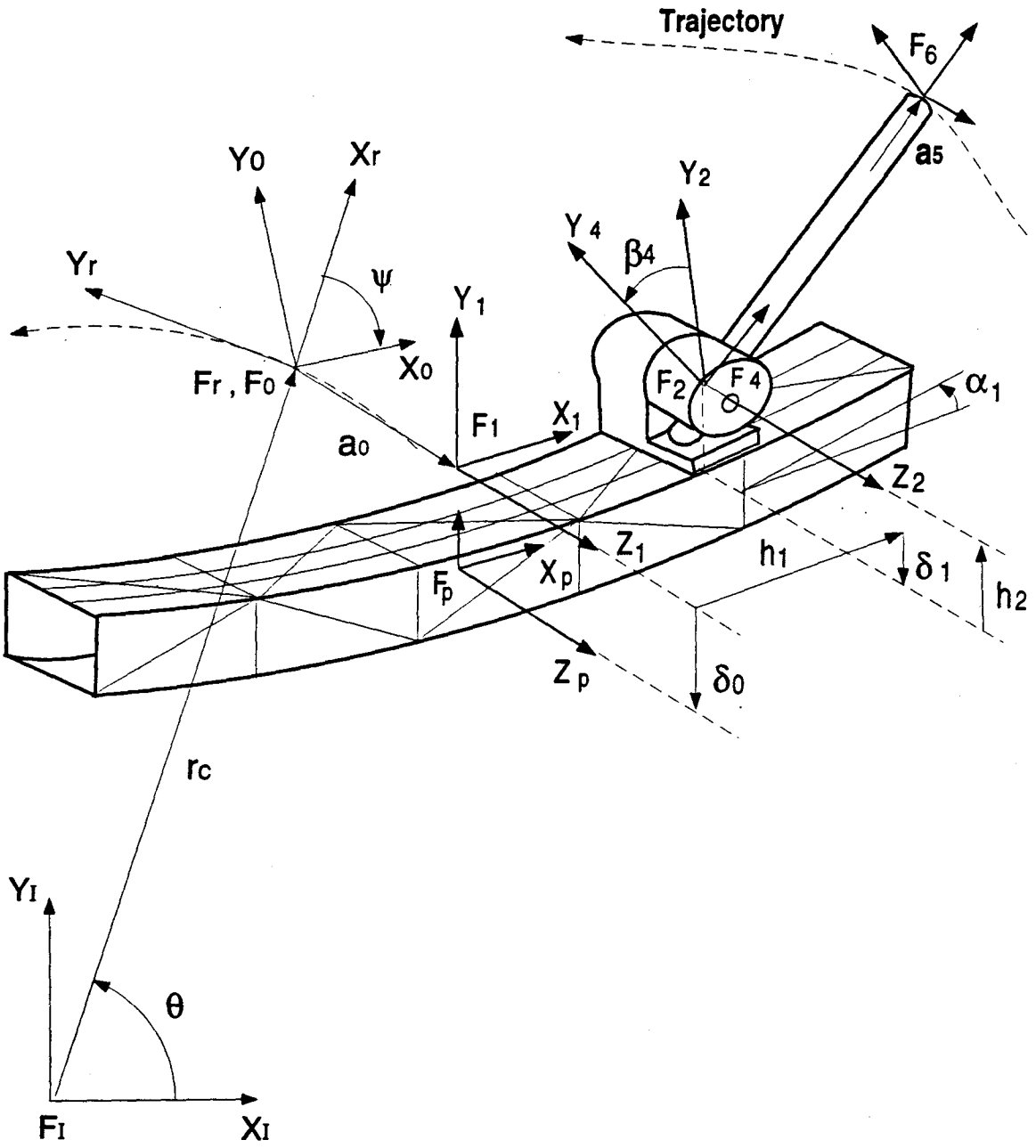

Figure 4-1 Reference coordinate frames established for the inverse kinematics study of the MDM system.

$$[T_2] = [A_1] \cdot [A_2], \tag{4.2}$$

where:

$[A_1]$ homogeneous transformation matrix relating the coordinate frame F_4 of the slewing arm to the base frame F_2;

$[A_2]$ homogeneous transformation matrix relating the deployable arm frame F_6 to the slewing arm frame F_4.

From Figure 4-1, which establishs the arm based coordinate frames, it is possible to determine the homogeneous transformation for each arm:

$$[A_1] = \begin{bmatrix} cos\beta_4 & 0 & sin\beta_4 & 0 \\ sin\beta_4 & 0 & -cos\beta_4 & 0 \\ 0 & 1 & 0 & 0 \\ 0 & 0 & 0 & 1 \end{bmatrix}; \tag{4.3}$$

$$[A_2] = \begin{bmatrix} 1 & 0 & 0 & 0 \\ 0 & 1 & 0 & 0 \\ 0 & 0 & 1 & a_5 \\ 0 & 0 & 0 & 1 \end{bmatrix}. \tag{4.4}$$

Substituting $[A_1]$ and $[A_2]$ into Eq. (4.2) gives the arms' homogeneous transformation matrix $[T_2]$ as

$$[T_2] = \begin{bmatrix} cos\beta_4 & 0 & sin\beta_4 & a_5 sin\beta_4 \\ sin\beta_4 & 0 & -cos\beta_4 & -a_5 cos\beta_4 \\ 0 & 1 & 0 & 0 \\ 0 & 0 & 0 & 1 \end{bmatrix}. \tag{4.5}$$

The task to be performed by the MDM can be defined w.r.t. the platform reference frame F_p (Figure 4-1), the orbital frame F_r or to the inertial frame F_I (Figure 2-2). The platform reference frame is fixed to the geometric center of the platform and displaced by an amount δ_0 (due to the platform deflection at h_1=0) from F_1,

which is fixed to the center of mass of the platform as shown in Figure 4-1,

$$\delta_0 = \bar{\phi}_1^T(0)\bar{q}_1, \tag{4.6}$$

where δ_0 is the platform's deflection at its center.

The orbital refernce frame F_r is displaced through $\bar{a}_0$ and rotated by an angle ψ w.r.t. F_1. The inertial reference frame F_I is translated through $\bar{r}_c$ and rotated by an amount θ w.r.t. F_r as shown in Figures 2-2, and 4-1.

As most of the tasks planned for the MDM are confined to the space station, they are defined in this study w.r.t. the frame F_p.

The MDM base homogeneous transformation $[B_p]$ takes into account the translations (TRANS) and rotations (ROT) of the base frame F_2 w.r.t. the chosen reference frame F_p as follows,

$$[B_p] = TRANS[(h_1 - h_2 sin\alpha_1), (\delta_1 + h_2 cos\alpha_1 - \delta_0), 0]ROT[Z_p, (\frac{\pi}{2} + \alpha_1)], \tag{4.7}$$

where:

$[B_p]$ MDM base homogeneous transformation to the platform reference frame F_p;

h_1 location of the base along the platform;

h_2 distance between joint 1 and the center line of the platform;

δ_1 platform deflection at h_1.

In the matrix representation, the base homogeneous transformation has the following form,

$$[B_p] = \begin{bmatrix} -sin\alpha_1 & -cos\alpha_1 & 0 & h_1 - h_2^{\bullet} sin\alpha_1 \\ cos\alpha_1 & -sin\alpha_1 & 0 & \delta_1 - \delta_0 + h_2 cos\alpha_1 \\ 0 & 0 & 1 & 0 \\ 0 & 0 & 0 & 1 \end{bmatrix}. \tag{4.8}$$

The homogeneous transformation matrix $[H_p]$, which specifies the location of the MDM end coordinate frame F_6 w.r.t. the platform coordinate frame, is the chain product of the successive coordinate transformation matrices $[B_p]$ and $[T_2]$, and can be expressed as

$$[H_p] = [B_p][T_2]. \tag{4.9}$$

Substituting transformation matrices from Eqs. (4.5) and (4.8) into Eq. (4.9) gives

$$[H_p] = \begin{bmatrix} -sin\gamma & 0 & cos\gamma & a_5 cos\gamma + h_1 - h_2 sin\alpha_1 \\ cos\gamma & 0 & sin\gamma & a_5 sin\gamma + \delta_1 - \delta_0 + h_2 cos\alpha_1 \\ 0 & 1 & 0 & 0 \\ 0 & 0 & 0 & 1 \end{bmatrix}, \tag{4.10}$$

where $[H_p]$ is the homogeneous transformation between the MDM end and the platform based frame. Here: $\gamma = \alpha_1 + \beta_4$.

4.2 Inverse Kinematics for Point Tracking

In the previous section the relationships between the position and orientation of the coordinate frame that defines the MDM end and the actual system d.o.f. have been established. The relationships that define the position are also functions of the MDM base instanteneous location along the platform (h_1) and the shift of the revolute joint w.r.t. the platform center line (h_2).

In this section the above mentioned relationships are used with the inverse transform technique to determine the requied MDM d.o.f. (required control variables) for a desired position of the payload.

A given task for the MDM is defined by the instanteneous desired position and orientation of the end effector w.r.t. the chosen reference frame (F_p in this case). For time dependent variable position the desired task describes a trajectory in the reference frame.

A desired task, in the planar case, can be represented by a homogeneous transformation matrix $[H_{pd}]$ with known elements as

$$[H_{pd}] = \begin{bmatrix} n_x & 0 & a_x & p_x \\ n_y & 0 & a_y & p_y \\ 0 & 0 & 0 & 0 \\ 0 & 0 & 0 & 1 \end{bmatrix}, \tag{4.11}$$

where p_x,p_y are the components of the desired position, with n_x,n_y, and a_x,a_y as the components of the desired orientation. The required angular position β_{4d} of the slew arm and the required linear position a_{5d} of the deployable arm, to impart specified position and orientation to the payload (end effector), can be found using the inverse transform technique as follows.

Rewriting Eq. (4.9) for the desired case as

$$[H_{pd}] = [B_p][T_{2d}], \tag{4.12}$$

and premultiplying both sides with $[B_p]^{-1}$ gives

$$[B_p]^{-1}[H_{pd}] = [B_p]^{-1}[B_p][T_{2d}]. \tag{4.13}$$

After some mathematical manipulations, it is possible to present Eq. (4.13) in the form

$$\begin{bmatrix} f_1(n) & 0 & f_1(a) & f_1(p) \\ f_2(n) & 0 & f_2(a) & f_2(p) \\ f_3(n) & 0 & f_3(a) & f_3(p) \\ 0 & 0 & 0 & 1 \end{bmatrix} = [T_{2d}], \tag{4.14}$$

$[T_{2d}]$ is the homogeneous transformation $[T_2]$ of Eq. (4.5) with the required values of β_4 and a_5;

$$f_1 = -sin\alpha_1(x) + cos\alpha_1(y) + h_1 sin\alpha_1 - (\delta_1 - \delta_0)cos\alpha_1 - h_2; \tag{4.15}$$

$$f_2 = -cos\alpha_1(x) - sin\alpha_1(y) + h_1 cos\alpha_1 + (\delta_1 - \delta_0)sin\alpha_1; \tag{4.16}$$

$$f_3 = 1(z); \tag{4.17}$$

and x,y,z refer to components of the vectors given as arguments of f_1,f_2, and f_3.

Equating the fourth column on both sides of Eq. (4.14) gives the following relations:

$$f_1(p) = a_{5d} sin\beta_{4d}; \tag{4.18}$$

$$f_2(p) = -a_{5d} cos\beta_{4d}. \tag{4.19}$$

Dividing Eq. (4.18) by Eq. (4.19), β_{4d} can be evaluate from

$$tan\beta_{4d} = -\frac{f_1(p)}{f_2(p)}. \tag{4.20}$$

Substituting $f_1(p)$ and $f_2(p)$ from Eqs. (4.15) and (4.16), respectively into Eq. (4.20) gives the required value for the slew,

$$\beta_{4d} = tan^{-1}\left[\frac{(p_x - h_1)sin\alpha_1 + (\delta_1 - \delta_0 - p_y)cos\alpha_1 + h_2}{(\delta_1 - \delta_0 - p_y)sin\alpha_1 + (h_1 - p_x)cos\alpha_1}\right]. \tag{4.21}$$

Note, β_{4d} is a function of the trajectory parameters p_x and p_y, the instanteneous base location h_1 along the platform, the location of the joint w.r.t. the platform h_2, the instanteneous platform deflections δ_0, δ_1, and the local slope α_1. It should be recognized that β_{4d} is a function of time even for the stationary end effector (p_x, p_y constants) w.r.t. the reference frame.

To determine the required value of the deployment a_5, Eq. (4.13) is premultiplied by $[A_1]^{-1}$,

$$[A_1]^{-1}[B_p]^{-1}[H_{pd}] = [A_1]^{-1}[T_{2d}] = [A_{2d}]. \tag{4.22}$$

Algebraic manipulations lead to the relation

$$\begin{bmatrix} f_1(n) & 0 & f_1(a) & f_1(p) \\ f_2(n) & 0 & f_2(a) & f_2(p) \\ f_3(n) & 0 & f_3(a) & f_3(p) \\ 0 & 0 & 0 & 1 \end{bmatrix} = [A_{2d}], \tag{4.23}$$

where $[A_{2d}]$ is the homogeneous transformation of Eq.(4.4) with the required value of a_5.

Here:

$$f_1 = -s(\alpha_1+\beta_4)(x)+c(\alpha_1+\beta_4)(y)+h_1 s(\alpha_1+\beta_4)-(\delta_1-\delta_0)c(\alpha_1+\beta_4)-h_2 c\beta_4; \quad (4.24)$$

$$f_2 = 1(z); \quad (4.25)$$

$$f_3 = c(\alpha_1+\beta_4)(x)+s(\alpha_1+\beta_4)(y)-h_1 c(\alpha_1+\beta_4)-(\delta_1-\delta_0)s(\alpha_1+\beta_4)$$
$$-h_2 s\beta_4. \quad (4.26)$$

Equating the third element of the fourth column on two sides of Eq. (4.23) gives the following relation for a_{5d} (with β_4=β_{4d} as obtained from Eq. 4.21),

$$a_{5d} = (p_x - h_1)cos(\alpha_1+\beta_{4d})+(p_y-\delta_1+\delta_0)sin(\alpha_1+\beta_{4d})-h_2 sin\beta_{4d}. \quad (4.27)$$

As in the case of the β_{4d}, a_{5d} is also a function of time, even for the stationary end effector (p_x, p_y constants) w.r.t. the reference frame.

Let the MDM degrees of freedom β_4 and a_5 be the required value as given in Eqs. (4.21) and (4.27), respectively. Now the end effector will meet the desired trajectory position. For the control purpose, it is important to have required velocity and acceleration for the degrees of freedom. From Figure 4-2, the following kinematic relationships for the desired trajectory can be obtained,

$$tan\beta_{4d} = \frac{u}{v}, \quad (4.28)$$

with u and v defined from Eq. (4.21) as:

$$u = (h_1 - p_x)sin\alpha_1 + (p_y+\delta_0-\delta_1)cos\alpha_1 - h_2; \quad (4.29)$$

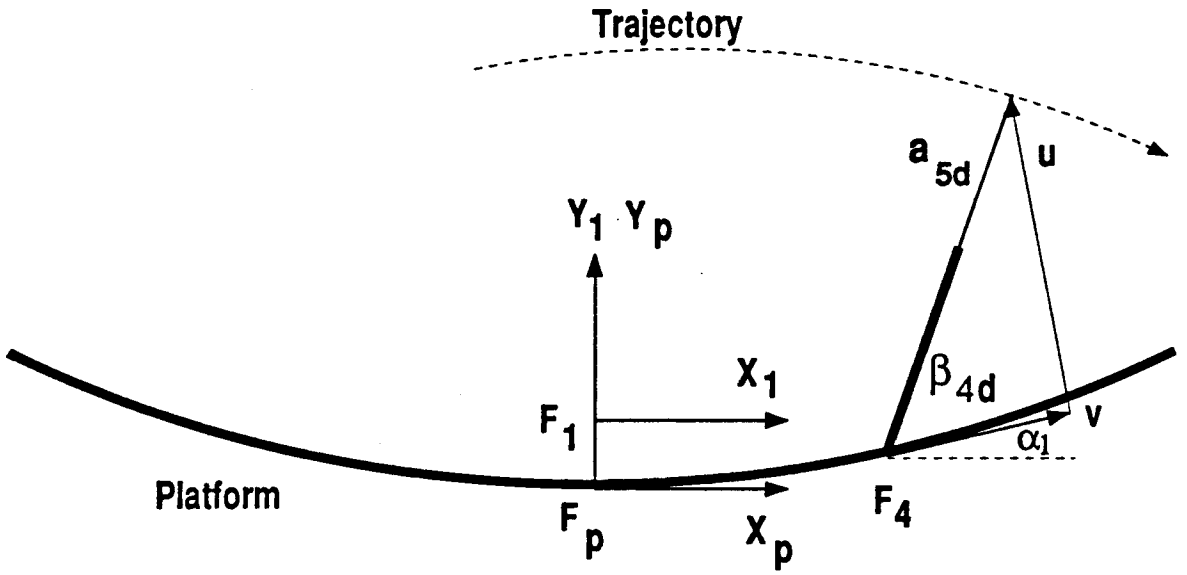

$$tan\beta_{4d} = \left[\frac{(p_x - h_1)sin\alpha_1 + (\delta_1 - \delta_0 - p_y)cos\alpha_1 + h_2}{(\delta_1 - \delta_0 - p_y)sin\alpha_1 + (h_1 - p_x)cos\alpha_1}\right] = \frac{u}{v}$$

$$u = (h_1 - p_x)sin\alpha_1 + (p_y + \delta_0 - \delta_1)cos\alpha_1 - h_2$$

$$v = (p_y + \delta_0 - \delta_1)sin\alpha_1 + (p_x - h_1)cos\alpha_1$$

$$\dot{a}_{5d} = \dot{v}cos\beta_{4d} + \dot{u}sin\beta_{4d}$$

$$\ddot{a}_{5d} = \ddot{v}cos\beta_{4d} + \ddot{u}sin\beta_{4d}$$

$$\dot{\beta}_{4d} = \frac{\dot{u}cos\beta_{4d} - \dot{v}sin\beta_{4d}}{a_{5d}}$$

$$\ddot{\beta}_{4d} = \frac{\ddot{u}cos\beta_{4d} - \ddot{v}sin\beta_{4d}}{a_{5d}}$$

Figure 4-2 Kinematic relationships.

$$v = (p_y + \delta_0 - \delta_1)sin\alpha_1 + (p_x - h_1)cos\alpha_1. \tag{4.30}$$

Now the required velocity and acceleration can be obtained from the corresponding components of the trajectory as:

$$\dot{a}_{5d} = \dot{v}cos\beta_{4d} + \dot{u}sin\beta_{4d}; \tag{4.31}$$

$$\ddot{a}_{5d} = \ddot{v}cos\beta_{4d} + \ddot{u}sin\beta_{4d}; \tag{4.32}$$

$$\dot{\beta}_{4d} = \frac{\dot{u}cos\beta_{4d} - \dot{v}sin\beta_{4d}}{a_{5d}}; \tag{4.33}$$

$$\ddot{\beta}_{4d} = \frac{\ddot{u}cos\beta_{4d} - \ddot{v}sin\beta_{4d}}{a_{5d}}; \tag{4.34}$$

where $\dot{u}$, $\dot{v}$, $\ddot{u}$, $\ddot{v}$ are obtain by differentiating u,v in equations (4.29) and (4.30) w.r.t. time.

4.3 Matching of the End Effector Position and Orientation

In the previous section, the required MDM degrees of freedom β_{4d}, a_{5d} and their first and second time derivatives were evaluated in order to negotiate the desired end effector trajectory. For some tasks, orientation of the MDM end effector, w.r.t. the reference coordinate, may also be importent, in addition to its position. For the planar case, this would require an additional degree of freedom besides the slew and deployment. To meet this requirment, the proposed space station based Mobile Servicing System (MSS) is equipped with the Special Purpose Dexterous Manipulator (SPDM). In the present study, the obvious solution is to consider the translation h_1 along the platform as the additional degree of freedom. Of course, addition of a generalized coordinate will further complicate the simulation. As no flexibility is involved in the base translation system, and the base's mass is negligible compared to those of the platform, arm and the payload, it is taken to be specified. Thus the motion of the base (h_1) is specified in such a way that the MDM orientation

requirment is met. Note, the system degrees of freedom are coupled with the base motion (h_1,$\dot{h}_1$, $\ddot{h}_1$) as apparent from the r.h.s. of Eq. (III.1). However, as mentioned before, the base motion is not affected by the system generalized coordinates.

To evaluate the required base position h_{1d}, the third columns from two sides of Eq. (4.14) are equated giving:

$$f_1(a) = sin\beta_{4d}; \tag{4.35}$$

$$f_2(a) = -cos\beta_{4d}. \tag{4.36}$$

Dividing Eq. (4.35) by Eq. (4.36) gives β_{4d} as a function of the desired end effector orientation

$$\beta_{4d} = tan^{-1}[-\frac{f_1(a)}{f_2(a)}]. \tag{4.37}$$

Substiting for $f_1(a)$ and $f_2(a)$ from Eqs. (4.15) and (4.16), respectively into Eq. (4.37) leads to

$$\beta_{4d} = tan^{-1}\left[\frac{(a_x - h_1)sin\alpha_1 + (\delta_1 - \delta_0 - a_y)cos\alpha_1 + h_2}{(\delta_1 - \delta_0 - a_y)sin\alpha_1 + (h_1 - a_x)cos\alpha_1}\right]. \tag{4.38}$$

Note, the required slew β_{4d} is a function of the desired orientation parameters a_x, a_y and the instanteneous base location h_1 along the platform.

The required base position h_{1d} is now found by equating the two expressions for β_{4d} in (4.21) and (4.38),

$$h_{1d} = \frac{-p_x a_y + p_y a_x - (a_x - p_y)(\delta_1 - \delta_0 + h_2 cos\alpha_1)}{p_y - a_y} + h_2 sin\alpha_1. \tag{4.39}$$

Note,, h_{1d} is a function of the desired trajectory (p_x, p_y) as well as the orientation (a_x, a_y). Furthermore, the h_{1d} depends on the platform deflections δ_1, δ_0 and the local slope α_1 which are functions of $\bar{q}_1$. From the equations of motion (2.37) and Appendix III, it is clear that the platform flexibility generalized coordinate $\bar{q}_1$ itself is

a function of h_1, $\dot{h}_1$, $\ddot{h}_1$. This suggests that the h_{1d} must be calculated by an iterative procedure.

To have a constant arm orientation while the end is tracking a desired trajectory, the base must translate at a velocity $\dot{h}_{1d}$ which is proportional to the trajectory velocity and the platform deflection rate. It can be determined by differentiating Eq. (4.39) w.r.t. time.

4.4 Task with respect to the orbit

In this case, the homogeneous transformation from the MDM base frame F_2 to the orbital frame F_r takes into account the system libration ψ and shift in the center of mass $\bar{a}_0$,

$$[B_r] = TRANS[(a_{0x} + h_1 - h_2 sin\alpha_1), (a_{0y} + \delta_1 + h_2 cos\alpha_1), 0] ROT[Z_r, (\psi + \frac{\pi}{2} + \alpha_1)], \tag{4.40}$$

where:

$[B_r]$ MDM base homogeneous transformation to the orbital refernce frame F_r;

ψ system libration;

a_{0x},a_{0y} components of the shift of the system c.m. w.r.t. the frame F_0.

In the matrix notation, the base homogeneous transformation has the form

$$[B_r] = \begin{bmatrix} -s(\psi+\alpha_1) & -c(\psi+\alpha_1) & 0 & (a_{0x}+h_1)c\psi - (\delta_1+a_{0y})s\psi - h_2 s(\psi+\alpha_1) \\ c(\psi+\alpha_1) & -s(\psi+\alpha_1) & 0 & (a_{0x}+h_1)s\psi + (a_{0y}+\delta_1)c\psi + h_2 c(\psi+\alpha_1) \\ 0 & 0 & 1 & 0 \\ 0 & 0 & 0 & 1 \end{bmatrix}. \tag{4.41}$$

The homogeneous transformation matrix $[H_r]$, which specifies the location of the MDM end effector frame F_6 w.r.t. the orbital coordinate frame, is the chain product of the successive coordinate transformation matrices $[B_r]$, $[T_2]$ and can be expressed

as

$$[H_r] = [B_r][T_2]. \tag{4.42}$$

Substituting from Eqs. (4.5) and (4.41) into Eq. (4.42) gives the transformation as

$$[H_r]=$$

$$\begin{bmatrix} -s(\psi+\gamma) & 0 & c(\psi+\gamma) & a_5c(\psi+\gamma)+(h_1+a_{0x})c\psi-(\delta_1+a_{0y})s\psi-h_2s(\psi+\alpha_1) \\ c(\psi+\gamma) & 0 & c(\psi+\gamma) & a_5s(\psi+\gamma)+(h_1+a_{0x})s\psi+(\delta_1+a_{0y})c\psi+h_2c(\psi+\alpha_1) \\ 0 & 0 & 1 & 0 \\ 0 & 0 & 0 & 1 \end{bmatrix}, \tag{4.43}$$

were $\gamma = \alpha_1+\beta_4$, and β_{4d}, a_{5d}, h_{1d} are obtained using the inverse kinematic technique as developed in Sections 4.2 and 4.3.

4.5 Parametric Study

In the previous section the MDM required degrees of freedom β_{4d}, α_{5d} and the base location h_{1d} to meet a desired payload trajectory and orientation w.r.t. the platform reference frame were defined.

An investigation to study the effects of the system parameters on the required degrees of freedom β_{4d} and a_{5d} has been carried out in this section. The main objective in the parametric study is to present the effects of the platform flexibility on the required d.o.f. when following various trajectories with different initial conditions. To begin with, the system is simulated with the rigid platform. The required d.o.f. obtained for this case will serve as the reference for the simulations that take into account the platform flexibility. Both the stationary point tracking as well as trajectory tracking are considered for the flexible system parameter study.

4.5.1 Trajectory tracking for the rigid system

In this subsection the required degrees of freedom for the rigid system tracking a

predefined trajectory, while the MDM base is moving, are presented. This case, where the desired trajectory is defined w.r.t. the platform, is similar to a rigid ground based robot moving on its track.

The simulation results for a constant speed base motion, as well as the accelerated base, starting from the center of the platform, are presented in Figures 4-3 and 4-4, respectively. In both the cases, the payload is initially located on the platform 10 m from its midpoint (arms' total length 10 m). The duration of the tasks are 0.02 orbit (111 s).

Figure 4-3(a) presents a desired trajectory, a straight path traversed at a constant velocity in the Y_p direction at $X_p = 10$ m. The translation of the MDM base at 0.01 m/s is shown in Figure 4-3(b). The required slew (β_{4d}) and deployment (a_{5d}) time histories are also presented (Figures 4-3c and 4-3d, respectively). As can be seen, close to the constant rates of 0.001 rad/s and -0.01 m/s are required for the slew and the deployment, respectively.

Figure 4-4 shows a more complex case where the desired trajectory forms a curved path. It represents the payload accelerating at $-0.005\ m/s^2$ and $0.002\ m/s^2$ in the X_p and Y_p directions, respectively where, at the starting point (10,0), the velocity is 0.2 m/s and 0.03 m/s in the X_p and Y_p directions, respectively. The payload must negotiate the desired trajectory, with the base accelerating at $0.001\ m/s^2$, as shown in Figure 4-4(b).

The time histories of the requirmed slew (β_{4d}) and deployment (a_{5d}) for the above mentioned task are indicated in Figures 4-4(c) and 4-4(d), respectively. Note, in this case, a relatively slow variation of the d.o.f. is required, hence the control problem can be solved relatively easily. It is important to remember that the MDM base is moving on a rigid platform while the joints, where the control input is applied, are

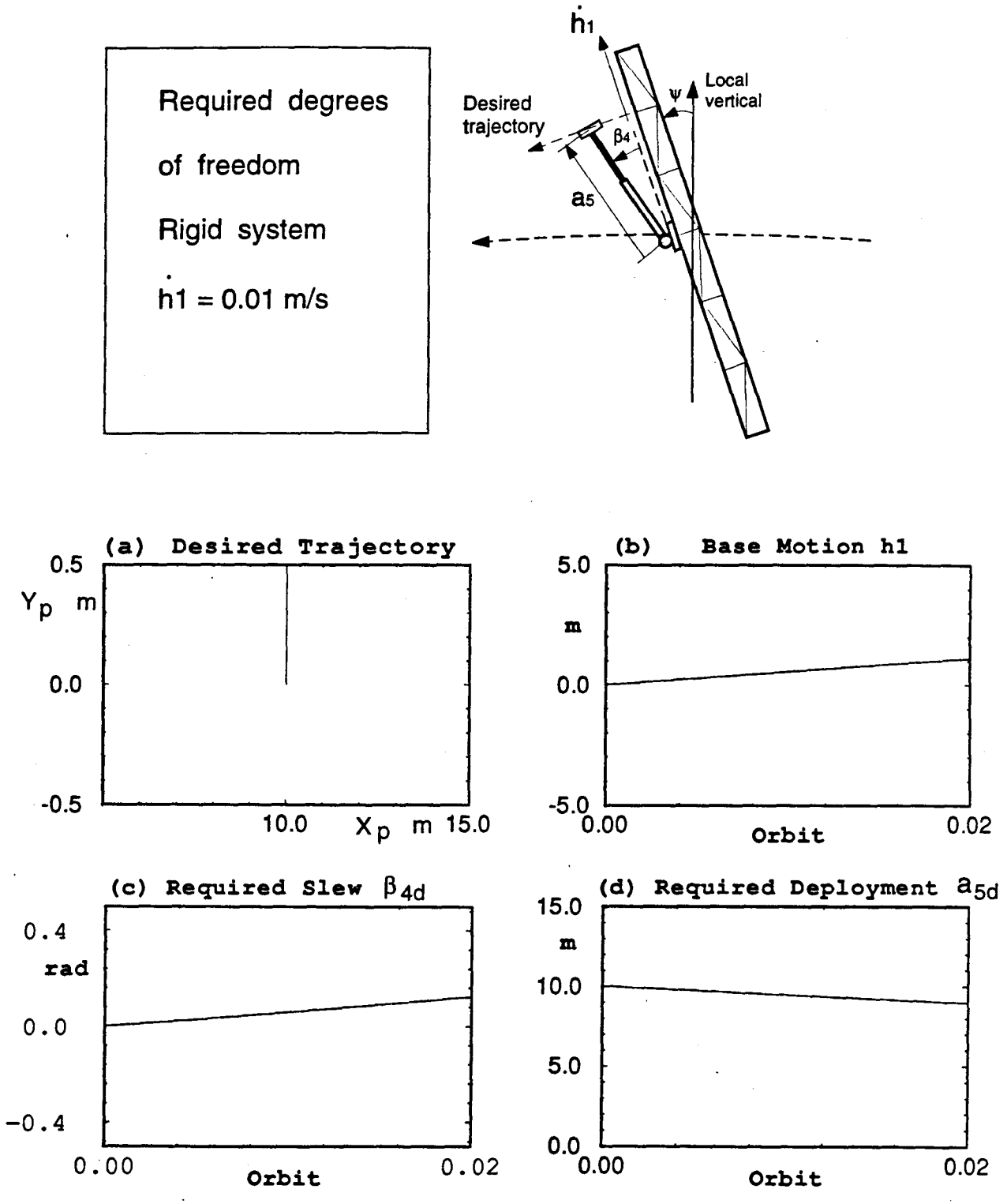

Figure 4-3 Time histories for the required positions of the degrees of freedom with a constant rate of base motion.

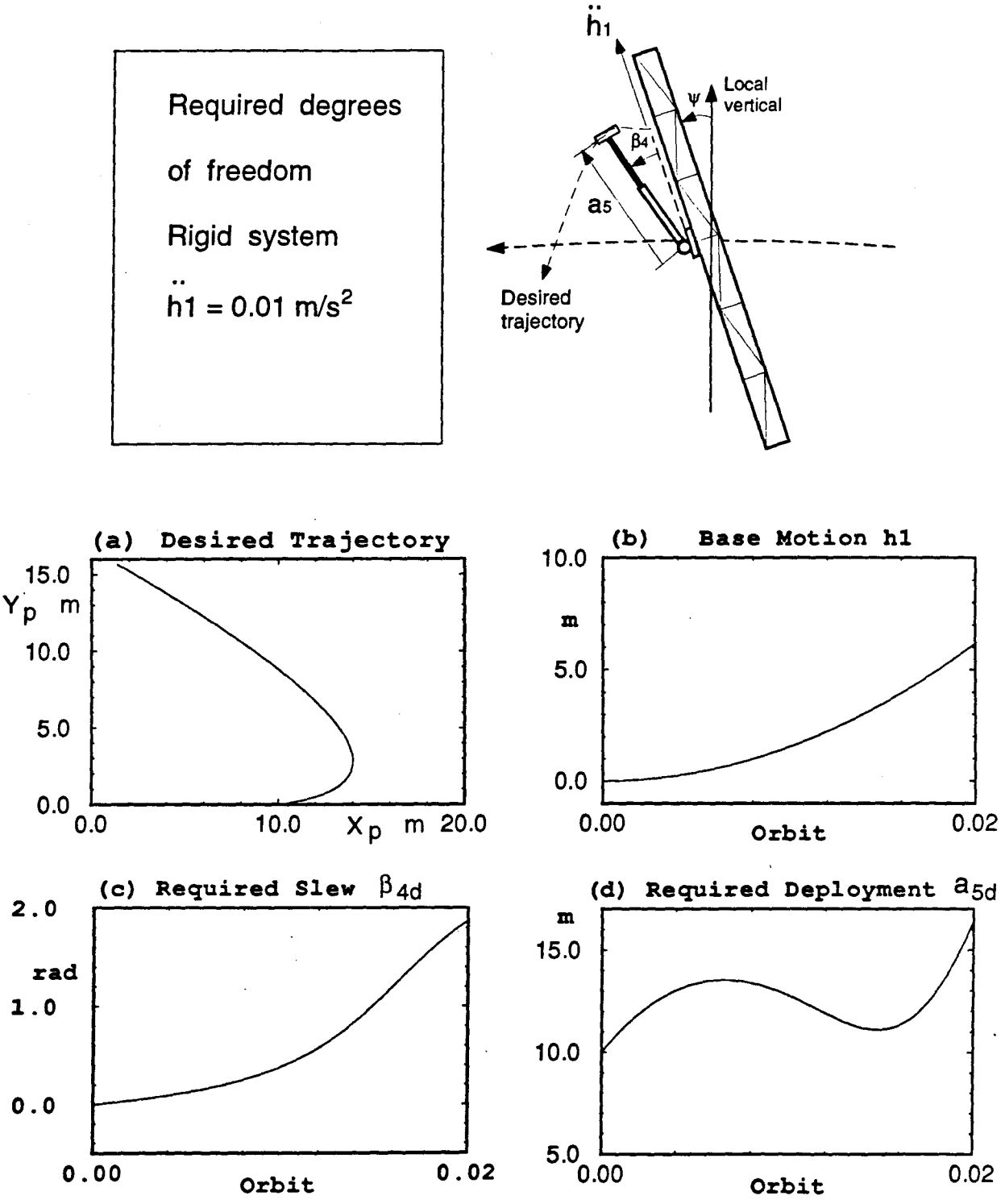

Figure 4-4 Time histories of the required degrees of freedom, for the rigid system, with an accelerating base and a specified trajectory.

flexible.

4.5.2 Trajectory tracking for the flexible system

In this subsection the effects of platform flexibility, MDM base location and initial conditions on the required position, velocity and acceleration of the d.o.f. are studied.

Figures 4-5 and 4-6 present the required d.o.f. time histories for a desired trajectory and base motion as described in Figure 4-4. The system is simulated for different initial conditions for the two generalized coordinates, associated with the first two modes, that represent the platform deflection.

In Figure 4-5, a relatively large initial disturbance of $q_1 = 1$ m, for $x_1 = 0$ (initial base location), is applied to the first mode. The initial condition for the second (antisymmetric) mode is zero.

As can be seen from Figure 4-5(c), the relatively large amplitude platform vibrations ($\delta_1 = 1.2$ m for $x_1 = 0$), do not affect the required values in the initial stage, when the base is located close to the center of the platform. As the base translates along the platform, oscillations of the local slope α_1 affect the required slew after 0.02 orbit. The required deployment remains virtually unaffected by the flexibility effect represented here with the first vibration mode (Figure 4-5d).

Figure 4-6 provides similar information to assess the effect of the second mode excitation. Now the slope initial condition of $q_2 = 1$ m is added to the displacement at $x_1 = 0$. Note, the local slope oscillations affect the required slew, β_{4d}. The nominal position is modulated at a high frequency of 0.5 Hz, the natural frequency of the second mode, as shown in Figure 4-6(c).

The required deployment time history is essentially unaffected in the beginning, however, high frequency modulations, growing in amplitude, do appear and become

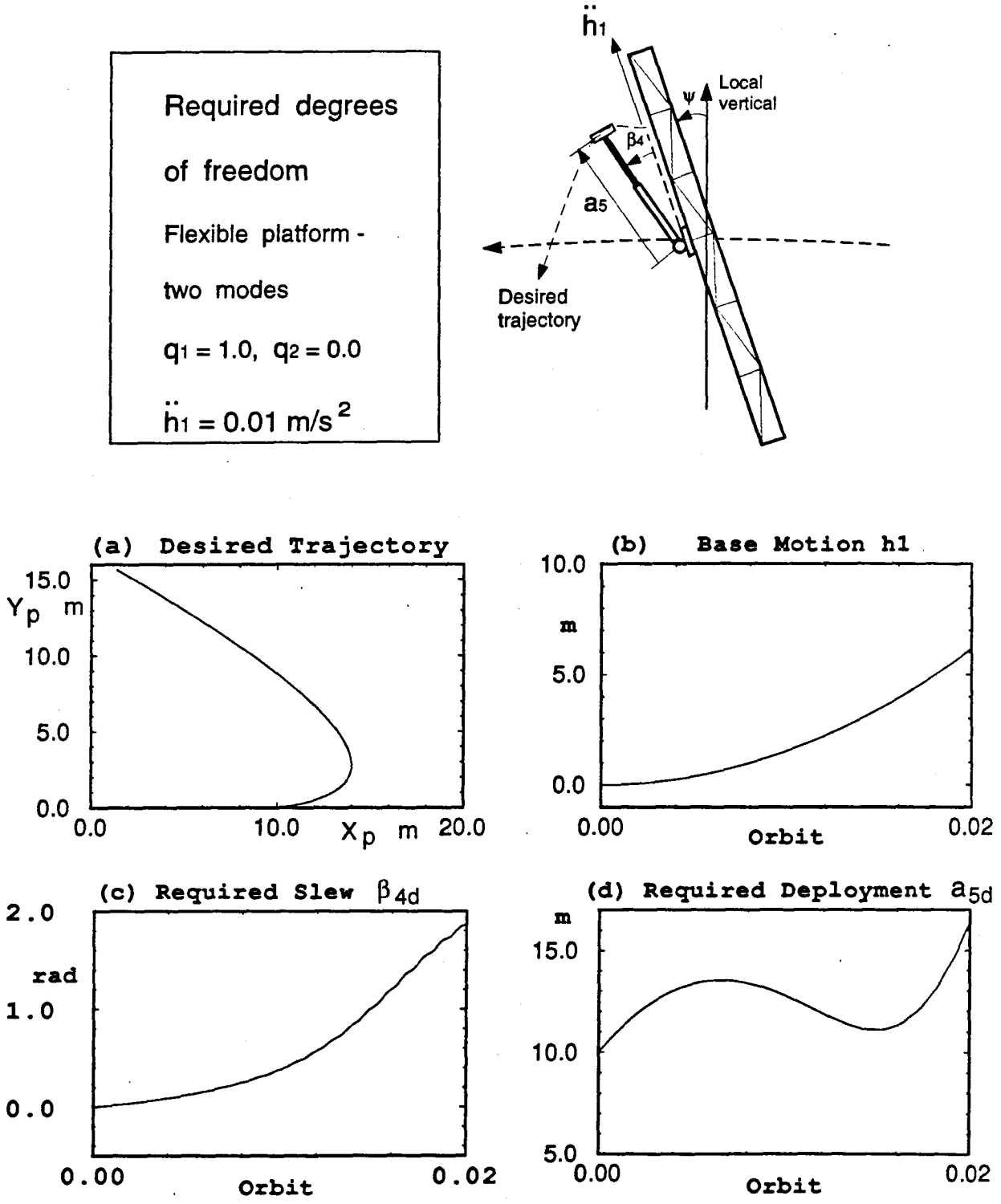

Figure 4-5 Time history of the required degrees of freedom for the flexible system with an accelerating base and prescribed trajectory. Initial modal excitations are: $q_1 = 1$ m; $q_2 = 0$.

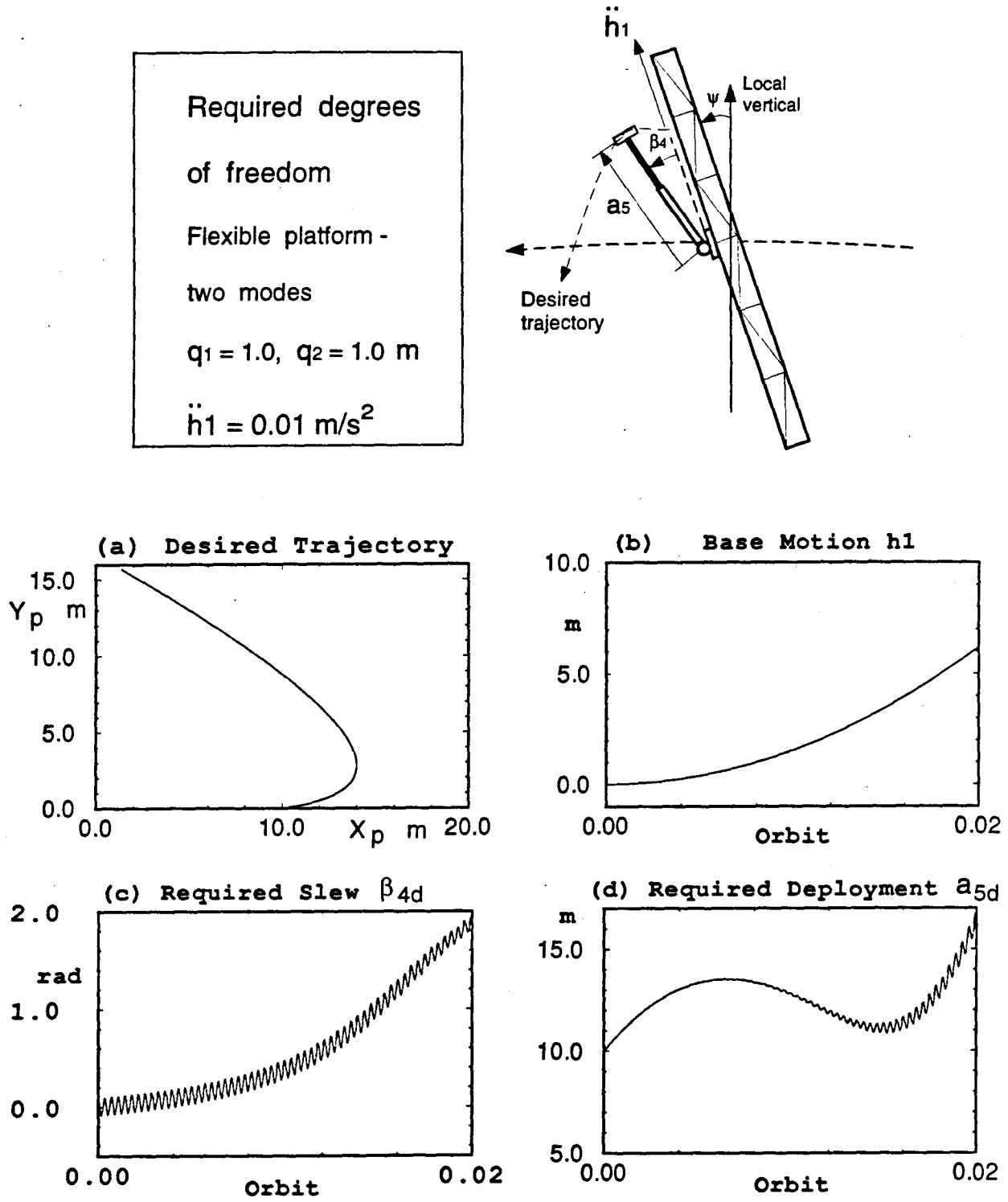

Figure 4-6 Time history of the required degrees of freedom for the flexible system with an accelerating base and prescribed trajectory. Initial modal excitations are: $q_1 = 1$ m; $q_2 = 1$ m.

significant rather quickly (Figure 4-6d). The vibrations affect the required deployment when the displacement at the center of the platform, where the reference frame F_p is located, is different from the displacement at the base (δ_1-δ_0).

Next, the MDM base was initially located 50m from the center of the platform. The trajectory parameters and the base motion were kept the same as before. Effect of the magnitude of the initial conditions on the required time histories of the generalized coordinates β_4 and a_5 is discussed in Figures 4-7 and 4-8.

In the case presented in Figure 4-7, the initial conditions are $q_1 = q_2 = 0.1$ m with the base located at $x_1 = 50$ m.

It is apparent from Figure 4-7(c) that even a relatively small disturbance at the platform affects the required slew. In this case, the modulations are of about 0.05 rad amplitude and at the frequency reflecting the combined effect of the first (0.2 Hz) and the second mode (0.5 Hz). The required deployment is also affected as shown in Figure 4-7(d). Note, for the present case, the modulation amplitude appears to be rapidly increasing.

With an increase in the initial disturbance to $q_1 = q_2 = 0.5$ m, the required time histories of the generalized coordinates are strongly affected as can be seen in Figure 4-8. The required slew is modulated at a high frequency with a peak amplitude of 0.2 rad. The deployment time history is also modulated, at a high frequency, and the amplitude of 2 m reached in 0.02 orbit is still increasing. Obviously, an efficient controller would be necessary to obtain the desired performance.

As explained in the next chapter, for the control purpose, the required position as well as the velocity and acceleration of the d.o.f. will be needed to achieve the desired performance.

Figure 4-9 presents the required profile for the slew degree of freedom, β_4. The

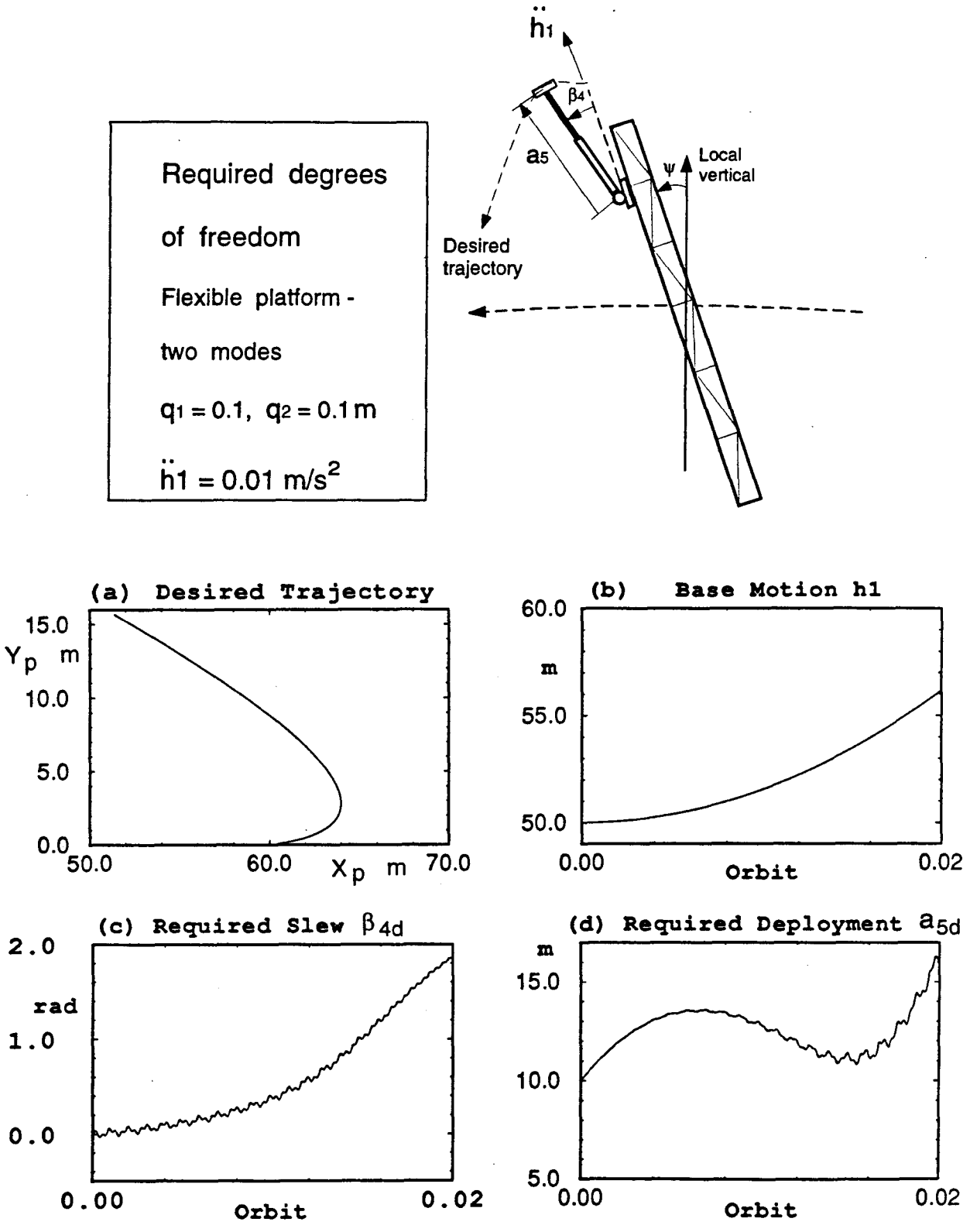

Figure 4-7 Required time histories of the generalized coordinates with the platform excitation of $q_1 = q_2 = 0.1$ m. The manipulator is located 50 m from the center (h_1=50 m).

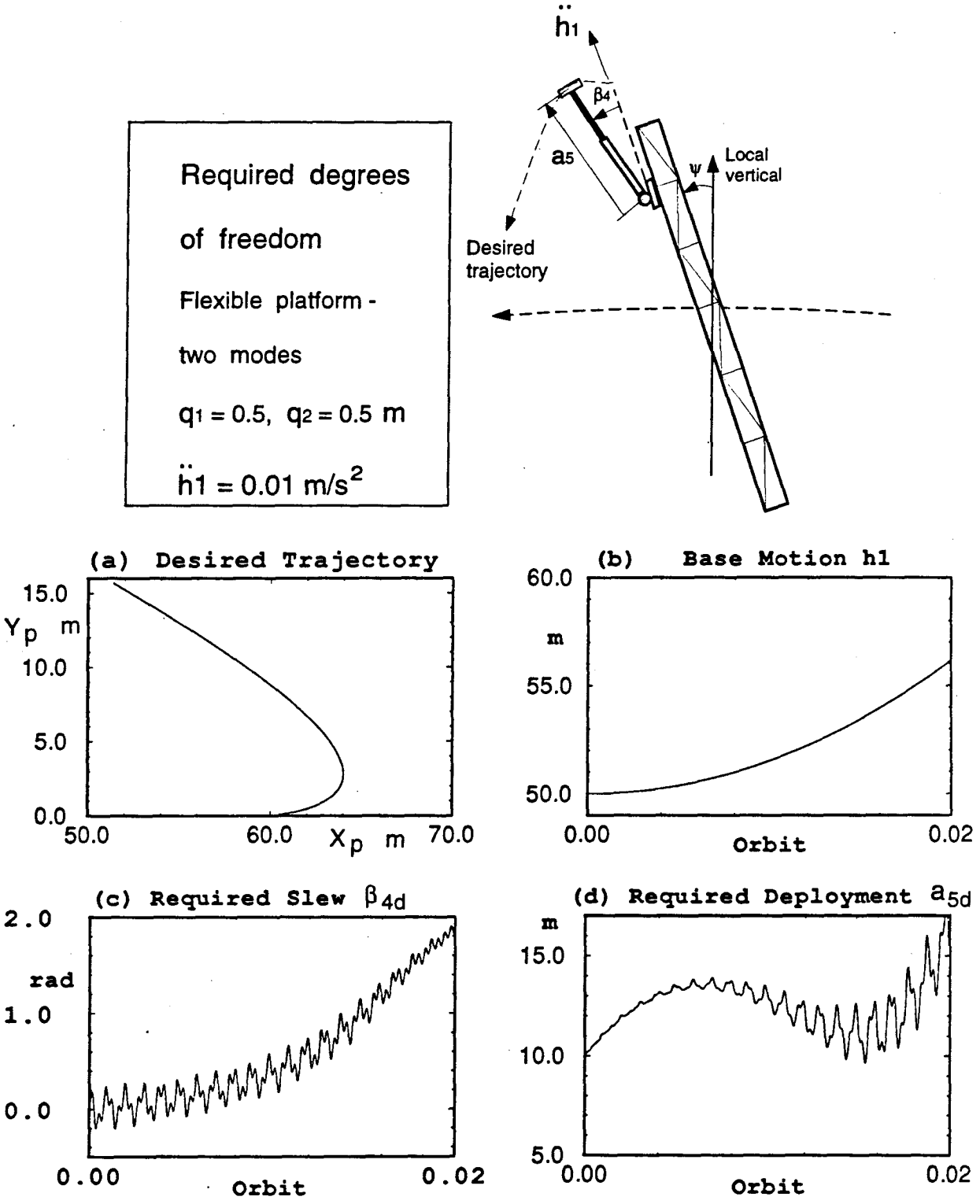

Figure 4-8 The effect of increased platform excitation of $q_1 = q_2 = 0.5$ m on the required time histories of the generalized coordinates β_4 and a_5 to track a desired trajectory. The base is located at $h_1 = 50$ m.

system parameters, the desired trajectory, and the base position as well as motion are the same as in the previous case. The system is simulated with $q_1 = q_2 = 0.5$ m as the initial values of the platform generalized coordinates, associated with the first two modes. The required slew time history, β_{4d}, is presented in Figure 4-9(b). The slew velocity $\dot{\beta}_{4d}$ is also recorded (Figure 4-9c). It is of interest to note that the nominal velocity is close to zero. Amplitude of the high frequency modulations is rather significant, 0.4 rad/s. The modulation frequency of 0.5 Hz is associated with the second mode. The required acceleration time history, $\ddot{\beta}_{4d}$ is presented in Figure 4-9(d). Note, that the acceleration remains positive with a peak modulation amplitude of 1.4 rad/s^2 at a frequency of 1 Hz.

The required position, velocity and acceleration for the deployment d.o.f. a_5 are presented in Figures 4-10 and 4-11. For zero initial conditions the required values are smooth as shown in Figure 4-10(b), 4-10(c) and 4-10(d). However, for the initial conditions of $q_1 = q_2 = 0.5$ m, the required velocity time history is modulated at high frequencies associated with the first and second flexible modes. The peak velocity is 3.5 m/s as shown in Figure 4-11(c), while the maximum required acceleration is $-2m/s^2$ (Figure 4-11d).

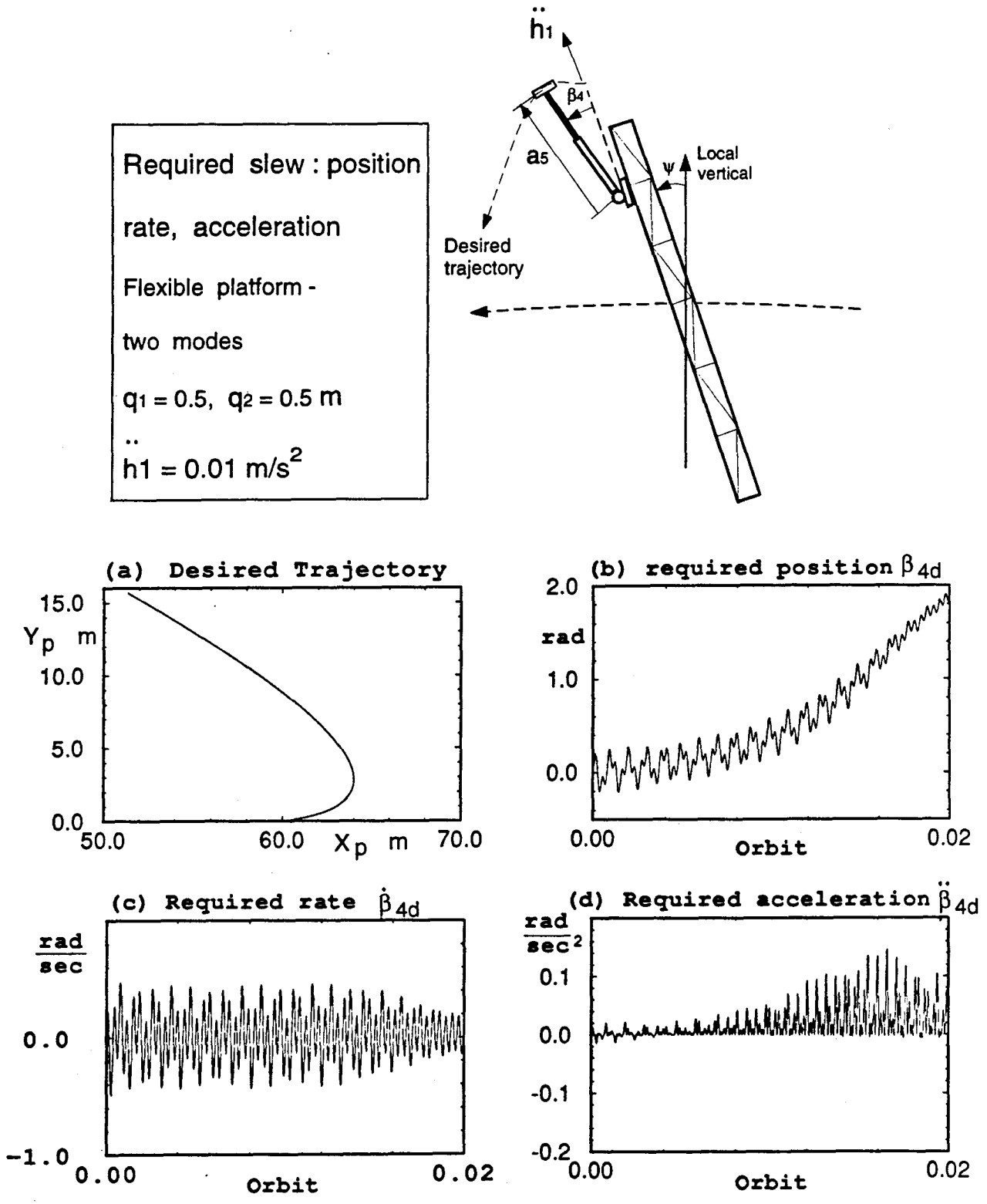

Figure 4-9 Required slew arm position, velocity and acceleration for the flexible system, with initial excitation of $q_1 = q_2 = 0.5$ m, to track the specified trajectory. The manipulator is positioned 50 m from the center of the platform.

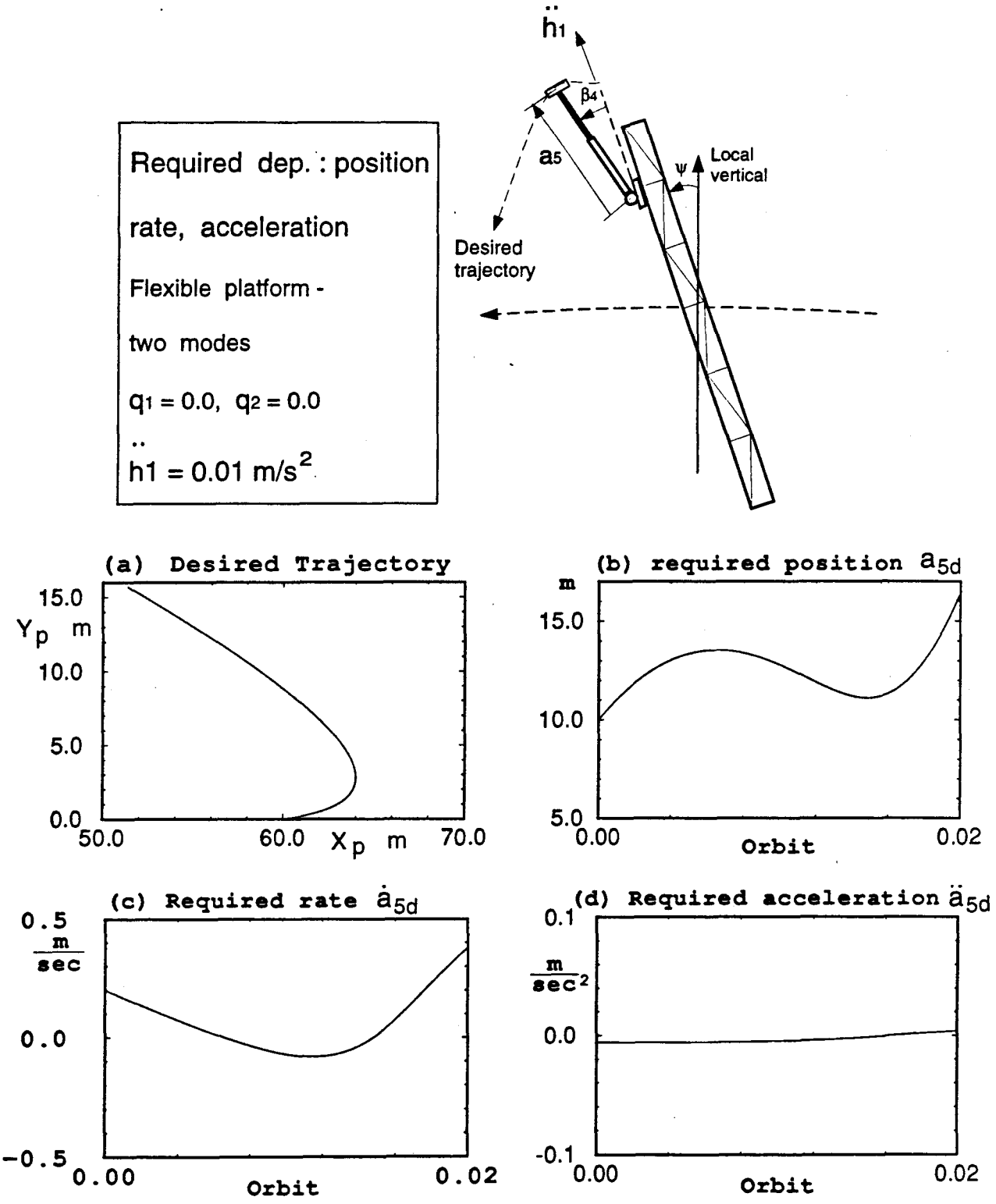

Figure 4-10 Required deployable arm position, velocity and acceleration in absence of the platform excitation ($q_1 = q_2 = 0$). The base is initially located at h_1 =50 m.

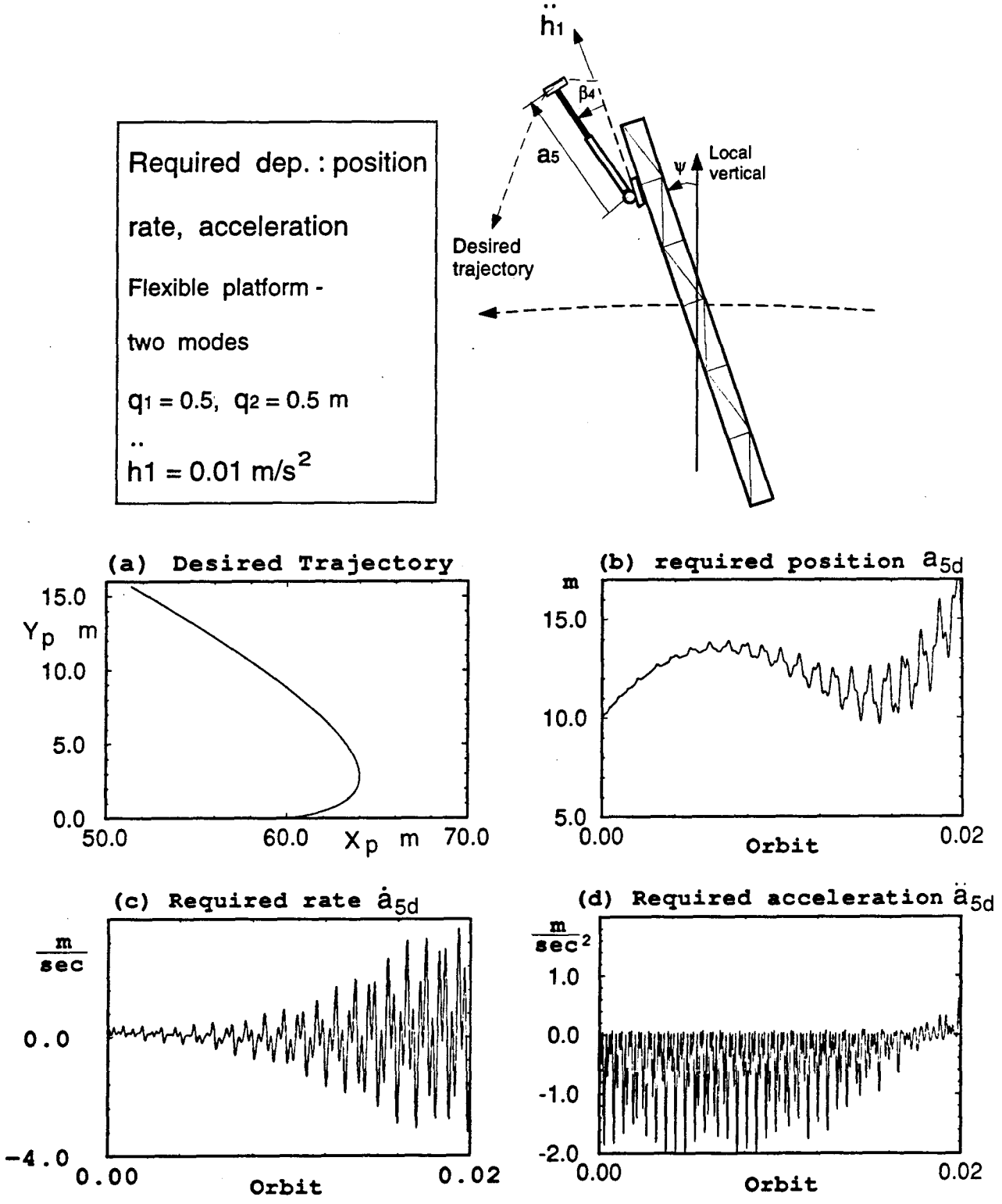

Figure 4-11 Effect of the platform excitation of $q_1 = q_2 = 0.5$ m on the required position, velocity and acceleration time histories of the deployment generalized coordinate a_5. The manipulator starts to translate from h_1=50 m.

4.6 Summary

Inverse kinematic relationships to evaluate the required MDM controlled variables when tracking a desired trajectory, defined w.r.t. the platform or the orbit, have been developed. It imparts the desired position and orientation to the payload by moving the MDM base to the appropriate location.

From the simulations results it is concluded that the platform vibrations affect the required degrees of freedom via the displacement and rotation at the base. To obtain required time histories of the slew and deployment generalized coordinates, at least the first two modes must be taken into account.

5. CLOSED LOOP STUDY

5.1 Preliminary Remarks

A relatively extensive open loop study was presented in Chapter 3 and the system dynamic simulation established. From the open loop study it can be concluded that it is impossible to achieve even an approximate trajectory tracking, and therefore it is necessary to close the loop with a controller.

From the control point of view, a given task is usually accomplished in two distinct steps: First, the gross motion control in which the arms move from an initial position/orientation to the desired target position/orientation along a planned trajectory. Next, the fine motion control in which the manipulator end-effector (SPDM) interacts with the object to complete the task.

The purpose of the control in this study is to achieve the desired trajectory motion of the manipulator end effector with respect to the reference coordinate frame. The trajectory tracking is achieved by controlling the required degrees of freedom as determined by the inverse transform technique in Chapter 4. The control action takes place in the presence of the platform pitch and transverse vibrations, as well as oscillations at the flexible joints.

This chapter focuses on development of a nonlinear control strategy, which utilizes the dynamic simulation discussed in Chapter 3, to efficiently control the MDM.

5.2 Nonlinear Control

This section is concerned with the design of a reliable control technique in order to ensure the desired trajectory tracking performance of the MDM. The highly nonlinear MDM dynamics were accurately modelled in Chapter 2. A control strategy accounting

for the complete nonlinear dynamical model is sought.

Control strategies based on linearized system models have been found to be inadequate because of the stability and robustness problems. Furthermore, there are situations of practical importance, where the contribution of the nonlinear dynamics cannot be neglected and must be modelled accurately. For example, a problem may involve precise trajectory tracking of a system governed by highly nonlinear dynamics and maneuvering histories as in the present study. To meet this challenging problem, an inverse control technique is suggested to achieve high tracking accuracy of the MDM, in presence of the platform libration, base translation, and system vibrations.

5.2.1 Computed torque technique

The inverse control method, also referred as the Computed Torque Technique, which is a particular case of the Feedback Linearization Technique (FLT), was first investigated by Beijezy [53], and applied to the rigid arm control by Fu [2]. In this approach, the nonlinear and coupling terms in the equations of motion are eliminated by judiciously selecting the control input to be a function of these terms. The advantages of this procedure are: accounts for the complete nonlinear dynamics of the system; simplicity of the control algorithm and compensator. Spong [54] later extended the method to control a robot with elastic joints. Recently the technique was extended by Modi and Karray [42] to deal with a flexible space based manipulator. For its application to a flexible orbiting manipulator, authors proposed two different control schemes: quasi-open loop; and quasi-closed loop.

Basically the computed torque technique is a nonlinear control with feedforward and feedback components. The feedforward components compensate for the interaction torques/forces at the joints, while the feedback component provides the necessary torque to correct any deviations from the desired trajectory.

For example, consider the MDM system described by the governing nonlinear equations in the form

$$[M](q,t)\ddot{\bar{q}} + \overline{N}(q,\dot{q},t) = \overline{Q}(t), \tag{5.1}$$

where $\bar{q}$ and $\overline{Q}$ are vectors of the generalized coordinates and generalized forces (control forces), respectively. $[M]$ is the symmetric positive definite mass matrix. It is a function of $\bar{q}$ and t due to the nonlinear and time varying nature of the system inertia. $\overline{N}$ is the noninertial, nonlinear force vector associated with Coriolis, centrifugal and gravitational forces. Note, the nonlinear force vector $\overline{N}$ also accounts for the structural and joints damping.

The main objective here is to design a control technique to implement values of the generalized coordinates for tracking the desired trajectory. To this end, a proportional plus derivative control is used to regulate the various MDM system actuators: momentum wheels at the platform, and torque motors at the joints. Thus the control law has the form

$$\overline{Q}(t) = [M](q,t)\{\ddot{\bar{q}}_d + [K_v][\dot{\bar{q}}_d - \dot{\bar{q}}] + [K_p][\bar{q}_d - \bar{q}]\} + \overline{N}(q,\dot{q},t), \tag{5.2}$$

where q_d, $\dot{q}_d$, $\ddot{q}_d$ are the desired (required) system degrees of freedom: position, velocity, and acceleration vectors, respectively, as obtained in Chapter 4 from the inverse kinematics of the desired trajectory. For the system pitch motion, the required and the desired values are the same as the platform reference frame F_p is parallel to the system frame F_0 (Figure 4.1). $[K_v]$ and $[K_p]$ are the $n \times n$ matrices, of velocity and position feedback gain, respectively, where n is the total number of the controllable degrees of freedom. Substituting the control torque vector $\overline{Q}(t)$ from Eq. (5.2) into the equations of motion (5.1), the following error dynamics equation is obtained,

$$[M](q,t)[\ddot{\bar{e}}(t) + [K_v]\dot{\bar{e}}(t) + [K_p]\bar{e}(t)] = 0, \tag{5.3}$$

where $\bar{e}(t) = \bar{q}_d(t) - \bar{q}(t)$ is the tracking position error. The mass matrix $[M](q,t)$ is always nonsingular, and $[K_p]$, $[K_v]$ can be chosen appropriately to get negative real roots for the characteristic equation (5.3), so that the position error vector $\bar{e}(t)$ approaches zero asymptotically. The optimal choice for $[K_v]$ and $[K_p]$ is:

$$[K_p] = diag[\omega_0^2, ..., \omega_n^2]; \qquad [K_v] = diag[2\omega_0, ..., 2\omega_n]. \tag{5.4}$$

This leads to a globally decoupled system with each generalized coordinate responding as a critically damped second order oscillator. ω_i is the closed loop natural frequency of the i^{th} degree of freedom. In order not to excite the platform oscillations and resonance at the joints, and to ensure system stability, the closed loop natural frequency ω_i should not exceed one-half of the structural natural frequency as suggested by Paul [1].

In the present study, the total number of the generalized coodinates is $nom + 5$, where nom indicates the number of modes representing the platform flexibility. Here the first two free-free modes were taken during the closed loop simulation study, hence the degrees of freedom are seven.

In the present control study, the main objective is to maintain the desired attitude of the platform while tracking a prescribed trajectory of the payload, and to ensure stable response of the flexible joints (elastic torsional deformations within the permissible limit). Consistent with the main objectives mentioned before, the flexible generalized coordinates are considered nonobservable. The stable response of the platform is assured because of the structural damping, and by designing the control to have a closed loop natural frequency less than one-half of the lowest structural frequency.

The desired or required values of the system degrees of freedom must be assigned

for application of the FLT to control the MDM. In the present study, required values were assigned to the platform pitch (ψ_d), and to the arms' degrees of freedom - β_{4d} for the slew, and a_{5d} for the deployment. The required values for the arms were obtained from the inverse tranform of the desired payload trajectory. No desired values were assigned for the joints degrees of freedom: β_3, and β_5. A method to determine the MDM joints' desired values, from the given desired values of the arms, has been developed. The system equations of motion (5.1) can be written as

$$[M](q,t)\ddot{\overline{q}} = \overline{F}(q,\dot{q},t) + \overline{T}(t) = \overline{Q}(t) - \overline{N}(q,\dot{q},t), \tag{5.5}$$

where $\overline{F}$ is the nonlinear force vector $\overline{N}$ without the coupling force/torque, and $\overline{T}$ is the control, coupling torque vector. Eq. (5.5) can be presented in a more detailed form as follows,

$$[M(i,j)] \begin{bmatrix} \ddot{\bar{q}}_1 \\ \ddot{\psi} \\ \ddot{\beta}_3 \\ \ddot{\beta}_4 \\ \ddot{\beta}_5 \\ \ddot{a}_5 \end{bmatrix} = \begin{bmatrix} \bar{F}_1 + T_0\bar{\phi}_1'(0) \\ F_0 + T_0 \\ F_3 + T_3 + T_4 \\ F_4 - T_4 \\ F_5 + T_5 + T_6 \\ F_6 - \frac{T_6}{r_5} \end{bmatrix}, \tag{5.6}$$

where:

$[M(i,j)]$ the mass matrix with elements as shown in Appendix III;

$\bar{q}_1$ the generalized coordinate vector associated with the platform flexibility;

T_0 the control input torque of the momentum wheels attached at the center of the platform;

$\bar{\phi}_1'(0)$ the value of the first derivative w.r.t. x_1 of the mode shapes at the platform's midpoint;

T_3, T_5 the control input torques acting at the joints of the slew and deployable arm, respectively;

T_4, T_6 coupling torques at the joints.

T_4 and T_6 can be expressed as follows:

$$T_4 = k_3(\beta_4 - \frac{\beta_3}{n_3}); \tag{5.7}$$

$$T_6 = k_5(\frac{a_5}{r_5} - \frac{\beta_5}{n_5}). \tag{5.8}$$

Applying the FLT (Eq. 5.2) to the: pitch (ψ); slew (β_4) and the deployment (a_5) degrees of freedom, and introducing the required values ψ_d, β_{4d} and a_{5d}, respectively, the following control laws can be obtained:

$$T_{0d} = M(2,2)[\ddot{\psi}_d + K_{v0}(\dot{\psi}_d - \dot{\psi}) + K_{p0}(\psi_d - \psi)] - F_0 + [M(2,1)\ddot{\bar{q}}_1$$

$$+M(2,3)\ddot{\beta}_3 + M(2,4)\ddot{\beta}_4 + M(2,5)\ddot{\beta}_5 + M(2,6)\ddot{a}_5]; \tag{5.9}$$

$$T_{4d} = -M(4,4)[\ddot{\beta}_{4d} + K_{v4}(\dot{\beta}_{4d} - \dot{\beta}_4) + K_{p4}(\beta_{4r} - \beta_4] + F_4$$

$$-[M(4,1)\ddot{\bar{q}}_1 + M(4,2)\ddot{\psi} + M(4,5)\ddot{\beta}_5]; \tag{5.10}$$

$$\frac{T_{6d}}{r_5} = -M(6,6)[\ddot{a}_{5d} + K_{v6}(\dot{a}_{5d} - \dot{a}_5) + K_{p6}(a_{5d} - a_5)] + F_6$$

$$-[M(6,1)\ddot{\bar{q}}_1 + M(6,2)\ddot{\psi}]. \tag{5.11}$$

Here:

K_{p0}, K_{v0} position and velocity feedback gains in the pitch (ψ) degree of freedom;

K_{p4}, K_{v4} position and velocity feedback gains in the slew (β_4) degree of freedom;

K_{p6}, K_{v6} position and velocity feedback gains in the deployment (a_5) degree of freedom.

T_{0d} is the required control input in pitch; and T_{4d} T_{6d} are the required coupling torques in slew and deployable joint output, respectively, in order to asymptotically decrease the tracking error to zero.

Substituting for T_{4d} and T_{6d} into Eq. (5.7) and (5.8), respectively, the required values for the joint rotor positions β_{3d} and β_{5d}, can be written as:

$$\beta_{3d} = (\beta_4 - \frac{T_{4d}}{k_3})n_3; \tag{5.12}$$

$$\beta_{5d} = (\frac{a_5}{r_5} - \frac{T_{6d}}{k_5})n_5. \tag{5.13}$$

The required velocity and acceleration can be obtained by differentiating β_{3d} and β_{5d} with respect to time:

$$\dot{\beta}_{3d} = \frac{d}{dt}\beta_{3d}, \qquad \ddot{\beta}_{3d} = \frac{d^2}{dt^2}\beta_{3d}; \tag{5.14}$$

$$\dot{\beta}_{5d} = \frac{d}{dt}\beta_{5d}, \qquad \ddot{\beta}_{5d} = \frac{d^2}{dt^2}\beta_{5d}. \tag{5.15}$$

Applying the FLT to the MDM joints, with the required values obtained in equations (5.12) to (5.15), the control laws for the joint motors take the form:

$$T_{3d} = M(3,3)[\ddot{\beta}_{3d} + K_{v3}(\dot{\beta}_{3d} - \dot{\beta}_3) + K_{p3}(\beta_{3d} - \beta_3)] + C_3\dot{\beta}_3 - \frac{T_{4d}}{n_3}$$
$$+M(3,1)\ddot{\bar{q}}_1 + M(3,2)\ddot{\psi}; \tag{5.16}$$

$$T_{5d} = M(5,5)[\ddot{\beta}_{5d} + K_{v5}(\dot{\beta}_{5d} - \dot{\beta}_5) + K_{p5}(\beta_{5d} - \beta_5)] + C_5\dot{\beta}_5 - \frac{T_{6d}}{n_5}$$
$$+M(5,1)\ddot{\bar{q}}_1 + M(5,2)\ddot{\psi} + M(5,4)\ddot{\beta}_4. \tag{5.17}$$

Here K_{p3}, K_{v3} are the position and velocity feedback gains for joint 1 (β_3) degree of freedom; and K_{p5}, K_{v5} are the corresponding gains for joint 2 (β_5) degree of freedom. T_{3d} and T_{5d} are the required control input torques at the slew and deployment joints' motors, respectively, in order to decrease the trajectory tracking error asymptotically to zero. The closed loop block diagram for the slew and deployable arm degrees of freedom are shown in Figures 5-1 and 5-2, respectively.

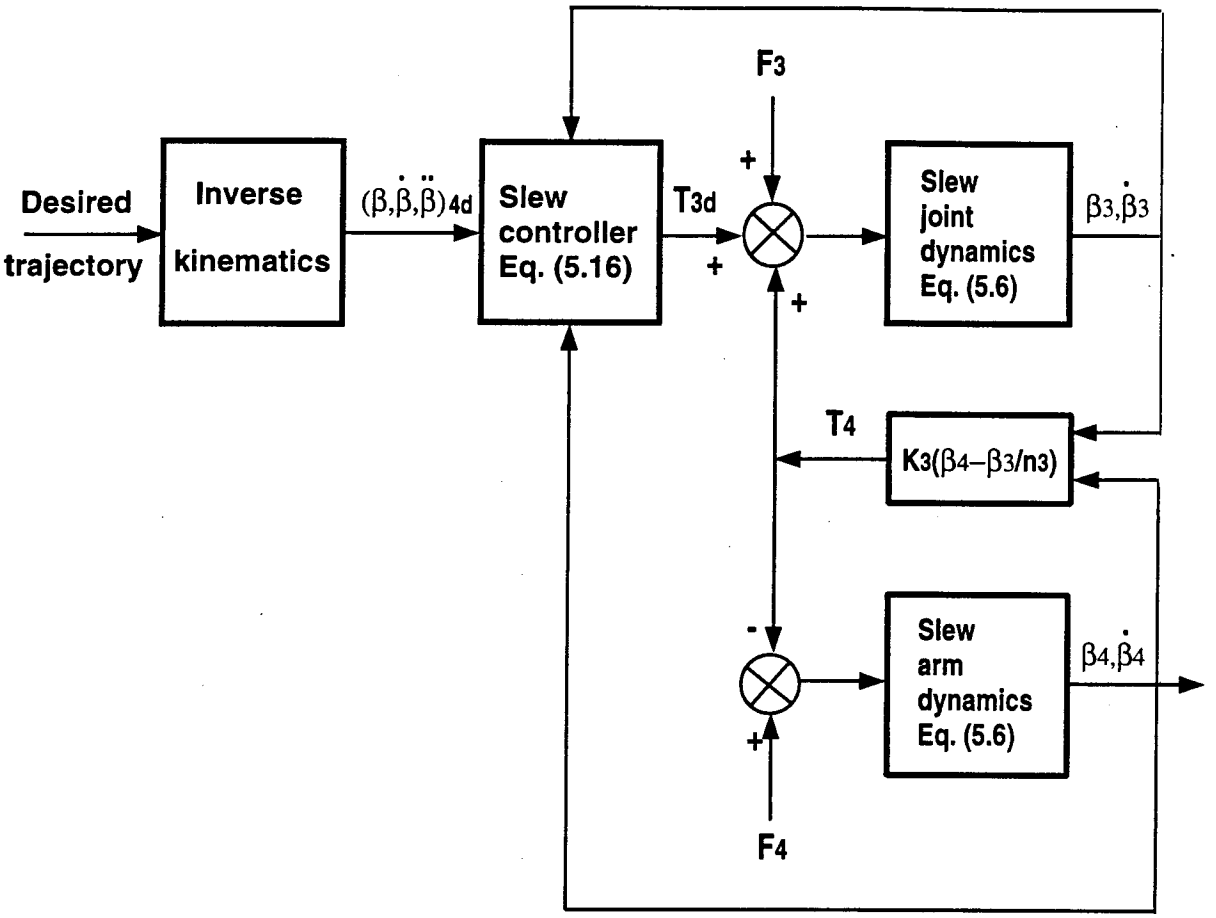

Figure 5-1 Closed loop block diagram for the slew degree of freedom.

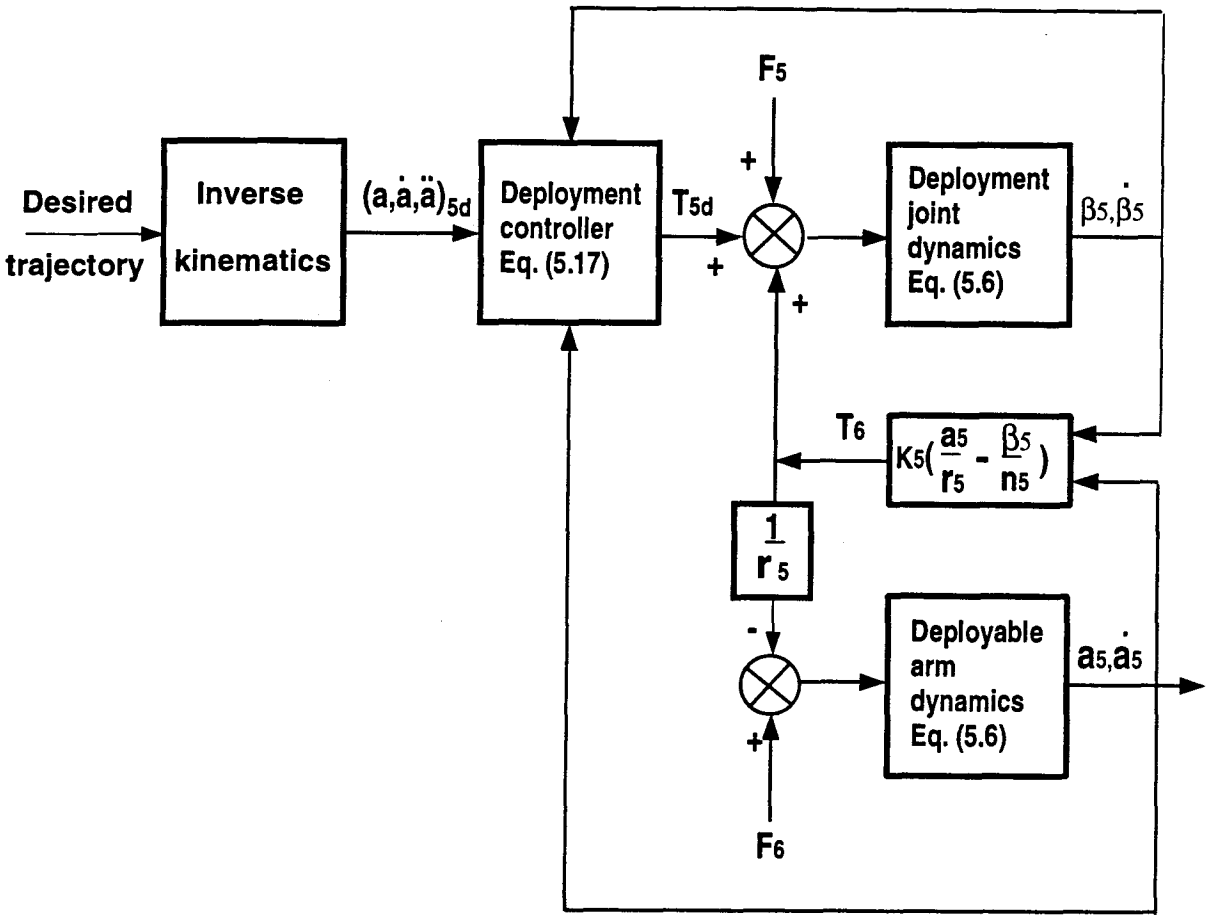

Figure 5-2 Closed loop block diagram for the deployment degree of freedom.

As mentioned before, the process of getting the required velocity and acceleration of the joints degrees of freedom involves differentiation with respect to time. In real systems the signals contain noise; hence it is necessary to include some filtering procedure in the numerical differentiation. To avoid this problem a different approach is suggested as discussed in the following section.

5.2.2 Joints stiffness control

A new control approach is proposed in order to avoid the numerical differentiation of the required joint degrees of freedom when applying the FLT. It is suggested that the joint stiffness be controlled according to the actual twist at the joints and the required input torque to the arms. Thus, the stiffness of the joint, represented by the flexural rigidity of the torsional shaft, is not constant. For example, an arrangement that varies the equivalent length of the shaft can be adopted. This can be achieved by shifting the point of application of the torque to the shaft by the joint motor. Alternatively, a controllable clutch (say, a magnetic clutch) may be introduced to change the equivalent shaft cross-section moment of inertia. A multiple element clutch can engage with different sections of the shaft thus changing the cross-section area effective in transmitting the torque.

The main objective in this new approach is to determine the required joint stiffnesses k_{3d} and k_{5d} in order to obtain the required torques T_{4d} and T_{6d} given in Eqs. (5.10) and (5.11), respectively. For this case the arms' required position and velocity as obtained from the inverse kinematics are assumed to be the required values for the joints degrees of freedom. Applying Proportional plus Derivative (PD) control to the joints' degrees of freedom, the control law takes the form:

$$T_{3d} = [K_{v3}(\dot{\beta}_{4d} - \frac{\dot{\beta}_3}{n_3}) + K_{p3}(\beta_{4d} - \frac{\beta_3}{n_3})]K_{m3}; \tag{5.18}$$

$$T_{5d} = [K_{v5}(\frac{\dot{a}_{5d}}{r_5} - \frac{\dot{\beta}_5}{n_5}) + K_{p5}(\frac{a_{5d}}{r_5} - \frac{\beta_5}{n_5})]K_{m5}. \tag{5.19}$$

T_{3d} and T_{5d} are the control input torques at the slew and deployable joint motors, respectively, in order to decrease the error at the joints to zero. K_{m3}, K_{m5} are the slew and deployable torque motor gains, respectively.

Application of the control inputs T_{3d}, T_{5d} to the joints with the nominal constant stiffness K_3, K_5 may not necessarily meet the requirement of the input torques to the arms, T_{4d} and T_{6d}, as found by the FLT (Eqs. 5.10, 5.11). As a consequence tracking may not be possible. To overcome this problem, the joint stiffnesses must be changed, as proposed.

The relations governing the input torques to the arms and the stiffness of the joints are given in Eqs. (5.7), (5.8). The required joint stiffnesses can be calculated as follows:

$$k_{3d} = \frac{T_{4d}}{(\beta_4 - \frac{\beta_3}{n_3})}; \tag{5.20}$$

$$k_{5d} = T_{6d}(\frac{a_5}{r_5} - \frac{\beta_5}{n_5}); \tag{5.21}$$

which provide the required input torques to the slew and deployable arms, respectively.

5.3 Controlled System Study

An extensive open loop study was presented in Chapter 3. The simulation results clearly showed that a controller must be incorporated in the MDM system in order to successfully perform any desired task. Now the control law developed in Section 5.1 is to be implemented to achieve a closed loop response. The system parameters are the same as for the open loop case (Table 3-1). The only additional parameters are the position and the velocity gains K_p K_v, respectively.

As mentioned in the previous section, with an appropriate choice of the feedback gain K_v and K_p, each degree of freedom can be made to respond as a decoupled critically damped second order oscillator. In this case, the gains are functions of the system closed loop natural frequencies as shown in Eq. (5.4). For stability reasons, the closed loop natural frequency for each degree of freedom cannot exceed one-half the value for the associated open loop case. The feedback gains can be obtained from the open loop simulation results presented in Chapter 3, and are given in Table 5-1.

Table 5-1 MDM closed loop velocity and position feedback gains.

d.o.f	ω_o, rad/s	ω_c, rad/s	$K_v = 2\omega_c$	$K_p = \omega_c^2$
q_1	1.13	—	—	—
q_2	3.11	—	—	—
ψ	0.002	0.001	0.002	$1 \cdot 10^{-6}$
β_3 $(n_3 = 1)$	9.6	1.5	3	2.25
β_4	0.002–0.01	0.001	0.002	$1 \cdot 10^{-6}$
β_5 $(n_5 = 1)$	9.6	0.6	1.2	0.36
a_5 $(r_5 = 0.1)$	2.8	0.6	1.2	0.36

Here:

ω_o open loop natural frequency as found from the simulation results;

ω_c the desired closed loop natural frequency;

K_v the velocity feedback gain;

K_p the position feedback gain.

It is apparent from Table 5-1 that not all the closed loop natural freequencies,

ω_c, have been chosen according to the rule of one-half. For example, in the case of joint 1 (β_3), the dynamic coupling between the platform and oscilations at the joint will exite the second mode with a frequency of 3.11 rad/s. Hence, the joint 1 closed loop natural frequency is chosen to be 1.5 rad/s.

An extensive study of the MDM closed loop response was carried out. For better appreciation the system was analyzed in an increasing order of complexity. The study starts with the stationkeeping mode (fixed desired position) for a rigid or flexible platform. This is followed by the response investigation during trajectory tracking with stationary or moving base. Note, the effects of initial position error are accounted for. Finally, the attention is focused on the trajectory tracking for system with external disturbances.

The main goal of this closed loop simulation study is to assess the controlled tracking performance of flexible space based manipulator, i.e. trajectory tracking in the presence of system libration, base translation and rotation.

The amount of information obtained through a planned variation of the system parameters in the above mentioned case is rather extensive. For conciseness, only the typical results useful in establishing trends are presented here.

The MDM closed loop simulation flow chart is shown in Figure 5-3. The system properties and the initial conditions are supplied by the input data to the main program. The input to the inverse kinematics block is the desired trajectory, the actual state of the platform (deflections and slope) and the MDM base location. The output of the inverse kinematic analysis gives the required values for the system degrees of freedom which serve as an input to the control block (actual state variables). Output from the control block is the control efforts (generalized torques) for various degrees of freedom. Input to the dynamics block are the generalized forces, system

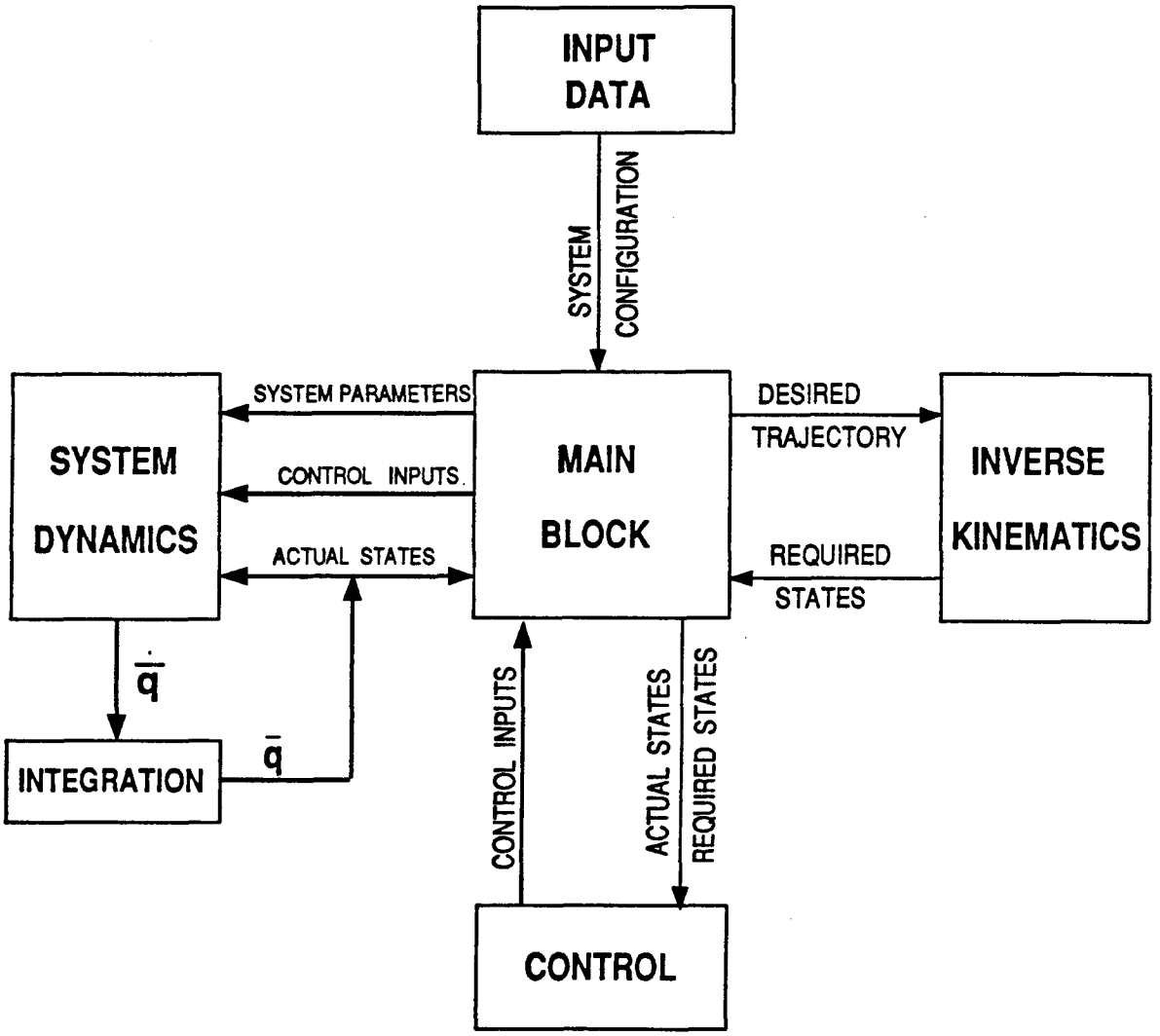

Figure 5-3 MDM closed loop simulation flow chart.

parameters and the actual state of the system. The output from the integration block is the new state of the system.

5.3.1 Stationkeeping

The system closed loop response, when the desired payload position is fixed with respect to the platform, is studied here. The tracking error and the control efforts have been evaluated, for a rigid or flexible platform, when the pitch initial condition is 0.02 rad (1.1 deg from the local vertical). The desired payload position in this case was $P_x = 10m$, $P_y = 0$ in the X_p and Y_p coordinates, respectively (Figure 4-1). In others words, the desired position of the payload is on the platform 10 m from its center. The desired position of the platform is along the local vertical ($\psi = 0$).

The closed loop responses for both the rigid and flexible platforms are shown in Figure 5-4 and 5-5, respectively.

Figure 5-4 presents simulation results over 0.02 orbit (110 s). The parameters of importance are the degrees of freedom, tracking error, control efforts and twist at the joints.

Figure 5-4(c) shows controlled response of the degrees of freedom ψ, β_3, β_4. The pitch (ψ) decreases asymptotically to zero. As a consequence, joint 1 motor (β_3) reacts relatively fast to drive the slew arm (β_4), in order to decrease the error. Figure 5.4(b) shows the tracking errors in platform pitch, slew and deployment. As can be seen, the initial pitch error of 0.02 rad is asymptotically decreased to zero with the time constant determined by the feedback gains. The deployment error remains essentially zero. The maximum slew error is about 0.0005 rad and decreases to zero asymptotically as can be seen from the expanded view of β_4. Figure 5-4(a) shows the desired and the actual positions of the payload in the platform reference frame

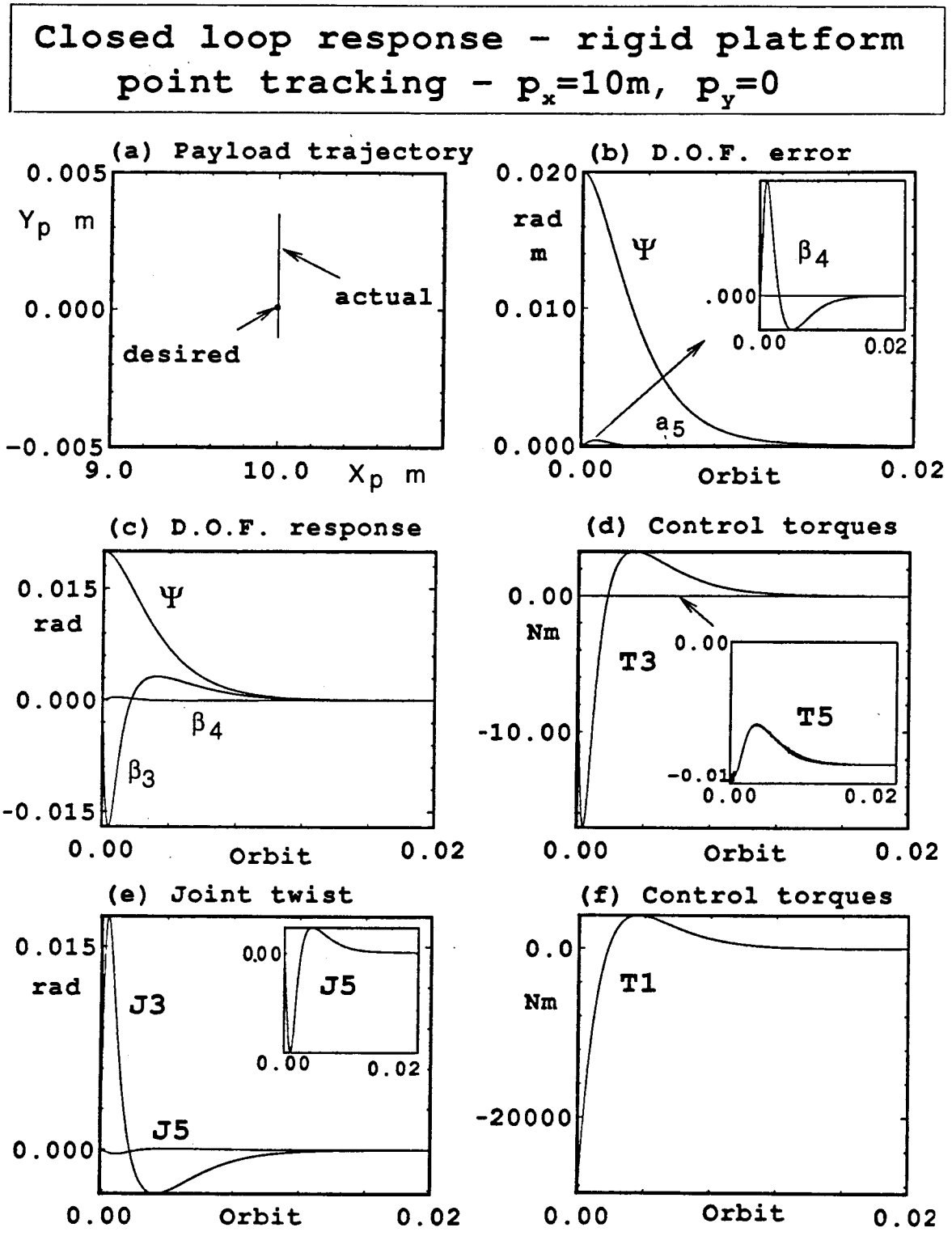

Figure 5-4 Closed loop response during stationkeeping for the rigid platform case with an initial disturbance of $\psi = 0.02$ rad.

X_p, Y_p. Note, the resultant position error is between -0.001 m to 0.0035 m along the Y_p direction.

The control effort and twist at the joints are shown in Figures 5-4(d), 5-4(e), 5-4(f). The maximum control effort at the slew joint T_3 was found to be around -17 Nm (Figure 5-4d). The torque decreased to zero asymptotically with an overshoot of 4 Nm. The associated twist at the slew joint J_3 is 0.003 rad, as can be seen in Figure 5-4(e). The maximum control effort at the deployment joint T_5 was approximately -0.01 Nm, and the steady state value of around -0.008 Nm is required in order to overcome the gravitational effect (Figure 5-4d). The associated twist at the joint J_5 remains relatively small due to the low torque value and the equivalent gear ratio of 10 ($r_5 = 0.1$ m). The control effort provided by the momentum wheels (T_1) is $-2.9 \cdot 10^4$ Nm as shown in Figure 5-4(f). The huge demand is due to the large moment of inertia of the platform and the relatively high feedback gains.

Figure 5-5 presents the same case as discussed in Figure 5-4 but now accounting for the platform flexibility. The platform is modelled by the first two free-free modes with the natural frequencies of 1.13 rad/s and 3.11 rad/s, respectively.

At the outset it is apparent from Figure 5-5(c) that the pitch response is not affected by the platform vibrations. The initial pitch disturbance of 0.02 rad decreases to zero asymptotically. The response of the slew joint motor (β_3) is the reaction to the error that has been developed by the pitch motion. The associated impulse excites the platform vibrations (Figure 5-5f). In this case, the MDM base is located at the center of the platform, hence the displacement δ_1 and the rotation α_1 of the base are related to the first and second mode, respectively. The deflections are modulated at the high frequency associated with the second mode. The rotational oscilations of the base affects the required slew as apparent from the responses β_3 and β_4 in Figure

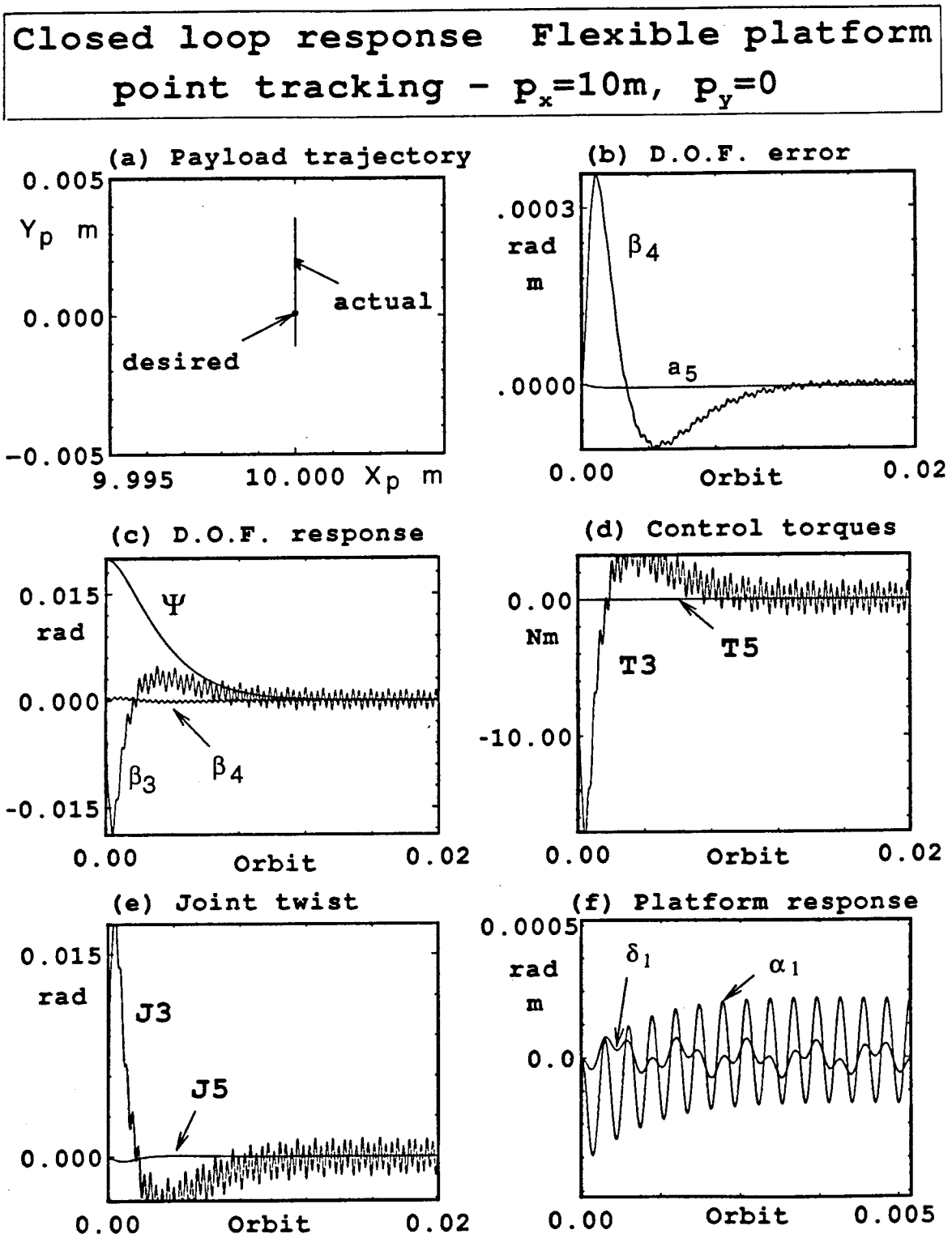

Figure 5-5 Closed loop response for point-tracking (stationkeeping) of the payload, supported by the manipulator, located on the flexible platform. The manipulator is at the center of the platform, and arm 2 is deployed 10 m. The initial disturbance is 0.017 rad in pitch.

5-5(c). The residual tracking error, because of the base vibrations, are negligible compared to the oscillation amplitude (Figure 5-5b). The small steady state error in the deployment degree of freedom is attributed to the gravitational force acting on the payload, which is deployed 10 m from the orbit along the local vertical. As can be expected, the control efforts at the slew joint and the twist (T_3, J_3) are affected by the base rotational oscillations as shown in Figures 5-5(d) and 5-5(e), respectively.

The main conclusions from the closed loop simulation results for the stationkeeping case are: a) it is possible to achieve point tracking (stationkeeping) for this class of space-based manipulators in the presence of platform maneuvers and base vibrations; b) the tracking error is essentially unaffected by the flexibility of the platform; c) the error in the controlled variables approaches to zero asymptotically.

5.3.2 Trajectory tracking

The next logical step would be to assess performance of the controller in tracking the desired trajectory. This subsection presents the closed loop response when the specified payload position describes a trajectory with respect to the platform. The tracking error and the control effort have been evaluated for the fixed as well as the moving base. The prescribed position of the platform is along the local vertical. The specified initial velocity components of the payload are 0.2 m/s and 0.03 m/s in the X_p and Y_p directions, respectively. The corresponding desired acceleration components are -0.005 m/s^2 and 0.002 m/s^2. The base is initially located at the center of the platform, and the payload is deployed 10 m along the platform ($P_x = 10$ m, $P_y = 0$). The closed loop responses for stationary as well as the moving base are presented in Figure 5-6 and 5-7, respectively.

Figure 5-6 shows the simulation results over 0.02 orbit (110 s). The parameters discussed are the degrees of freedom response, tracking error, control effort and the

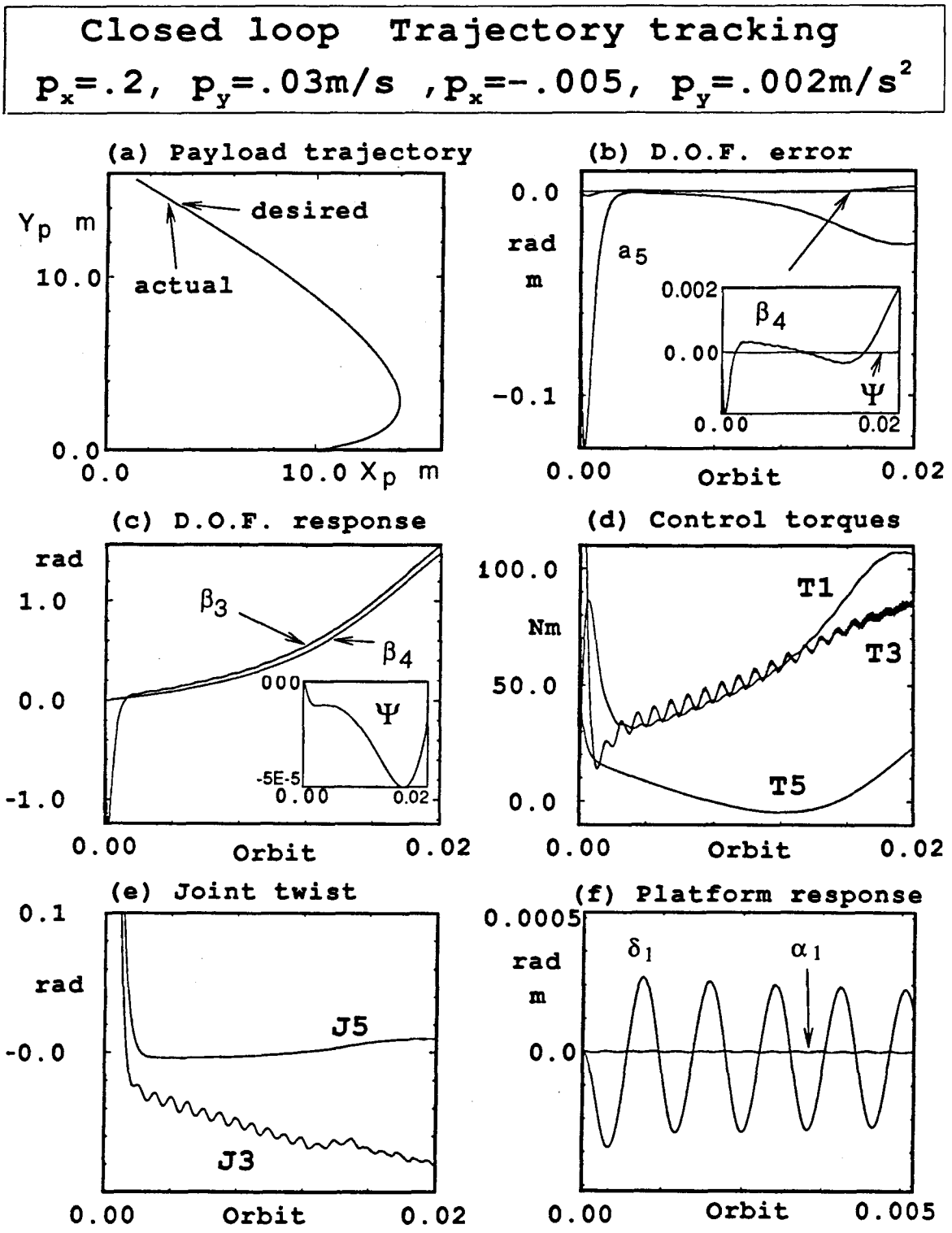

Figure 5-6 Closed loop response during the trajectory tracking, with the base held fixed and arm 2 initially deployed 10 m along the platform.

twist at the joints.

Figure 5-6(a) depicts the desired trajectory with respect to the platform reference frame F_p. The controlled response of the degrees of freedom is shown in Figure 5-6(c). The large displacement at joint 1 (β_3) is due to the initial desired values (velocity and acceleration) when the initial conditions of the controlled variables are all zero. Note, the slew of arm 1, β_4, follows the joint motion. The slew response excites the pitch with a maximum attitude error of $-5 \cdot 10^{-5}$ rad. The tracking error was relatively significant in the beginning and reached a steady state value of -0.025 m for the deployment degree of freedom (Figure 5-6b). The slew error increases as the arm approaches the orientation of 90 deg w.r.t. the platform. In that position, a relatively large desired maneuver causes the tracking error to increase to 0.002 rad, as seen in the expanded view of β_4 (Figure 5-6b). The payload follows the desired trajectory (Figure 5-6a) with the tracking accuracy according to the error in the individual arm (Figure 5-6b).

The time histories of the control efforts are presented in Figure 5-6(d). In the beginning, the control efforts are relatively large, as expected, in order to decrease the initial error in velocity and acceleration. As a result, the flexible platform is excited with linear and angular oscillations δ_1 and α_1, respectively, as shown in Figure 5-6(f). A small reduction in amplitude is attributed to the structural damping. The angular oscillations of the platform affect the control effort of the slew joint T_3 and platform pitch T_1 as can be seen in Figure 5-6(d). The control effort of the deployment degree of freedom is not affected because of the gear ratio and the relatively small oscillations of $5 \cdot 10^{-4}$. The twist at the joints is large at the begining in order to meet the demand, of required output torques, as shown in Figure 5-6(e).

Figure 5-7 presents the system response while performing a task in which the

payload is required to translate, along the platform at a constant speed of 0.5 m/s, over a distance of 10 m. Simultaniously, the MDM base is moving in the same direction at the same velocity. In others words, the slew arm is perpendicular to the platform while the base is translating along the platform, and the deployable arm keeps the payload at a constant distance from the undeformed centerline of the platform.

The control efforts for this case are shown in Figure 5-7(d). To overcome the initial error as a result of the fact that the payload has no initial velocity, the control effort T_3 at the slew joint is relatively large. Once the payload achieves the desired velocity, the demand on the controller decreases to the level required to compensate for the gravitational force. As the arms and payload deviate from the system c.m., more control effort is needed to overcome the gravitational effect. The control effort T_5 at the deployment joint is required to compensate for the Coriolis reaction due to the translation of the payload.

As a result of the input torques, the platform flexible modes are excited as shown in Figure 5-7(f). Here δ_1 represents the linear displacement at the base and α_1 the corresponding rotation. Note, while moving along the platform, the base crosses the nodal points: i.e. zero slope and displacement, at 0.008 orbit and 0.016 orbit, respectively. The effect of the platform oscillations can be clearly discerned from the response of the deployment and slew degrees of freedom as presented in Figures 5-7(c) and 5-7(e), respectively. As can be expected, at the nodal points, effect of the platform vibrations is relatively small, as apparent from the control inputs.

The tracking errors for the individual degrees of freedom are shown in Figure 5-7(b). For all practical purposes they are negligible. The steady state error for the deployment arm is 10^{-5} m, and the corresponding errors in pitch and slew are also of

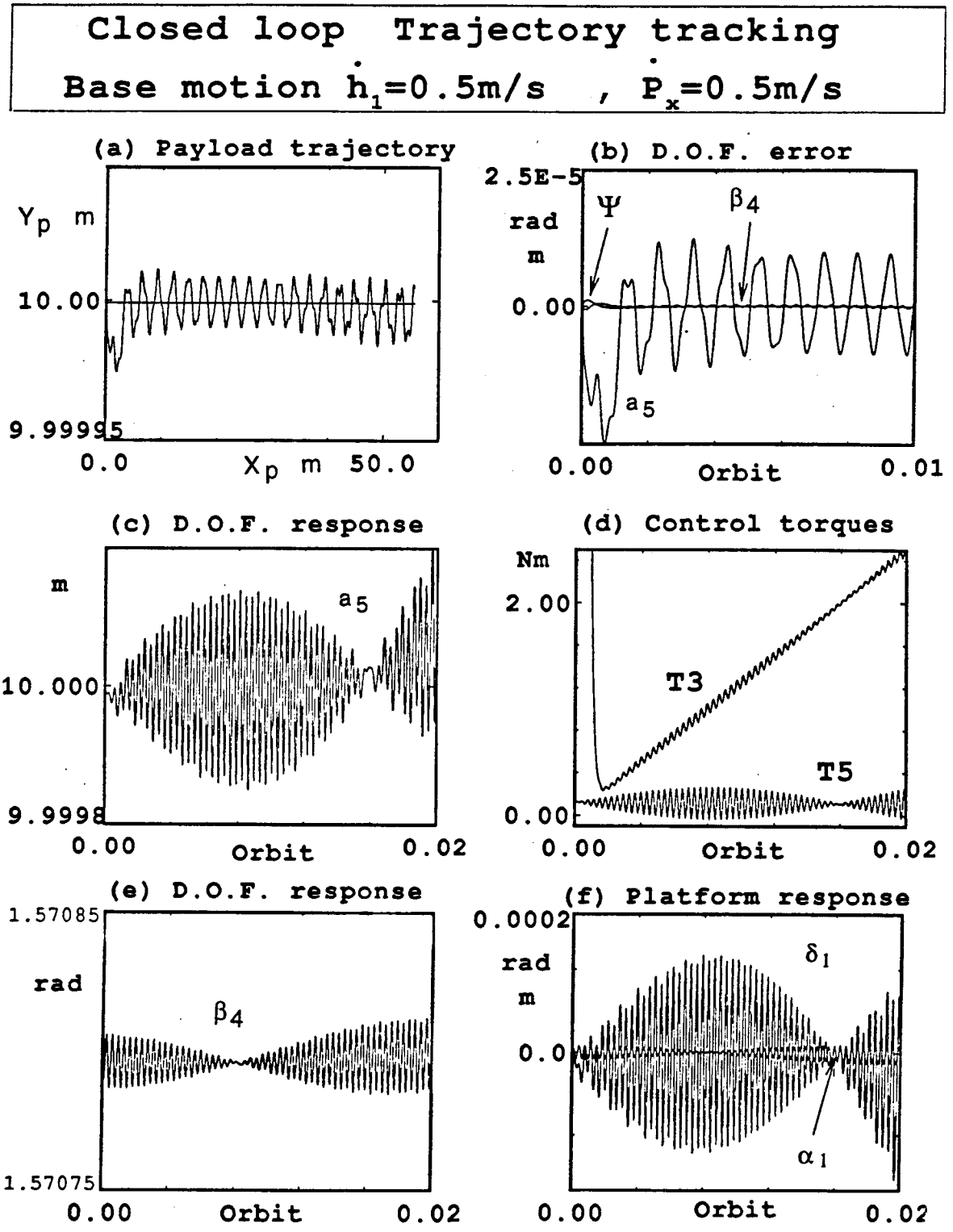

Figure 5-7 Closed loop response during the trajectory tracking for the MDM with the arm perpendicular to the platform.

the same order of magnitude. The actual and the desired trajectories are compared in Figure 5-7(a). Note, the total tracking error is small even compared to the vibrations amplitude of the platform.

The simulation results clearly point out effectiveness of the nonlinear control strategy even when applied to such highly flexible space-based manipulator. It is important to recognize that the tracking performance is essentially unaffected by the vibration of the MDM base.

5.3.3 Special cases

It was decided to assess effectivness of the nonlinear controller under several, particular demanding situations such as: the system with a relatively large initial error for the payload position; the system subjected to an external disturbance; and an inherently unstable orientation of the system. The issue concerning the choice of the feedback gains also must be addressed. With this objective in mind, to begin with, the system with initial position errors of $\beta_4 = 0.02$ rad in slew and $a_5 = 1.0$ m in the deployment degree of freedom is considered. The simulation results for this case are shown in Figure 5-8.

Figure 5-8(b) presents time histories of the errors corresponding to the generalized coordinates associated with the platform pitch (ψ), slew (β_4) and deployment (a_5). Note, the initial errors decrease significantly as a result of the control effort. The control torques and the dynamic reactions excite the flexible platform (Figure 5-8f). The manipulator base is initially located at the center of the platform, hence, the contribution to the displacement δ_1 is mainly from the first mode. The base is moving with a constant velocity of 0.01 m/s and the vibration amplitudes decrease.

The actual and the desired payload trajectories are shown in Figure 5-8(a). It

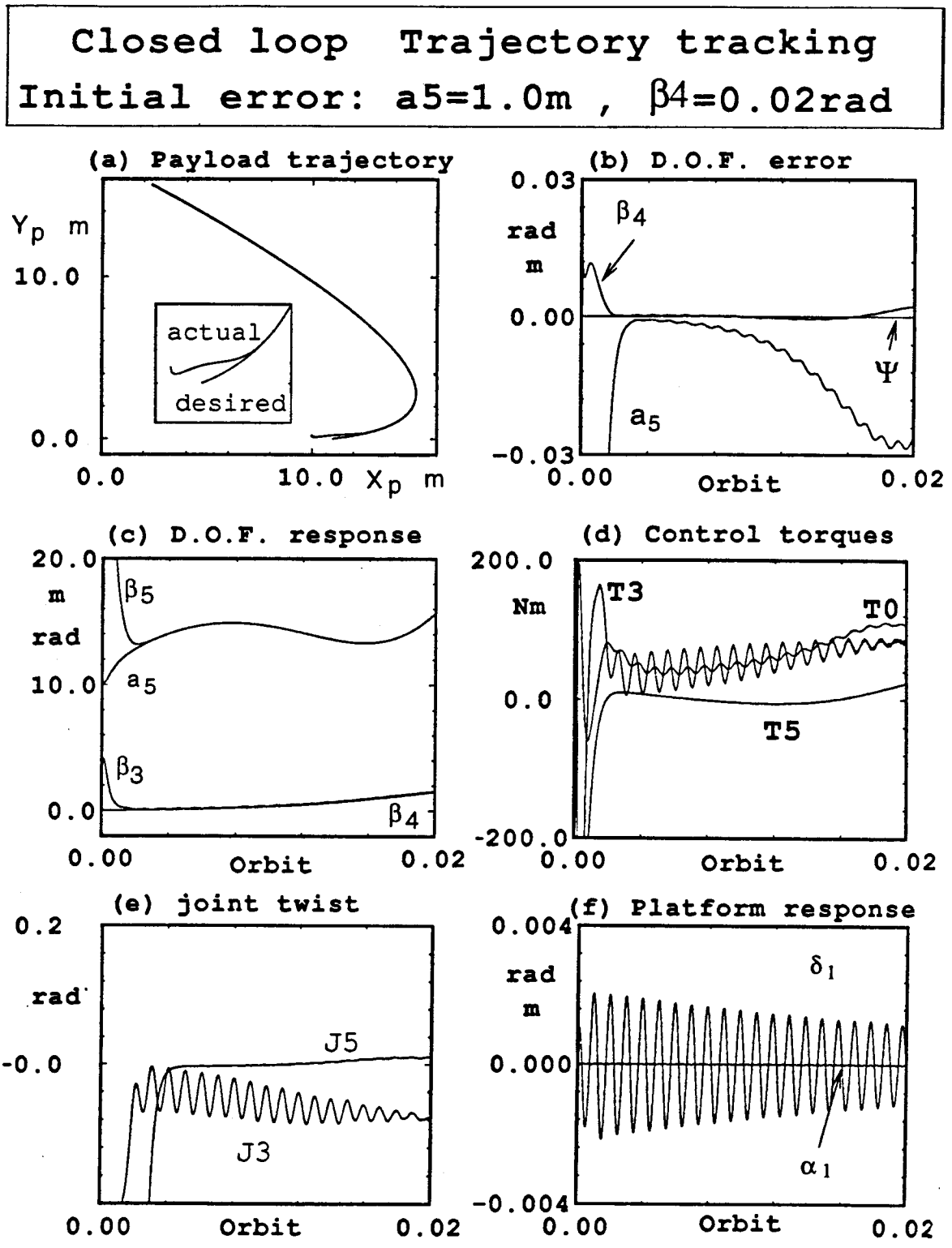

Figure 5-8 Closed loop response for trajectory tracking with initial position errors.

is apparent from the expanded view of the start of the tracking maneuver that the MDM has a relatively slow response. This is a consequence of the relatively low feedback gains selected to avoid excitation of the structure. After 0.001 orbit (5.5 sec) the initial error has diminished significantly. From Figure 5-8(c), it can be seen that the joint degrees of freedom β_3 and β_5 react relatively fast and strongly to the initial error. In real systems, for such a case, the joint motors may get saturated and hence may not be able to supply the required torques. To overcome this problem a gear ratio of more than 1:1 has to be considered. After the transient maneuver, the arms follow the joints up to the twist angle as shown in Figure 5-8(e).

In the earlier closed loop simulations, the platform initial conditions were taken to be zero. Yet the platform was excited due to coupling between the degrees of freedom. In the present tracking simulation, the platform is initially disturbed equally in all the modes to give $\bar{q}_1 = 0.1$ m. The effect of the platform initial condition and the feedback gains on the tracking performance are presented in Figure 5-9. Note, the configuration here is similar to that described in Figure 5-7. The slew arm is forced by the motion of the base and the desired payload trajectory to align perpendicular to the platform.

Figure 5-9(f) shows the platform deflection δ_1 and slope α_1 at the location of the base. The initial displacement for the base located at the center of the platform is 0.12 m (due to the modal disturbances). The platform dynamics is affected by the MDM and the maximum amplitude is 0.2 m. When the base is close to the nodal point, the platform response at the base reaches a minimum. Note, in the present case, the vibration of the base primarily affects the deployable arm. The control effort at joint 2 is shown in Figure 5-9(b) for the velocity and position feedback gains of $K_v = 1.2$ and $K_p = 0.36$, respectively. The peak control effort is around 150 Nm.

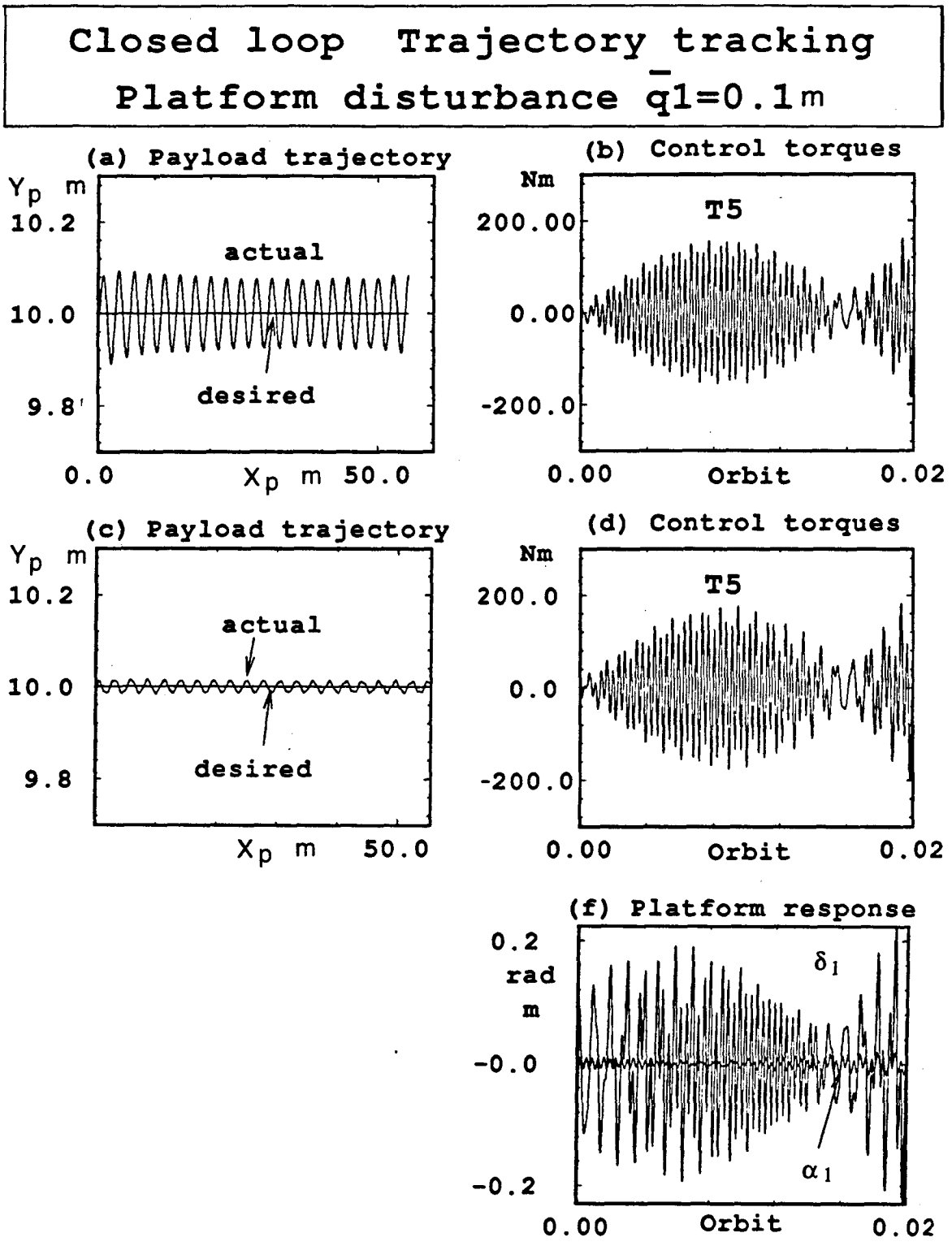

Figure 5-9 Controlled response for trajectory tracking with base motion 0.5 $\frac{m}{s}$ and the initial conditions of $\bar{q}_1 = 0.1$ m imposed on the platform.

The resultant tracking performance is shown in Figure 5-9(a). Note, even with such a severe disturbance, the controller is successful in limiting the peak error to around 0.1 m. The performance can be improved further by increasing the gains to $K_v = 6$ and $K_p = 9$. As a result the closed loop bandwidth has increased. The tracking performance for the high feedback gains is shown in Figure 5-9(c). The maximum tracking error is now reduced to 0.03 m and the peak control effort is slightly increased (Figure 5-9d).

From the simulation results it can be concluded that: external disturbances to the platform can adversely affect the tracking performance; the feedback gains dominate the closed loop behavior; and by proper selection of the gains, the controller can provide an acceptable performance.

The question concerning preferred orientation of the platform from the manipulator's performance consideration has not been addressed yet. The obvious choice was the gravity gradient configuration where the system is inherently stable. In the next closed loop simulation, the platform was aligned with the local horizontal, i.e., an unstable orientation, and the control effort in pitch compared with that of the gravity gradient case. The results are presented in Figure 5-10. The configuration of the system is similar to that described in Figure 5-9, except for the platform which is now oriented along the local horizontal.

The tracking performance data in Figure 5-10(a), clearly show that the orientation of the platform has virtually no effect on the trajectory tracking. The attitude error in pitch and the associated control effort are shown in Figures 5-10(b) and 5-10(d), respectively. The control effort is a function of the base and payload locations as well as the platform vibrations. As can be seen, the attitude error is kept low while the control effort is increasing according to the MDM base location along the

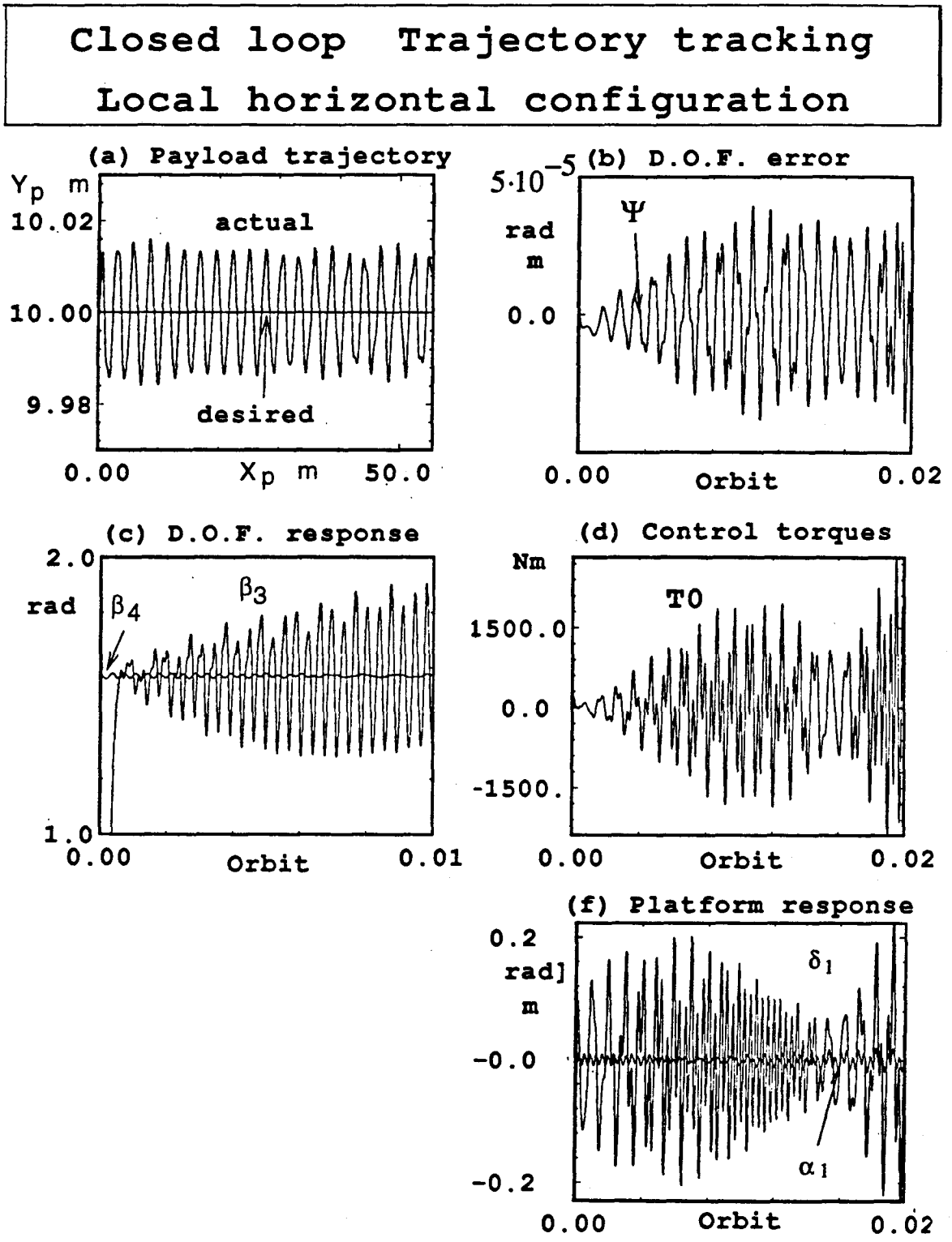

Figure 5-10 FLT controlled response for the trajectory tracking with the platform along the local horizontal and the base translation at 0.5 $\frac{m}{s}$. The initial condition is $\bar{q}_1 = 0.1$ m.

platform and the local vibration amplitude as shown in Figure 5-10(f). As expected, the control effort required to keep the platform in the desired orientation, when the base is close to the tip of the platform, is less compared to the corresponding gravity gradient case with MDM arm normal to the platform.

To assess effectivness of the controller in enabling the MDM-payload to follow a desired trajectory, even when subjected to disturbances of extreme severity, the initial conditions were increased to $\bar{q}_1 = 0.5$ with the position errors for the slewing and deploying arms set at 0.3 rad and 2 m, respectively. The tracking performance results for the MDM are presented in Figure 5-11. The desired trajectory properties were described earlier in Figure 5-6.

Figure 5-11(b) shows the resultant linear and angular oscilations at the center of the platform where the MDM base is located. The displacement amplitude δ_1 associated with the first mode is 0.6 m and the slope angle α_1 associated with the second mode is 0.04 rad. The tracking performance results are presented in Figure 5-11(a). As the initial position error is large, the transient response is relatively short and the tracking error decays to less than the vibration amplitude. From the expanded view, it can be seen that the tracking error in the transient is 0.1m. It diminished to almost zero after 0.02 orbit as shown in the enlarged view.

The control effort time-histories for this case are shown in Figure 5-12. Figure 5-12(a) presents the control efforts for a gear ratio of $n_3 = 1$ at the slew joint. Note, the torque (T_3) required to control the slew arm is enormous due to the large vibrations of the platform. When the slew arm approaches the 90^o position, the effect of the vibrations is gradually diminished. In fact, now the vibrations begin to affect the deployable arm. The control effort for this case is relatively small due to the effective gear ratio of 10. The torque required to maintain the desired attitude of the platform

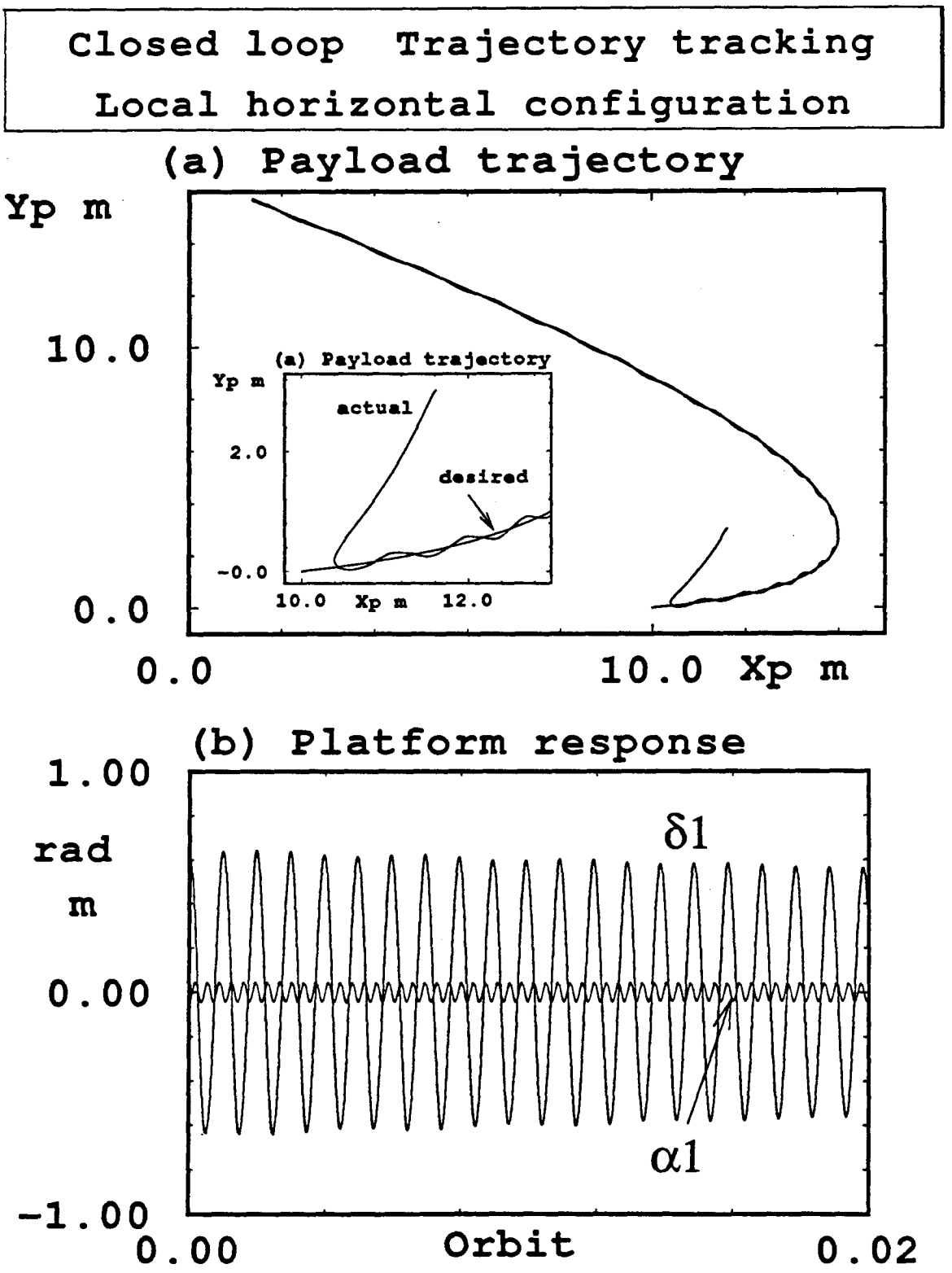

Figure 5-11 Controlled response during the trajectory tracking for the local horizontal configuration of the platform. The initial condition is $\bar{q}_1 = 0.5$ m for the platform. The initial position error are: 2 m in deployment; and 0.3 rad in slew.

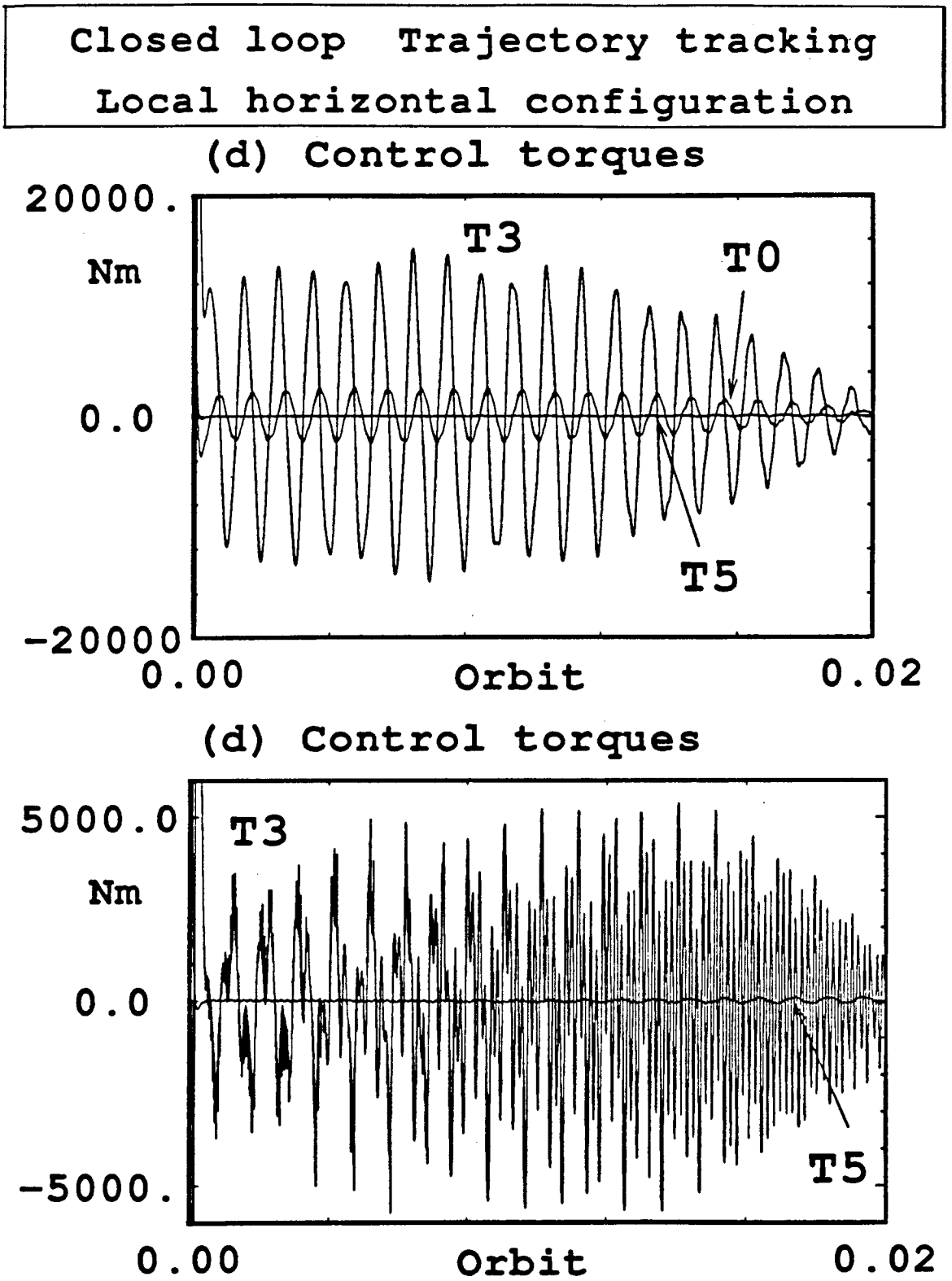

Figure 5-12 Control effort time histories for the system described in Figure 5-11: (a) gear ratio $n_3 = 1$; (b) gear ratio $n_3 = 10$.

is the result of the reaction moment from slew joint torque motor.

To reduce the control effort at the slew joint, gear ratio of $n_3 = 10$ was introduced (Figure 5-12b). The higher gear ratio reduces the torque demand to slew the arm from around 15,000 Nm to around 5,000 Nm. The joint rotor oscillates (β_3) at higher frequency and amplitude when the gear ratio is increased in order to supply the torque in the right direction.

Thus the results suggest that the gear ratio is an important parameter in the design and closed loop simulation of flexible space based manipulators.

5.4 Summary

The control study showed that it is possible to achieve high tracking performance with the end effector of a flexible space based manipulator, even under extreme conditions of platform maneuvers and base oscillations.

The strategy based on the FLT has been found to be effective in controlling the manipulator arms as well as the attitude motion of the space station. To successfully implement the controller, the MDM base must be provided with sensors to measure the local slope and the deflection of the flexible platform. The robustness issue, though not addressed here, is a valid one for the present study where the system is represented by a relatively accurate model.

The most important parameter is the feedback gain. Performance of the manipulator, tracking a desired trajectory, is not satisfactory when the gains are selected according to the common recommendation of one-half the lowest structural frequency. When the system is subjected to external disturbances, for example docking of the space shuttle, higher gain values may be necessary.

To implement the FLT, desired values must be assigned to each degree of freedom.

A procedure for real time evaluation of the joint parameters has been developed. To avoid numerical differentiation required for this purpose, introduction of the joint stiffness as a control variable is suggested.

6. CLOSING REMARKS

6.1 Concluding Comments

A relatively general formulation and associated simulation tool for studying the nonlinear dynamics and control of a space based flexible, mobile, deployable manipulator have been presented. The formulation employs Lagrange's approach. It leads to a set of nonlinear, nonautonomous and coupled equations of motion, governing the system dynamics.

In general, implementation of the equations into a comprehensive computer code involves enormous amount of effort. This is minimized through the use of vector operations and judicious synthesis of mathematical expressions leading to a relatively compact form of the equations of motion. The system is amenable to further simplification by neglecting the effect of the shift in the center of mass. This is justifiable for relatively small slewing maneuvers and slow deployment of the second arm.

To close the loop, a nonlinear control strategy based on the Feedback Linearization Technique (FLT) is adopted and incorporated in the program to form a complete simulation tool for design and performance evaluation of a large class of MDM systems.

Validity of the formulation and the computer code is established through comparison with particular cases and by checking the conservation of the total energy. The computer program is so structured, in a modular fashion, to permit detailed parametric analysis. The versatile simulation is applied to study three major aspects: open loop response; inverse kinematics; and closed loop performance.

A manipulator with a synthesis of revolute and prismatic joints is a novel idea, never explored in depth before, for application to space based platforms. Thus the

formulation, associated computer code, parametric analysis and control strategy represent original contributions of far-reaching significance. Of particular importance is the application of the FLT for control, which accounts for the complete nonlinear dynamics of a class of complex flexible, orbiting MDM's. This has never been attempted before, and presents possibilities of exciting developments in the areas of robotics and adaptive structures.

Based on the open loop and control analysis, following general conclusions can be made:

Open-Loop Systems

(i) Even for simple configurations the response of the MDM system is complex and unpredictable.

(ii) The MDM system is unstable even when the platform and the slew arm are in the gravity gradient orientation, especially when the MDM base is located away from the mid-point of the platform.

(iii) The flexibility of the platform affects the dynamic response of the system significantly and hence cannot be neglected. Platform vibrations change the frequency, amplitude and the equilibrium position of the slew arm.

(iv) Even small vibrations of the platform can create significantly different environment for the MDM, and the resulting coupling dynamics can cause the system to become unstable.

(v) Introduction of damping in the degrees of freedom adversely changes the system's dynamical response by exerting moments at the joints.

(vi) To obtain an accurate response, it is necessary to take into account more than one flexible modes for discretization of the platform deformations, This

removes constraints on slope and deflection at any station along the platform.

(vii) The vibration of the platform creates a pseudo-gravity field in the direction of the deflections which, in some cases, can be used to advantage for locating the slew arm in a position perpendicular to the platform.

(viii) For space based manipulators of the class discussed here, it is necessary to control the degrees of freedom to achieve desired performance. It is unsafe to depend even on the so called stable equilibrium positions to locate the arm, as in the case of ground based robots.

Inverse Kinematics

(i) It is possible to achieve trajectory and orientation tracking for a class of two degrees of freedom manipulators with a coordinated base motion.

(ii) The parametric study suggests that the platform vibrations affect the required degrees of freedom for tracking via the displacements and the rotations at the MDM base.

(iii) In order to take into account the effect of the base motion (displacement, slope) on the required values at each location along the platform, at least two flexible modes are necessary.

Closed-Loop Systems

(i) The control strategy based on the FLT is found to be effective in controlling the manipulator arms as well as the attitude motion of the platform.

(ii) The flexibility of the platform has significant influence on the control effort, which is proportinal to the vibration amplitude.

(iii) It is possible to reduce the control effort by increasing the gear ratio, implying

a need for the controller with a higher bandwidth.

(iv) To achieve better tracking accuracy in the precence of extreme external disturbances, higher gains than that those normally recomended in the standard textbooks are required.

6.2 Original Contributions

A complete simulation tool that can handle a flexible space based deployable type manipulator has been developed and analyzed in this thesis. The distinctive features of this simulation are:

- two degrees of freedom slewing-deployable type robot, with two more degrees of freedom for the flexible, dissipative joints;
- torque motors with gears at the joints;
- moving base traversing a vibrating platform free to librate in orbit;
- arbitrarily shaped payload supported at the tip of the deployable arm;
- inverse kinematics for flexible systems;
- payload capable of tracking any predefined trajectory.

The presentation of a novel concept, demonstration of its advantages, and thorough dynamical as well as nonlinear control analyses provide a rather selfcontained character to this innovative contribution. It leads to some interesting observations, analysis and discussions concerning:

- the pseudo gravitational field induced by the platform vibrations;
- the coordinated base motion in order to position and orient the payload;
- the variable joint stiffness and its use as a control variable.

6.3 Recommendations for Future Study

The study of the mobile flexible manipulator, free to slew and deploy, though reasonably comprehensive with reference to the stated objectives aimed at laying a sound foundation, represents only the first step in the development of an innovative idea. The possible exciting developments are indeed many. Some thoughts concerning its future evolution, which are likely to be satisfying, are indicated below:

(i) Introduction of the out-of-plane degrees of freedom will expand the capability of the MDM making it more versatile. It will be able to deal with the orbit normal configuration and assess gyroscopic effects on the MDM's performance.

(ii) In the present study, flexible character of the manipulator is reflected by the flexibility of the joints. For the out-of-plane study, it would be useful to incorporate flexibility of the deployable arm, as well as the torsional degree of freedom of the platform and the arm.

(iii) When dealing with relatively heavy payloads, the boundary conditions at the platform change with respect to time and must be taken in account in order to get accurate mode shapes.

(iv) For the time varying systems such as the MDM, an adaptive control strategy may be incorporate in order to improve the tracking performance.

(v) Extension of the FLT for nonlinear control with flexible degrees of freedom particularly with reference to the robustness, is necessary.

(vi) A systematic approach to select the controller gains and gear ratios is required. The tracking performance in the presence of system constraints (maximum power, bandwidth) needs further attention.

vii) Application of the concept to the development of adaptive structures appears

quite exciting. It can lead to the development of an entirely new field with a wide range of applications. Dynamics and control of variable geometry structures obtained through slewing-deploying links have never been studied before.

BIBLIOGRAPHY

[1] Paul, P.R.,*Robot Manipulators: Mathematics, programing and Control*, The MIT Press, Cambridge, Massachusetts, 1983.

[2] Fu, K.S., Gonzales, R.C., and Lee, C.S.G., *Robotics: Control, Sensing, Vision and Intelligence,* McGraw-Hill, Inc., New York, 1987.

[3] Chan, J.K.W, *Dynamics and Control of an orbiting Space Platform Based Mobile Flexible Manipulator,* M.Sc. Thesis, The University of British Columbia, April 1990.

[4] Forrest-Barlach, M.G., "On Modeling a flexible Robot Arm as a Distributed Parameter System with Nonhomogeneous, Time-Varying Boundary Conditions," *Proceedings of the 4th Symposium on Control of Distributed Parameter Systems,* Los Angeles, U.S.A., June - July 1986.

[5] Naganathan, G., and Soni, A.H., "Coupling Effects of Kinematics and Flexibility in Manipulators," *International Journal of Robotics Research*, Vol. 6, No. 1, Spring 1987, pp. 75-85.

[6] Book, W.J., "Recursive Lagrangian Dynamics of Flexible Manipulator Arms," *International Journal of Robotics Research*, Vol. 3, No. 3, Fall 1984, pp.87-101.

[7] Cetinkunt, S., and Book, W.J., "Symbolic Modeling of Flexible Manipulator," *Proceedings of the IEEE International Conference on Robotics and Automation*, Raleigh, USA, 1987, pp. 2074-2080.

[8] Nurre, G.S., Ryan, R.S., Scotfield, H.N., and Sims, J.L., "Dynamics and Control of Large Space Structures," *Journal of Guidance Control and Dynamics*, Vol. 7, No.5, Sept. 1984, pp. 514-526.

[9] Modi, V.J., "Attitude Dynamics of Satellites with Flexible Appendages - A Brief Review," *Journal of Spacecraft and Rockets*, Vol. 11, No. 11, November 1974, pp. 743-751.

[10] Hablani, H.B., "Constrained and Unconstrained Modes: Some Modeling Aspects of Flexible Spacecraft," *Journal of Guidance Control and Dynamics*, Vol. 5, No. 2, March-April 1982, pp. 164-173.

[11] Hughes, P.C., "Modal Identites for Elastic Bodies, with Application to vehicle Dynamics and Control," *Trans. of ASME, Journal of Applied Mathematics*, Vol. 47, March 1980, pp. 177-184.

[12] Achille M., and Deborah H., "Discret Dynamics Modelling of a Rigid Body Moving on a Flexible Structure," *AAS/AIAA Astrodynamics conference*, Durango, Colorado, U.S.A. August 1991, Paper No. AAS 91-399.

[13] Singh, R.P., Vandervoort, R.J., and Likins, P.W., "Dynamics of Flexible Bodies in Tree-Topology - A Computer Oriented Approach," Paper No. AIAA-84-1024, *AIAA/ASME/ASCE 25th Structural Dynamics, and Materials Conference*, Palm Spring, U.S.A., May 1984.

[14] Kane, T.R., Ryan, R.R., and Banerjee, A.K., "Dynamics of a Cantilever Beam Attached to a Moving Base," *Journal of Guidance, Control, and Dynamics*, Vol. 10, No. 2, March-April 1987, pp. 139-151.

[15] Reddy, A.S.S.R., Bainum, P.M., and Krisna R., "Control of a Large Flexible Platform in Orbit," *Proceedings of the AIAA/AAS Astrodynamics Conference*, Danvers, Massachussetts, August 1980, Paper No. AIAA 81-122.

[16] Bainum, P.M., and Kumar, V.K., "On the Dynamics of Large Orbiting Flexible Beams and Platforms Oriented Along the Local Horizontal," *Proceedings of the 31st International Astronautical Congress*, Tokyo, Japan, September 1980.

[17] Lang, W., and Honeycutt, G.H., "Simulation of Deployment Dynamics of spining Spacecraft," *NASA* TN-D-4074, 1967.

[18] Cloutier, G.J., "Dynamics of Deployment of Extendible Booms from Spinning Space Vehicles," *Journal of Spacecraft and Rockets*, Vol. 5, May 1968, pp. 547-552.

[19] Hughes, P.C., "Dynamics of a spin-Stabilized Satellite during Extension of Rigid Booms," *CASI Transactions*, Vol. 5, 1972, pp. 11-19.

[20] Sellappan, R., and Bainum, P.M., "Dynamics of Spin- Stabilized Spacecraft during Deployment of Telescopic Appendages," *Journal of Spacecraft and Rockets*, Vol. 13, October 1976, pp. 605-610.

[21] Modi, V.J., and Ibrahim, A.M., "A General Formulation for Librational Dynamics of Spacecraft with Deploying Appendages," *Journal of Guidance, Control, and Dynamics*, Vol. 7. No. 5, September-October 1984, pp. 563-569.

[22] Hablani, H.B., "Attitude Dynamics of a Rotating Chain of Rigid Bodies in a Gravitational Field," *Journal of Guidance, Control, and Dynamics*, Vol. 8, No. 4, July-August 1985, pp. 471-477.

[23] Conway, B.A., and Widhalm, J.W., "Equations of Attitude Motion for a N-Body Satellite with Moving Joints," *Journal of Guidance Control and Dynamics*, Vol. 8, No. 4, July-August 1985, pp. 537-539.

[24] Millar, R.A., Graham, W.R., and Vigneron, F.R., "Simulation of the Motion of a Shuttle Attached Flexible Manipulator Arm," *Proceedings of the Tenth International Association for Mathematics and Computers in Simulation*, World Congresss on System Simulation and Scientific Computation, Montreal, Canada, August 1982, Vol. 3, pp. 225-227.

[25] Ravindran, R., Sachdev, S.S., and Aikenhead, B., "The Shuttle Remote Manip-

ulator System and its Flight Tests" *Proceedings of the 14th International Symposium on Space Technology and Science*, Tokyo, Japan 1984, pp. 1125-1132.

[26] Meissinger, H.F., and Spector, V.A., "The role of Robotics in Space Systems Operations", *A Collection of technical papers of the AIAA Guidance, Navigation and Control Conference*, Snowmass, Colorado, U.S.A. August 1985, pp.223-236.

[27] Gardner, B.E., McLaughlin, J.S., Tucker, T.E., and Williamson, R.K., "Aerospace Initiative in Robotics Research," *A Collection of Technical Papers of the AIAA Guidance, Navigation and Control Conference*, Snowmass, Colorado, U.S.A. August 1985, pp. 237-245.

[28] Bejczy, A.K., Kan, E.P., and Killion, R.R., "Integrated Multi-Sensory Contol of Space Robot Hand," *A Collection of Technical Papers of the AIAA Guidance, Navigation and Control Conference*, Snowmass, Colorado, U.S.A. August 1985, pp. 253-259.

[29] Chase, C., Chase, W., Lohr, M., Lee, G.K.F., and Dwyer, T.A.W., III, "An Operational 1/16th Size Model of the Space Shuttle Manipulator," *A Collection of Technical Papers of the AIAA Guidance, Navigation and Control Conference*, Snowmass, Colorado, U.S.A. August 1985, pp. 269-277.

[30] Shiraki, K., Marumo, H., Sugasawa, Y., and Nishida, S., "Preliminary Concept of RMS for Japanese Experiment Module of the Space Station," *Joint AAS/Japanese Rocket Society (JRS) Symposium*, Honolulu, Hawaii, Dec. 1985, Paper No. 85-662.

[31] Meirovitch, L., and Quinn, R.D., "Equations of Motion for Maneuvering Flexible Spacecraft," *Journal of Guidance, Control, and Dynamics*, Vol. 10, No. 5, September-October 1987, pp.453-465.

[32] Longman, R.W., Lindberg, R.E., and Zedd, M.F., "Satellite Mounted Robot

Manipulators - New Kinematics and Reaction Moment Compensation," *The International Journal of Robotics Research*, Vol. 6, No. 3, Fall 1987, pp. 87-103.

[33] Hale, A.L, Lisowski, R.J., and Dahl, W.E., "Optimal Simultaneous Structural and Control Design of Maneuvering Flexible Spacecraft," *Journal of Guidance, Control, and Dynamics*, Vol. 8, No. 1, January-February 1985, pp. 86-93.

[34] Carrington, C.K., and Junkins, J.L., "Optimal Nonlinear Feedback Control for Space attitude Maneuvers, "*Journal of Guidance, Control, and Dynamics*, Vol. 9, No. 1, January-February 1986, pp. 99-107.

[35] Yuan, J.S.C., and Stieber, M.E., "Robust Beam-Pointing and Attitude Control of a Flexible Spacecraft," *Journal of Guidance, Control, and Dynamics*, Vol. 9, No. 2, March-April 1986, pp. 228-234.

[36] Garcia, E., and Inman, D.J., "Modeling of the Slewing Control of a Flexible Structure",*Journal of Guidance, Control, and Dynamics*, Vol. 14, No. 4, Sep.-Oct. 1991, pp. 736-742.

[37] Spong, M.W., and Vidyasagar, M., "Robust Linear Compensator Design for Nonlinear Robotic Control", *Proceeding of IEEE Conference on Robotics and Automation*, St. Louis, Missouri, March 1985, pp. 954-959.

[38] Widmann, G.R., and Ahmad, S., "Control of Industrial Robots with Flexible Joints," *Proceeding of the IEEE International Conference on Robotics and Automation*, Raleigh, USA, 1987, Vol. 3, pp. 1561-1566.

[39] De Luca, A., "Dynamic Control of Robots with Joint Elasticity,"*Proceeding of the IEEE International Conference on Robotics and Automation*, Philadelphia, USA, 1988, Vol. 1,pp.152-158.

[40] De Wit, C.C., and Lys, O., "Robust Control and Parameter Estimation of Robots with Flexible Joints,"*Proceeding of the IEEE International Conference*

on Robotics and Automation , Philadelphia, USA, 1988, Vol. 1, pp. 324-329.

[41] Ahmad, S., and Guo, H., "Dynamic Coordination of Dual-Arm Robotic Systems with Joint Flexibility ," *Proceeding of the IEEE International Conference on Robotics and Automation,* Philadelphia, USA, 1988, Vol. 1, pp. 332-337.

[42] Modi, V.J., Karray, F. and Chan, J.K., "On the Control of a Class of Flexible Manipulators Using Feedback Linearization Approach," *42nd Congress of the International Astronautical Federation* , Montreal, Canada, October 1991, Paper No. IAF-91-324; also *Acta Astronautica*, Vol. 29, No. 1, 1993, pp. 17-27.

[43] Marom, I, "A Closed-Form Dynamical Analysis of an Orbiting Single Link Manipulator," Technical Report.

[44] Ng, A.C., *Dynamics and Control of Orbiting Flexible System: a Formulation with Applications,* Ph.D. Thesis, The University of British Columbia, April 1992.

[45] Butenin, N.V., *Elements of Nonlinear Oscillations,* Baisdell Publishing Company, New York, U.S.A. pp. 102-137.

[46] Blevins, R., *Formulas for Natural Frequencies and Mode Shapes*, Robert E. Krieger Publishing Co., Malabar, Florida, U.S.A., 1984, pp. 107-109.

[47] Yu, E. Y., "Long-term Coupling Effects Between the Librational and Orbital Motion," *AIAA Journal,* Vol. 2, No. 3, March 1964, pp. 553-555.

[48] Misra, A. K., and Modi, V. J., "The Influence of Satellite Flexibility on Orbital Motion," *Celestial Mechanics,* Vol. 17, 1978, pp. 145-165.

[49] Brereton, R.C., *A Stability Study of Gravity Oriented Satellites*, Ph.D. Thesis, The University of B.C., November 1967.

[50] Silver, W.M., "On the Equivalence of Lagrangian and Newton-Euler Dynamics for Manipulators," *The International Journal of Robotics,* Vol. 1, No. 2, 1982,

pp. 60-70.

[51] Modi, V.J., Pradhan, S., and Misra, A.K., "On the Parametric Response and Control of a Flexible Tethered Two-Body System," in preparation for publication in *Acta Astronautica.*

[52] Space Station Engineering Data Book, NASA Space Station Program Office, Washington, D.C., NASA SSE-E-87-R1, November 1987.

[53] Beijczy, A.K., *Robot Arm Dynamics and Control,* JPL TM 33-669, California Institute of Institute of Technology, Pasadena, California, 1974.

[54] Spong, M.W., "Modelling and Control of Elastic Joint Robots" *Journal of Dynamic Systems, Measurement and Control,* Vol. 109, December 1987, pp. 310-319.

APPENDIX I : MODE SHAPES

The modal functions for the platform, treated as a free-free beam, as given in Blevins [46] are

$$\bar{\phi}_1(x) = coshp_i(x_1 + l_1) + cosp_i(x_1 + l_1) - \sigma_i[sinhp_i(x_1 + l_1) + sinp_i(x_1 + l_1)], \quad (I.1)$$

with

$$\sigma_i = \frac{cosh2p_il_1 - cos2p_il_1}{sinh2p_il_1 - sin2p_il_1}, \quad (I.2)$$

where p_i is the spatial frequency parameter of the i^{th} mode. $2p_il_1$ is the i^{th} root of the characteristic equation associated with the i^{th} mode,

$$cos2p_il_1 cosh2p_il_1 = 1. \quad (I.3)$$

This transendental equation has infinite number of roots, thus leading to an infinite number of mode shapes, listed below:

Mode	$2p_il_1$	σ_1
1	4.7300407448627	0.98250221457624
2	7.8532046240958	1.0007773119073
3	10.995607838002	0.99996645012541
4	14.137165491257	1.00000144989770
5	17.278596573990	0.99999993734438
$i > 5$	$\frac{(2i+1)\pi}{2}$	1.00

In formulating the governing equations of motion, it is necessary to evaluate the displacement and slope of the modal functions at the location of the manipulator base. Furthermore, it is required to evaluate integrals, involving the modal functions, over the length of the platform. These integrals are given below:

$$\bar{\Phi}_1^T = \frac{1}{2l_1}\int_{-l_1}^{l_1} \bar{\phi}_1^T(x)dx_1 = 0; \tag{I.4}$$

$$\Phi_{11} = \frac{1}{2l_1}\int_{-l_1}^{l_1} \bar{\phi}_1(x)\bar{\phi}_1^T(x)dx_1 = 1; \tag{I.5}$$

$$\bar{\Phi}_{1x}^T = \frac{1}{2l_1}\int_{-l_1}^{l_1} x_1\bar{\phi}_1^T(x)dx_1 = 0; \tag{I.6}$$

$$\bar{\phi}_1' = \frac{\partial\bar{\phi}_1}{\partial x_1}; \tag{I.7}$$

$$\bar{\Phi}_1' = \int_{-l_1}^{l_1} \bar{\phi}_1' dx_1; \tag{I.8}$$

$$\bar{\Phi}_1''^T = \int_{-l_1}^{l_1} [\bar{\phi}_1''^T(x)]^2 dx_1 = 2l_1(\bar{p}_i^4)^T. \tag{I.9}$$

APPENDIX II : THE SYSTEM INERTIA MATRIX

The instantaneous system inertia diadic about the system frame is given by

$$[I] = \sum_{i=1}^{n} \int_{m_i} \{(\bar{r}_i^T \bar{r}_i)[U] - (\bar{r}_i \bar{r}_i^T)\} dm_i, \qquad (II.1)$$

where [U] is the unit matrix.

According to the system model as described in Chapter 2, the MDM base moment of inertia I_2 is small comared to the platform moment of inertia I_1. As no generalized coordinate is associated with the base motion, I_2 has been neglected in the present study. The system moment of inertia w.r.t. the system frame, is the sum of contributions coming from the bodies constituting the system,

$$[I] = [I_1] + [I_3] + [I_4] + [I_5] + [I_6]. \qquad (II.2)$$

The platform mass moment of inertia matrix is

$$[I_1] = m_1 \begin{bmatrix} a_{0y}^2 + \bar{q}_1^T \Phi_{11} \bar{q}_1 + \frac{d_1^2}{3} & -a_{0x}a_{0y} - \Phi_{1x}^T \bar{q}_1 & 0 \\ -a_{0x}a_{0y} - \Phi_{1x}^T \bar{q}_1 & a_{0x}^2 + \frac{l_1^2}{3} + \frac{d_1^2}{6} & 0 \\ 0 & 0 & a_{0x}^2 + a_{0y}^2 + \frac{l_1^2}{3} + \bar{q}_1^T \Phi_{11} \bar{q}_1 + \frac{d_1^2}{6} \end{bmatrix}, \qquad (II.3)$$

where a_{0x}, a_{0y} are the shifts of the system c.m. w.r.t. F_0.

Neglecting the mass of the joints, the torque motor rotor inertias are given as:

$$[I_3] = \begin{bmatrix} 0 & 0 & 0 \\ 0 & 0 & 0 \\ 0 & 0 & I_3 \end{bmatrix}; \qquad [I_5] = \begin{bmatrix} 0 & 0 & 0 \\ 0 & 0 & 0 \\ 0 & 0 & I_5 \end{bmatrix}; \qquad (II.4)$$

The moment of inertia of arm 1 is

$$[I_4] = m_4 \begin{bmatrix} [a_{0y} + \bar{\phi}_1^T(h_1)\bar{q}_1][a_{0y} + \bar{\phi}_1^T(h_1)\bar{q}_1 + l_4 s\psi_4] & -[(a_{0y} + \bar{\phi}_1^T(h_1)\bar{q}_1)(a_{0x} + h_1 + \frac{l_4}{2}c\psi_4) & 0 \\ +\frac{l_4^2}{3}s^2\psi_4 + \frac{d_4^2}{4} & +(a_{0x} + h_1)\frac{l_4}{2}s\psi_4 + \frac{l_4^2}{6}s2\psi_4] & \\ ------ & --------- & --- \\ -[(a_{0y} + \bar{\phi}_1^T(h_1)\bar{q}_1)(a_{0x} + h_1 + \frac{l_2}{2}c\psi_4)+ & (a_{0x} + h_1)(a_{0x} + h_1 + l_4 c\psi_4)+ & 0 \\ (a_{0x} + h_1)\frac{l_4}{2}s\psi_4 + \frac{l_4^2}{6}s2\psi_4] & \frac{l_4^2}{3}c^2\psi_4 & \\ ----- & ---------- & --- \\ 0 & 0 & I_4(3,3) \end{bmatrix}, \tag{II.5}$$

with

$$I_4(3,3) = (a_{0x}+h_1)(a_{0x}+h_1+l_4c\psi_4)+(a_{0y}+\bar{\phi}_1^T(h_1)\bar{q}_1)(a_{0y}+\bar{\phi}_1^T(h_1)\bar{q}_1+l_4s\psi_4)+\frac{l_4^2}{3}.$$

Here, $\psi_4 = \alpha_1 + \beta_4$, and l_4 is the length of arm 1.

The moment of inertia of the arm 2 assembly is

$$[I_6] = m_6 \begin{bmatrix} (a_{0y} + \bar{\phi}_1^T(h_1)\bar{q}_1 + a_5 s\psi_4)^2 & -(a_{0x} + h_1 + a_5 c\psi_4) & 0 \\ & (a_{0y} + \bar{\phi}_1^T(h_1)\bar{q}_1 + a_5 s\psi_4) & \\ ----- & ----- & ----- \\ -(a_{0x} + h_1 + a_5 c\psi_4) & (a_{0x} + h_1 + a_5 c\psi_4)^2 & 0 \\ (a_{0y} + \bar{\phi}_1^T(h_1)\bar{q}_1 + a_5 s\psi_4) & & \\ ----- & ----- & ----- \\ 0 & 0 & I_6(3,3) \end{bmatrix}$$

$$+\frac{1}{2}\begin{bmatrix} I_{6x} + I_{6y} + I_{6z} & 0 & 0 \\ 0 & I_{6x} + I_{6y} + I_{6z} & 0 \\ 0 & 0 & I_{6x} + I_{6y} + I_{6z} \end{bmatrix}$$

$$-\frac{1}{2}\begin{bmatrix} I_{6x}(s^2\psi_4 - c^2\psi_4) + I_{6y}(c^2\psi_4 - s^2\psi_4) + I_{6z} & -2s\psi_4 c\psi_4(I_{6y} - I_{6x}) & 0 \\ -2s\psi_4 c\psi_4(I_{6y} - I_{6x}) & I_{6x}(c^2\psi_4 - s^2\psi_4) + I_{6y}(s^2\psi_4 - c^2\psi_4) + I_{6z} & 0 \\ 0 & 0 & 0 \end{bmatrix}$$

$$+\begin{bmatrix} 0 & 0 & 0 \\ 0 & 0 & 0 \\ 0 & 0 & I_{6x} + I_{6y} - I_{6z} \end{bmatrix},$$

$$with \qquad I_6(3,3) = (a_{0x} + h_1 + a_5 c\psi_4)^2 + (a_{0y} + \bar{\phi}_1^T(h_1)\bar{q}_1 + a_5 s\psi_4)^2, \tag{II.6}$$

where I_{6x}, I_{6y}, I_{6z} are the principal moments of inertia of the arm 2 payload assembly w.r.t. the frame F_6.

APPENDIX III : MASS MATRIX [M] AND THE NONLINEAR VECTOR {N}

The MDM system equations of motion have the form

$$[M]\{\ddot{q}\} = \{N\}. \qquad (III.1)$$

The mass matrix is symmetric and positive definite, therefore $M(i,j) = M(j,i)$ where:

$$\begin{aligned}
M(1,1) =& m_1\Phi_{11} + m_a[(\bar{\phi}_1^T(h_1))^2 - 2\bar{\phi}_1^T(h_1)\bar{\Phi}_1^T] \\
&+ 2m_b c\psi_4\bar{\phi}_1'^T(h_1)\phi + (\bar{\phi}_1'^T(h_1))^2[m_c + I_3 + I_5 + I_{6z}]; \\
M(1,2) =& m_1\Phi_{1x}^T + m_a[\phi]h_1 + m_b c\psi_4[\phi + \bar{\phi}_1'^T(h_1)] \\
&+ m_b s\psi_4\bar{\phi}_1'^T(h_1)\bar{q}_1\phi + \bar{\phi}_1'^T[m_c + I_3 + I_5 + I_{6z}]; \\
M(1,3) =& I_3\bar{\phi}_1'^T(h_1); \\
M(1,4) =& m_b c\psi_4\phi + \bar{\phi}_1'^T(h_1)[m_c + I_5 + I_{6z}]; \\
M(1,5) =& I_5\bar{\phi}_1'^T(h_1); \\
M(1,6) =& m_6 s\psi_4\phi; \\
M(2,2) =& I_3 + I_5 + I_{6z} + m_1[\frac{l_1^2}{3} + \frac{d_1^2}{6} + \bar{q}_1^T\Phi_{11}\bar{q}_1] \\
&+ m_a[h_1^2 + (\bar{\phi}_1^T(h_1)q_1)^2] + m_c \\
&+ 2m_b[h_1 c\psi_4 + \bar{\phi}_1^T(h_1)\bar{q}_1 s\psi_4]; \\
M(2,3) =& I_3; \\
M(2,4) =& m_b[h_1 c\psi_4 + \phi\bar{q}_1 s\psi_4] + m_c + I_5 + I_{6z}; \\
M(2,5) =& I_5; \\
M(2,6) =& m_6[h_1 s\psi_4 + \phi\bar{q}_1 c\psi_4]; \\
M(3,3) =& I_3;
\end{aligned}$$

$$M(3,4) = 0;$$

$$M(3,5) = 0;$$

$$M(3,6) = 0;$$

$$M(4,4) = m_c + I_5 + I_{6z};$$

$$M(4,5) = I_5;$$

$$M(4,6) = 0;$$

$$M(5,5) = I_5;$$

$$M(5,6) = 0;$$

$$M(6,6) = m_6.$$

Here:

$$m_a = m_4 + m_6;$$

$$m_b = m_4 \frac{l_4}{2} + m_6 a_5;$$

$$m_c = m_4 \frac{l_4^2}{3} + m_6 a_5^2;$$

$$\phi = \bar{\phi}_1^T(h_1) - \bar{\Phi}_1^T.$$

The components of the nonlinear vector N, on the r.h.s. of the equation of motion, are as follow:

$$\begin{aligned} N(1) =& \ddot{h}_1\{m_b \bar{\phi}_1'^T(h_1) s\psi_4\} \\ &+ (\dot{\psi} + \dot{\theta})^2\{m_1 \Phi_{11} \bar{q}_1 + m_a \bar{\phi}_1^T(h_1) \bar{q}_1 \bar{\phi}_1^T(h_1) \\ &+ m_b[\bar{\phi}_1^T(h_1) s\psi_4 + (\bar{\phi}_1^T(h_1) \bar{q}_1 c\psi_4 - h_1 s\psi_4) \bar{\phi}_1'^T(h_1)]\} \\ &- 2(\dot{\psi} + \dot{\theta})\{m_a \dot{h}_1 \phi + m_6 \dot{a}_5[\phi c\psi_4 + a_5 \bar{\phi}_1'^T(h_1)] \\ &+ m_b[-\phi(\dot{\psi}_4 - \dot{\bar{q}}_1 \bar{\phi}_1'^T(h_1) s\psi_4 + \dot{h}_1 \bar{\phi}_1'^T(h_1) c\psi_4\} \\ &+ \dot{\psi}_4^2\{\phi m_b s\psi_4\} \end{aligned}$$

$$
\begin{aligned}
&- 2\dot{\psi}_4\dot{a}_5 m_6\{\phi c\psi_4 + a_5\bar{\phi}_1'^T(h_1)\} \\
&- EJ\bar{\Phi}_1''^T\bar{q}_1 - C_1\bar{\Phi}_1^T\dot{\bar{q}}_1 \\
&- \frac{3GM}{r_c^3}\{m_1[\Phi_{11}\bar{q}_1(c^2\psi - \frac{2}{3}) + \frac{s2\psi}{2}\bar{\Phi}_{1x}] \\
&+ m_a[\bar{\phi}_1^T(h_1)\bar{q}_1\bar{p}hi_1(h_1)(c^2\psi - \frac{2}{3}) + \frac{s2\psi}{2}h_1\bar{\phi}_1(h_1) \\
&+ [m_c + I_{6y} - I_{6x}]\bar{\phi}_1'^T(h_1)\frac{s2(\psi+\psi_4)}{2} + m_b[\phi_1^T(h_1)[c\psi s(\psi \\
&+ \psi_4) - \frac{2}{3}c\psi_4] + \bar{\phi}_1^T(h_1)\bar{q}_1\bar{\phi}_1'^T(h_1)[c\psi c(\psi+\psi_4) - \frac{2}{3}c\psi_4] \\
&+ h_1\bar{\phi}_1'^T(h_1)[s\psi c(\psi+\psi_4) \\
&+ \frac{2}{3}s\psi_4]]\}; \\
N(2) =& \ddot{h}_1\{m_a\phi\bar{q}_1 + s\psi_4 m_b\} \\
&+ \dot{\psi}_4^2\{m_b[h_1 s\psi_4 - \phi\bar{q}_1 c\psi_4]\} \\
&- 2\dot{\psi}_4\dot{a}_5 m_6\{h_1 c\psi_4 + a_5 + \phi\bar{q}_1 s\psi_4\} \\
&- 2(\dot{\psi}\dot{\theta})\{m_1\dot{\bar{q}}_1^T\Phi_{11}\bar{q}_1 + [h_1\dot{h}_1 + \bar{\phi}_1^T(h_1)\dot{\bar{q}}_1\bar{\phi}_1^T(h_1)\bar{q}_1]m_a \\
&+ m_6\dot{a}_5[h_1 c\psi_4 + a_5 + \bar{\phi}_1^T(h_1)\bar{q}_1 s\psi_4] \\
&+ m_b[\dot{h}_1 c\psi_4 - h_1\dot{\psi}_4 s\psi_4 + \bar{\phi}_1^T(h)_1\dot{\bar{q}}_1 s\psi_4 \\
&+ \bar{\phi}_1^T(h_1)\bar{q}_1\dot{\psi}_4 c\psi_4]\} \\
&- \frac{3GM}{r_c^3}\{m_1[(\frac{l_1^2}{3} - \frac{d_1^2}{6} - \bar{q}_1^T\Phi_{11}\bar{q}_1)\frac{s2\psi}{2} \\
&+ \bar{\Phi}_{1x}^T\bar{q}_1 c2\psi] \\
&+ m_a[(h_1^2 - (\bar{\phi}_1^T(h_1)\bar{q}_1)^2\frac{s2\psi}{2} + \bar{\phi}_1^T(h_1)\bar{q}_1 c2\psi] \\
&+ \frac{1}{2}[m_c + I_{6y} - I_{6x}]s2(\psi+\psi_4)] + m_b[h_1 s(2\psi+\psi_4) \\
&+ \bar{\phi}_1^T(h_1)\bar{q}_1 c(2\psi+\psi_4)]\} \\
&+ \bar{T}_0 - C_0\dot{\psi}; \\
N(3) =& k_3(\beta_4 - \beta_3) + \bar{T}_3 - C_3\dot{\beta}_3;
\end{aligned}
$$

$$
\begin{aligned}
N(4) =& \ddot{h}_1[m_b s\psi_4] \\
& - 2(\dot{\psi}+\dot{\theta})\{m_6 a_5 \dot{a}_5 + m_b[\dot{h}_1 c\psi_4 + \phi\dot{\bar{q}}_1 s\psi_4]\} \\
& - (\dot{\psi}+\dot{\theta})^2\{m_b[h_1 s\psi_4 - \bar{\phi}_1^T(h_1)\bar{q}_1 c\psi_4]\} \\
& - 2m_6\dot{a}_5[\dot{\psi}_4 a_5 - \bar{\Phi}_1^T\dot{\bar{q}}_1 c\psi_4] - k_3(\beta_4-\beta_3) - C_4\dot{\beta}_4 \\
& - \frac{3GM}{r_c^3}\{[m_c + I_{6y} - I_{6x}]\frac{s2(\psi+\psi_4)}{2} + m_b[h_1[s\psi c(\psi+\psi_4) \\
& + \frac{2}{3}s\psi_4] + \bar{\phi}_1^T(h_1)\bar{q}_1[c\psi c(\psi+\psi_4) - \frac{2c\psi_4}{3}]\}; \\
N(5) =& k_5(\frac{a_5}{r_5} - \beta_5) + \bar{T}_5 - C_5\dot{\beta}_5; \\
N(6) =& -\ddot{h}_1 m_6 c\psi_4 + \dot{\psi}_4^2 m_6 a_5 - 2(\dot{\psi}+\dot{\theta})m_6[\dot{h}_1 s\psi_4 - \phi\dot{q}_1 c\psi_4 - \dot{\psi}_4 a_5] \\
& + (\dot{\psi}+\dot{\theta})^2 m_3[h_1 c\psi_4 + \bar{\phi}_1^T(h_1)\bar{q}_1 s\psi_4 + a_5] \\
& - \frac{k_5}{r_5}(\frac{a_5}{r_5} - \beta_5) - C_6\dot{a}_5 \\
& - \frac{3GMm_3}{r_c^3}\{a_5[s^2(\psi+\psi_4) - \frac{2}{3}] + h_1[s\psi s(\psi+\psi_4) - \frac{2}{3}c\psi_4] \\
& + \bar{\phi}_1^T(h_1)\bar{q}_1[c\psi s(\psi+\psi_4) - \frac{2}{3}s\psi_4].
\end{aligned}
$$